Cranfield University

Andrea Battisti

Conductive Carbon Nanotube Thermosetting Polyester Nanocomposites

School of Applied Sciences

PhD Thesis
2009

Cranfield University
School of Applied Sciences

PhD Thesis
2009

Andrea Battisti

Conductive Carbon Nanotube Thermosetting Polyester Nanocomposites

Supervisors
Prof Ivana K. Partridge
Dr Alexandros A. Skordos
September 2009

Abstract

A commercial unsaturated polyester resin has been used in combination with commercial multiwalled carbon nanotubes (MWNTs) to study the effects of this nanofiller on the electrical properties of the mix in the liquid state, during the cure and in the solid state. The level of addition of the nanotubes ranged from 0.05 to 0.3 wt%.

The dispersion of the filler particles in the matrix was carried out combining triple roll milling, horn sonication and high shear mixing. Qualitative optical and electronic microscopy characterisation supports the development of novel techniques for real-time quantitative assessments of dispersion quality. Fitting of shear dependent viscosity, measured between 0.1 and 100 s^{-1}, to Carreau's model has been shown to provide an indicator of the state of nanotube dispersion in the mixture. Additionally, liquid electrical conductivity measurements offer the option of on-line monitoring, providing a promising tool for process optimisation. The formation of an effective conductive network of nanotubes during the cure was investigated by combining impedance spectroscopy measurements and equivalent circuit modelling with two parallel RC circuit in series with each other. This allows in-situ observation of the key phenomenon responsible for the electrical conductivity of the nanocomposite, namely the filler re-aggregation during cure.

Optimisation of dispersion and cure parameters results in a nanocomposite showing conductive behaviour in the solid state, achieving DC conductivity of 0.13 S/m at 0.30 wt% loading. The percolation threshold was estimated to occur at 0.026 wt% filler loading. The conductivity achieved is comparable to state-of-the-art epoxy thermosetting nanocomposites based on use of carbon nanotubes of equivalent quality.

Successful laboratory scale trials demonstrated the suitability of the materials in copper electroplating and resistance heating. An industrial scale up trial of a 40 kg batch was carried out, using the dispersion and the monitoring techniques developed in the study.

I love fools' experiments. I am always making them.

CHARLES ROBERT DARWIN

Acknowledgments

I wish to thank my supervisors for their support and guidance: Dr. Alex Skordos for continuously fuel my enthusiasm and Prof. Ivana Partridge for teaching me how important it is to slow down and think, among other things. I am particularly grateful to Neil Gray and Dr. Gavin Creech at Scott Bader, to let me work with them instead of for them. They have been more than supportive and I hope I learnt something that will help me in my future career.

Thanks also, in no particular order, to Silvia Marson, Mehdi Asareh, Christian Knipprath, Jim Hurley, Beth Costa, David Ayre, Usama Attia, Gary Muir, Johannes Treiber, Denis Cartie, Bojan Boskovic, Ben Hopper, Ippokratis Sitaras, Mar Salinas Ruiz, James Lander, Marco Longana, Sharon McGuire and all the people that helped me during my PhD.

A special thanks to all the new friends that I made during my time in Cranfield, luckily they are too many to name them all! Thanks to Fra', for everything.

Contents

List of Figures

List of Tables

Nomenclature

BSI British Standards Institution
CNTs Carbon nanotubes
COSHH Control of Substances Hazardous to Health
CVD catalytic vapour deposition
DSC Differential scanning calorimetry
EDI Electrical dispersion index
MWNTs Multi-walled nanotubes
RTM Resin Transfer Moulding
SEM Scanning Electron Microscope
SFEG-SEM Schottky Field Effect Gun Scanning Electron Microscope
SWNTs Single walled nanotubes
TEM Transmission Electron Microscope
TEPPE two exponents phenomenological percolation equation
TLD through lens detector
UPE unsaturated polyester

Publications

Edited version of the following chapters have been published or submitted for publication as follows:

Chapter 6 A. Battisti, A. A. Skordos, I. K. Partridge, Monitoring dispersion of carbon nanotubes in a thermosetting polyester resin, *Composites Science and Technology*, 69(10): 1516–1520, 2009.

Chapter 7 A. Battisti, A. A. Skordos, I. K. Partridge, Measurement of dispersion of carbon nanotubes in thermosets during processing, *Measurement Science and Technology*, submitted.

Chapter 8 A. Battisti, A. A. Skordos, I. K. Partridge, Dielectric monitoring of carbon nanotube network formation in curing thermosetting nanocomposites, *Journal of Physics D: Applied Physics*, 42 (15), 2009.

Chapter 9 A. Battisti, A. A. Skordos, I. K. Partridge, Percolation threshold of carbon nanotubes filled unsaturated polyesters, *Composites Science and Technology*, submitted.

Chapter 1

Introduction and Thesis structure

1.1 Motivation and goals

Over the past two decades considerable volume of study has appeared on the subject of thermosetting polymers loaded with carbon nanotubes. Nanocomposites based on epoxy resins have been by far the most intensively investigated systems [1]. This study, carried out in close liaison with Scott Bader Company Ltd., focuses on carbon nanotube/unsaturated polyester.

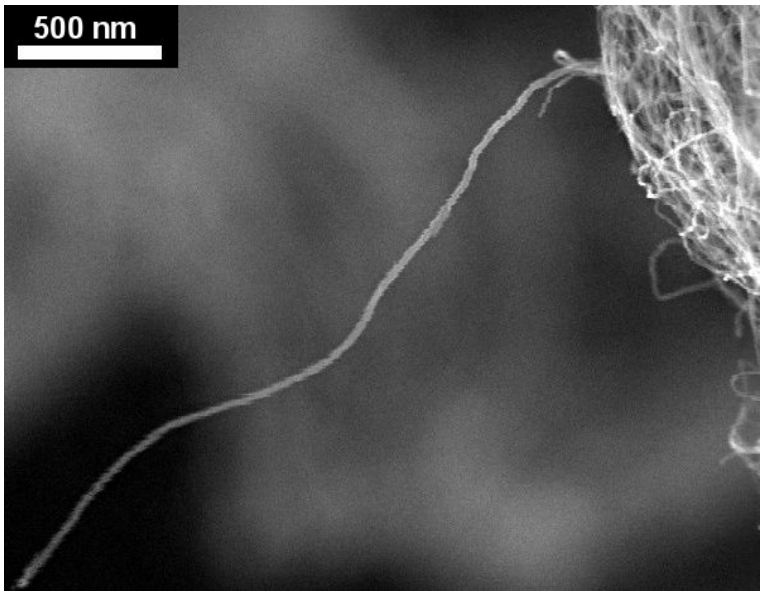

Figure 1.1: SEM micrograph of industrial grade multiwalled carbon nanotubes used in this study

The preparation of CNT composites is aimed at the improvement of multiple properties of the polymer by exploiting the outstanding electrical, mechanical and thermal properties of the CNTs. Additionally, because of the nanoscale dimension of the tubes, the filler loading required to generate such improvements is expected to be considerably lower for CNTs than for traditional fillers. This would result in nanocomposites that can be processed in the same way the corresponding resins are processed, with no additional difficulties. The studies carried out so far have demonstrated the actual capabilities of this class of nanocomposites [2, 3]: CNTs are very effective for electrical properties improvement, but less effective for imparting mechanical reinforcement. So far little success has been obtained in the improvement of the

thermal properties of polymers. The supply chain of nanotubes has expanded remarkably in the last few years. Good-quality entangled multiwalled CNTs, as the ones shown in figure 1.1, are nowadays produced in commodity volumes [4]. Their cost is decreasing rapidly, from the initial value of thousand of euros per gram down to the current value of about 0.1 euros per gram. This motivates the development of new commercial applications based on CNTs, such as the preparation of electrically conductive nanocomposites.

The present study uses commercial multiwalled carbon nanotubes and unsaturated polyester resin to prepare electrically conductive nanocomposites, with an electrical conductivity above $10^{-2}\,S/m$. The main aim is to determine what level of conductivity can be achieved, compared to state-of-the-art epoxy systems. Some significant knowledge gaps must also be addressed to bring manufacturing with these materials to the industrial scale at a competitive cost. The properties and applicability of nanocomposites based on commercial resins must be demonstrated. The processing of the nanocomposites selected must be industrially feasible and easily scalable. Specific tools for process control and optimisation need to be developed. The investigation of the possible applications of the prepared material and the knowledge transfer to industry constitute an integral part of this project.

1.2 Thesis structure

The bases for the preparation of electrically conductive carbon nanotubes nanocomposite are given in chapters 2 and 3. Chapter 2 reviews the structure of the nanotubes, the difficulties encountered in dispersing them and the most relevant results found in literature, with special regard to thermosetting matrices. The chapter also contains an account of the industrial relevance and applications of conductive nanocomposites. The final section of chapter 2 covers the basics of dielectric spectroscopy monitoring of curing thermosetting composites, the application of which to carbon nanotube composites will be reported in chapter 8. Chapter 3 gives an account of the materials used, with special regard to their safe handling.

The preparation, characterisation and monitoring techniques used in the study are covered in chapters 4 and 5. Chapter 4 lists in detail all the procedures used. Chapter 5 is a critical comparison of the available microscopy characterisations techniques.

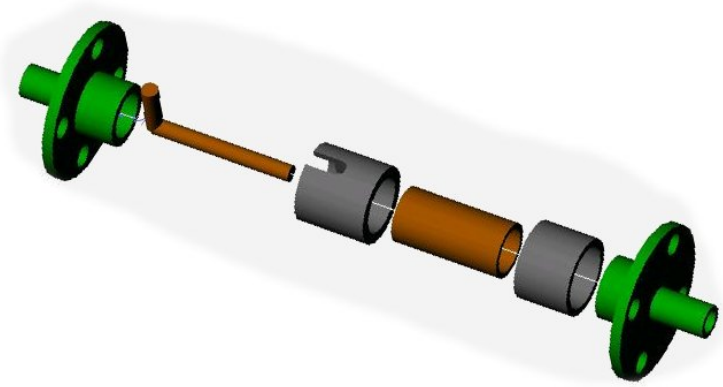

Figure 1.2: Design of the sensor developed for on-line measurement of liquid conductivity during processing

Chapters 6 to 9, which are edited versions of papers published or submitted for publication (see page xxi), form the scientific core of the study. Chapters 6 and 7 focus on the problem of CNT dispersion and on-line monitoring of dispersion during processing (figure 1.2). Chapter 8 describes the development of impedance spectroscopy techniques to monitor the development of the conductive network of nanotubes during cure. Chapter 9 reports

on the electrical conductivity of nanocomposites containing between 0.05 and 0.30 wt% of commercial multiwalled nanotubes.

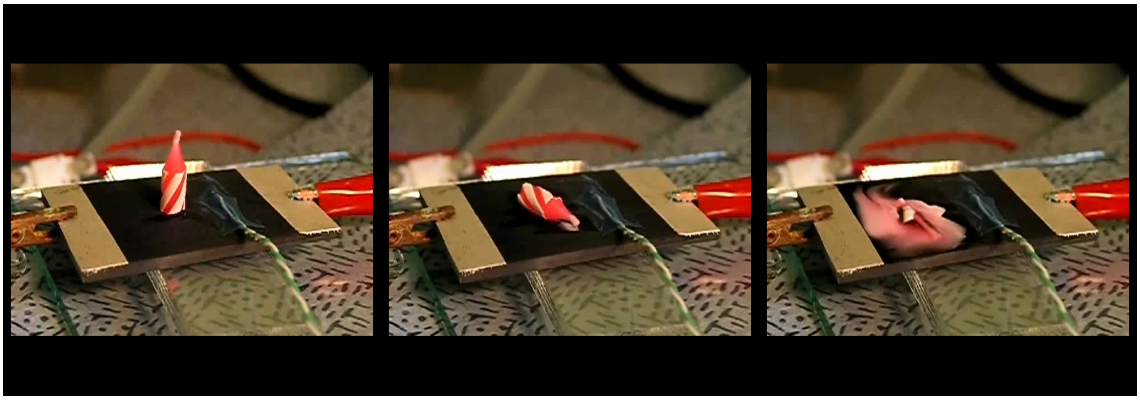

Figure 1.3: Example of application: resistance heating using carbon nanotubes/unsaturated polyester nanocomposites

The industrial developments of CNT/UPE nanocomposites, laboratory scale prototype applications such as the resistance heating of figure 1.3, and the scaling up of the preparation to 20 kg batches, are covered in chapter 10. This chapter constitutes the industrially sensitive content of this thesis.

Chapter 11 brings together the scientific advancements achieved in this study to give an overall picture of the electrical properties and the industrial exploitation of CNT/UPE nanocomposites. It also contains a list of questions that still remain unanswered and some suggestions for further investigation. The main conclusions are presented in chapter 12.

Chapter 2

Background

The first two sections of this chapter contain an overview of the characteristics of carbon nanotubes and of electrically conductive polymeric composites that are relevant to the scope of this study. Section 3 addresses the issue of the difficulties encountered in dispersing carbon nanotubes and the methodologies available to overcome the problem. Section 4 is an account of the work published on the topic of conductive carbon nanotube composites, with special attention paid to thermosetting matrices. Section 5 is an overview of the current and possible applications of electrically conductive CNT nanocomposites. Section 6 covers the basics of impedance spectroscopy for the cure monitoring of thermosetting polymers. Its application to carbon nanotube composites will be presented in chapter 8.

2.1 Carbon nanotubes

The first reports of tubular multilayer graphitic structures with a diameter in the range of nanometres date back to the 1970s by Endo and co-workers [4]. The term carbon nanotubes (CNTs) was first used by Iijima in 1991, during the TEM study of material produced by graphite arc-discharge, aimed at the synthesis of fullerene. [5]. In the last two decades CNTs have been the subject of extensive research programs worldwide and recent developments on their synthesis, molecular structure and properties are described in [6–8].

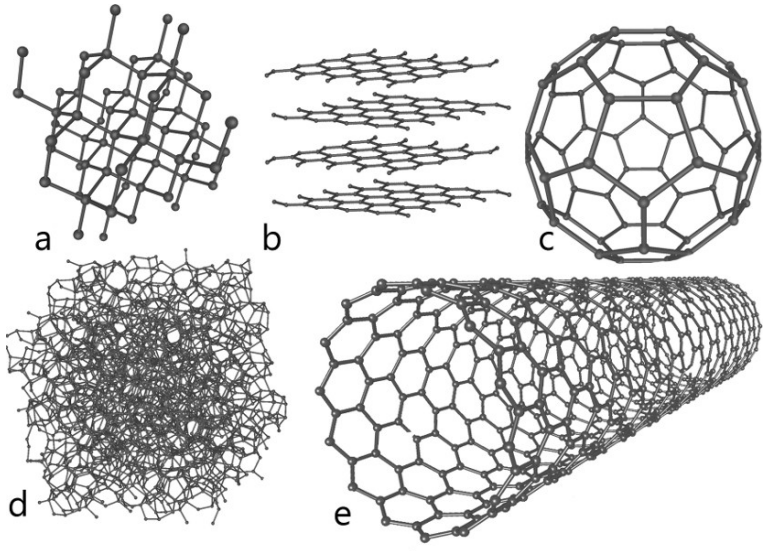

Figure 2.1: Some of the allotropic forms of carbon: (a) diamond (b) graphite (c) Buckminsterfullerene (d) amorphous carbon (e) single-walled carbon nanotube (adapted from [9])

Nanotubes are allotropic forms of carbon (figure 2.1) where the atoms form a highly regular, long and hollow cylinder. Each atom is covalently bonded with three other carbon atoms, forming a hexagonal lattice with carbon-carbon distance of 0.14 nm, as shown in figure 2.2. The sp^2 electronic structure is similar to graphite, possessing a significant π-delocalisation of electrons that allows electronic transport across the structure. Contrary to graphite, where the atoms rest on a plane, the hexagonal lattice is curved, causing a slight pyramidisation toward diamond structure (sp^3) and a lower electron density in the π-delocalisation compared

to graphite. The cylinder is capped at the extremities by hemi-fullerene structures.

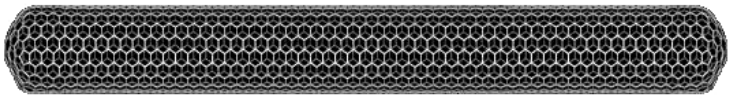

Figure 2.2: Schematic of the atomic structure of a single carbon nanotube [9]

There are two main types of carbon nanotubes. Tubes made of a single capped cylinder called single-walled nanotubes (SWNTs) have diameter close to 0.4 nm. Superstructures of concentric nanotubes, separated by an interlayer space similar to the one of graphite (0.34 nm), are called multi-walled nanotubes (MWNTs) and have diameters of up to 50 nm. The length of a nanotube is usually in the order of a few micrometres; however, lab-scale productions, currently under development, are able to synthesise much longer tubes, up to few millimetres in length [10].

The most common methods of growing CNTs are arc-discharge, laser ablation, high pressure carbon monoxide (HiPCO) and catalytic vapour deposition (CVD), as reviewed in [6–8]. All processes require a catalyst in the form of a nanoparticle of iron, nickel, cobalt or molybdenum to promote the growth of nanotubes. The HiPCO process, due to the yield and purity of the product prepared, is the method of choice for the production of commercial SWNTs [11]. The CVD process has been developed up to industrial scale and it is currently used by many producers to make MWNTs in commodity quantities. Commercial nanotubes are usually highly defective, with structural irregularities such as bends and branches (see figure 2.3). Single-walled nanotubes are generally less defective and usually more expensive than multi-walled nanotubes. Some synthesis methods, such as injection-CVD or plasma-CVD, have been developed to produce high-purity aligned nanotubes, which have fewer defects and less mechanical entanglement, therefore resulting in a product which is easier to disperse than standard commercial nanotubes [12].

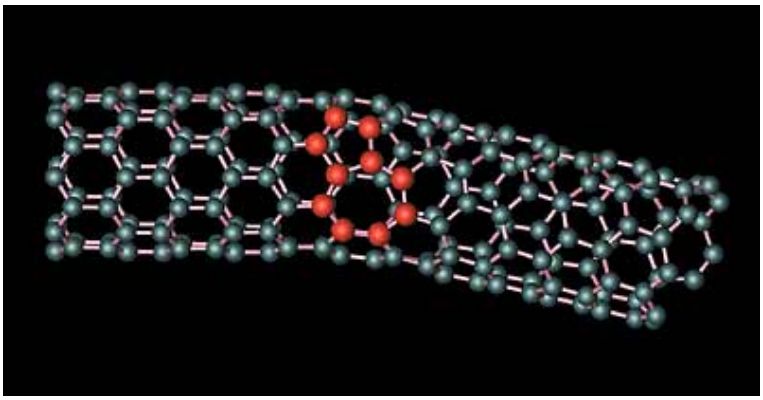

Figure 2.3: Pentagon-heptagon rearrangement in a nanotube [9]

Table 2.1: Physical properties of CNTs [13]. *in-plane properties.

Property	SWNT	MWNT	Graphite
Density $[g/cm^3]$	0.8	1.8	2.26
Elastic Modulus [TPa]	1	0.3 - 1	1 *
Strength [GPa]	50 - 500	10 - 60	10 - 20
Resistivity $[\Omega \cdot m]$	$5 \cdot 10^{-4} - 5 \cdot 10^{-5}$		$5 \cdot 10^{-4} - 5 \cdot 10^{-5}$*
Thermal Conductivity $[W \cdot m^{-1} \cdot K^{-1}]$	3000		3000*
Thermal Stability	>700°C		450-650°C

The high level of attention devoted to the study of CNTs is due to their remarkable theoretical properties: the main ones are listed in table 2.1. However, the real properties of CNTs are compromised by the presence of defects, impurities and by aggregation. As an example, the theoretical Young's modulus of CNTs is about 1 TPa, which has been confirmed experimentally for high quality SWNTs and MWNTs [3], but commercial MWNTs have a modulus of only about 0.4 TPa. The extremely high theoretical thermal conductivity of CNT (thousands of $W \cdot m^{-1} \cdot K^{-1}$) has not been confirmed experimentally yet, with a maximum observed value of about 30 $W \cdot m^{-1} \cdot K^{-1}$. This discrepancy has been attributed to high thermal resistance at the point of contact between tubes [2].

Electrically, SWNTs can act as quantum wires [14], with an electrical conductance close

to the quantomechanical limit[1] of a device

$$G = M \cdot G_0 = M \cdot \frac{2e^2}{h} \tag{2.1}$$

which, for a perfect SWNT, leads to a theoretical resistance of 6.45 $k\Omega$ [16], whereas the lowest value observed is about 10 $k\Omega$. Poncharal *et al.* [16] studied the resistance of individual MWNT at room temperature, using the experimental setup shown in figure 2.4. They observed transport of electrons in the absence of scattering (ballistic conduction) for distances of up to 65 μm. In the same study the electron transport was attributed entirely to the outermost layer of the nanotube, the integrity of which is therefore essential for the high conductivity.

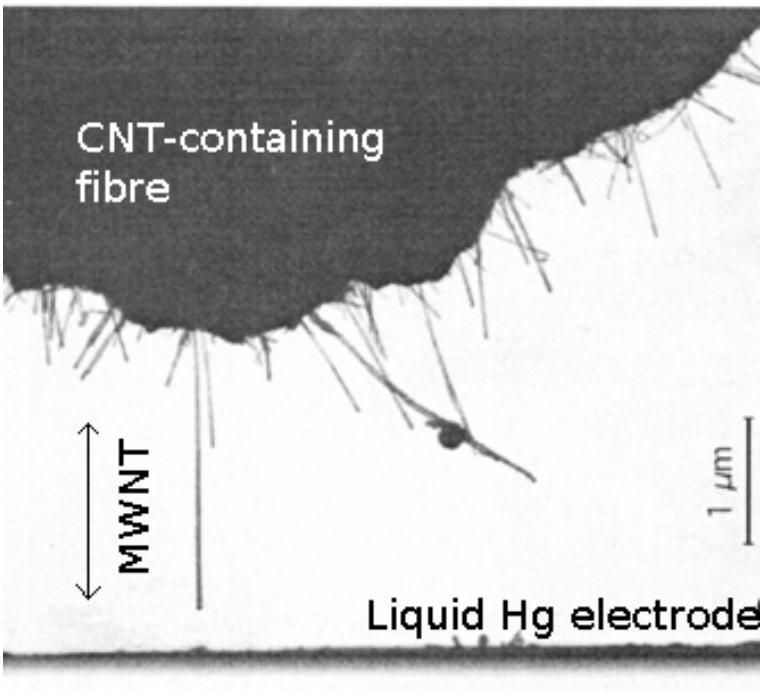

Figure 2.4: TEM imaging of direct measurement of the electron transport properties of an individual MWNT. The nanotube is lowered into the liquid mercury and conductance is measured as a function of position (adapted from [16])

[1] M is the number of conducting channels, 2 in a perfect SWNT; e is the electron charge; h is Plank's constant; G_0 is the quantum of conductance, i.e. the maximum conductance of a one-level device. [15]

2.2 Conductive polymeric composites

The electrical behaviour of conductive fillers, such as graphite, carbon black, fibres, nanofibres and nanotubes, in a polymeric matrix is described by percolation theory [17]. At a critical loading filler particles form a percolating network and the electrical conductivity of the system increases by up to ten orders of magnitude [18] (see figure 2.5). There are several

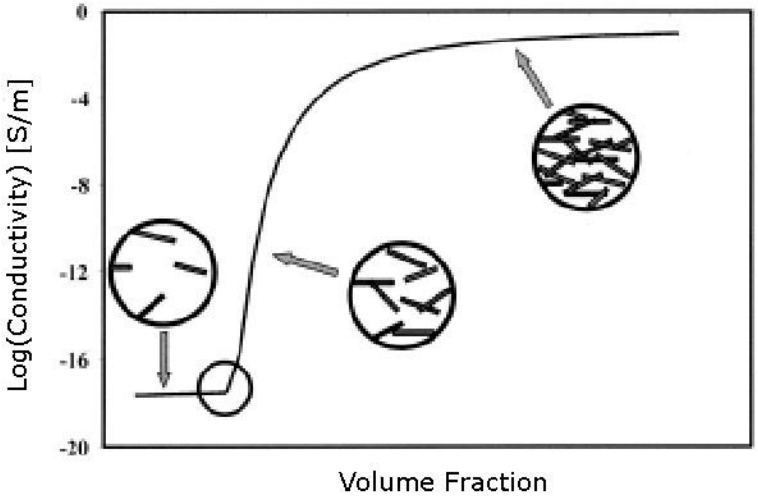

Figure 2.5: Electrical conductivity dependence on filler volume fraction. The small circle denotes the onset of electrical percolation (adapted from [19]).

models of percolation, accounting for factors such as surface energies, viscosity, orientation and shape of the filler [19]. The simplest model is the so-called "statistical percolation model", which describes the conductivity σ of a composite by calculation of the probability of particle-particle contact in a uniform random distribution [20]:

$$\sigma = \sigma_0 \cdot (\phi - \phi_c)^t \ , \ \phi > \phi_c \tag{2.2}$$

where ϕ is the loading as volume fraction, σ_0 is the filler conductivity and t is a critical exponent depending on the geometry of the lattice. The model is valid for filler loadings above the percolation threshold ϕ_c, the critical volume fraction at which the system changes from insulating to conductive.

A more exhaustive model of percolation, describing the behaviour of the system on the whole range of filler loadings ($0 < \phi < 1$), is the "two exponents phenomenological percolation equation" (TEPPE):

$$(1-\phi)\,\frac{\sigma_i^{1/s}-\sigma^{1/s}}{\sigma_i^{1/s}+A\sigma^{1/s}}+\phi\frac{\sigma_c^{1/t}-\sigma^{1/t}}{\sigma_c^{1/t}+A\sigma^{1/t}}=0 \tag{2.3}$$

where

$$A=\frac{1-\phi_c}{\phi_c} \tag{2.4}$$

Here σ_c and σ_i are the conductivities of the conductive filler and the matrix, respectively; s and t are critical exponents [21]. Above and below percolation TEPPE tends to:

$$\sigma = \sigma_i\left(\frac{\phi_c}{\phi_c-\phi}\right)^s,\ \phi<\phi_c \tag{2.5}$$

$$\sigma = \sigma_c\left(\frac{\phi-\phi_c}{1-\phi}\right)^t,\ \phi>\phi_c \tag{2.6}$$

Table 2.2: Total average excluded volume $\langle V_{ex}\rangle$ of objects (adapted from [22])

System	$\langle V_{ex}\rangle$
Deformable spheres or parallel objects	2.8
Randomly oriented infinitely thin rods	1.4
Randomly oriented infinitely thin	1.8

The value of the percolation threshold is directly related to the excluded volume V_{ex} of a particle [22, 23], i.e. "the volume around an object in which the centre of another object is not allowed to penetrate". The percolation threshold of filler particles shaped as capped cylinders is linked to the excluded volume as follows:

$$\phi_c=1-e^{\left(-\frac{\langle V_{ex}\rangle[(\pi/4)\eta+(\pi/6)]}{[(4\pi/3)+2\pi\eta+(\pi/2)\eta^2]}\right)} \tag{2.7}$$

where η is the ratio between the length L and the diameter W of the particle. The total average excluded volume $\langle V_{ex} \rangle$ can be approximated as a constant for particles of known shape (see table 2.2). The total excluded volumes of completely random and parallel orientations are 1.4 and 2.8, respectively; the percolation threshold of a real system of cylindrical particles falls within the range:

$$1 - e^{\left(-\frac{1.4[(\pi/4)\eta+(\pi/6)]}{[(4\pi/3)+2\pi\eta+(\pi/2)\eta^2]}\right)} \leq \phi_c \leq 1 - e^{\left(-\frac{2.8[(\pi/4)\eta+(\pi/6)]}{[(4\pi/3)+2\pi\eta+(\pi/2)\eta^2]}\right)} \tag{2.8}$$

Among the two extreme cases considered theoretically, a random orientation yields the most efficient conductive network. However, the excluded volume resulting from any kind of particle agglomeration has not been calculated theoretically yet. It should be also noted that equation 2.7 considers perfectly linear rods, whereas industrial grade nanotubes are generally wavy. The effect of waviness has been considered theoretically in [24], concluding that tortuosity increases the percolation threshold of a system by up to a factor of two and that the effect is more important for particles with higher aspect ratios.

2.3 Dispersion of carbon nanotubes

A "good" dispersion of filler particles in the matrix is crucial to improve the performance of a composite by addition of CNTs, but is also one of the most challenging aspects of the preparation of these materials [3, 13, 25–28]. Several of the publications that have reported improved properties also showed a good filler dispersion [29–35]. Conversely, a low level of dispersion generally leads to limited improvement of properties, if any [36, 37].

The difficulties encountered in trying to achieve effective dispersion are due to two physical characteristics of commercial nanotubes. The first reason is that the tubes grow in entangled assemblies, which hold them together mechanically. Commercial MWNTs produced by

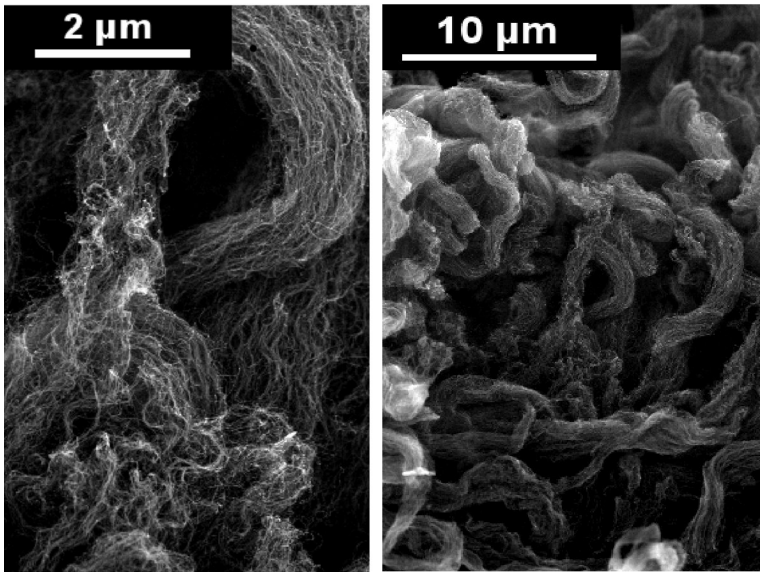

Figure 2.6: Commercial MWNTs grown by CVD (Nanocyl® NC7000)

CVD are extremely wavy and entangled, as shown in figure 2.6 for the nanotubes used in this study. The second reason is that attractive electrostatic forces keep the CNTs together: van der Waals bonds acting on a high surface, e.g. 300 m^2/g, result in a high overall attractive force.

A widely accepted definition of dispersion quality, as well as a quantitative index characterising the level of dispersion, is missing from the literature. The assessment of dispersion is typically based on the microscopical characterisation of the material, using techniques such as optical microscopy, SEM or TEM. The determination of the state of dispersion based on such techniques is qualitative. One notable exception is the introduction of the term 'optically dispersed' to define suspensions with an aggregate size that does not exceed the 1 micrometre threshold [38]. Another exception is the definition of a dispersion index as the ratio between the total area analysed and the area covered by aggregates [39]. The level of dispersion achieved is directly observed in some cases, e.g. [31, 37, 40, 41] or is inferred from the final properties of the material in some other cases, e.g. [34, 42–44]. The use of different characterisation techniques, host polymers, filler types, grades and loadings creates a

complex set of results. The absence of a universally accepted definition of dispersion and the use of the qualitative character of the term make difficult to compare the different preparation methods available. What follows is an account of dispersion methods that have been found effective for the dispersion of CNTs in polymers.

Dispersion methods

The methods for dispersion of CNTs can be classified into two main categories: the use of high-power direct mixing techniques without modification of the CNT structure and the chemical/physical modification of the nanotubes to diminish the forces holding them together. The techniques to disperse CNTs in thermosets and thermoplastics polymers have been reviewed by Grossindor *et al.* [45] and by Xie *et al.* [13].

Among the direct mixing techniques, the most common methods are high shear mixing, triple roll milling, ultrasonication and melt mixing. High shear mixing uses a dissolver disk rotating at up to 10000 rpm to deliver shear to the mixture; this has been applied to the preparation of state-of-the-art electrically conductive nanocomposites [30, 39, 41]. If the viscosity of the mixture is high more shear is applied and the dispersion is more efficient; the viscosity has been increased purposely either by processing at low temperature [32] or by preparing a highly loaded CNT mixture (masterbatch) which is then diluted as necessary [41]. Triple roll milling is a technique for the preparation of a homogeneous suspension commonly used in the pigment and pharmaceutical industry. It improves dispersion by breaking the agglomerates of CNTs by forcing a mixture in the gaps between cylinders rotating in opposite directions at different speeds, as shown in the schematic of figure 2.7.

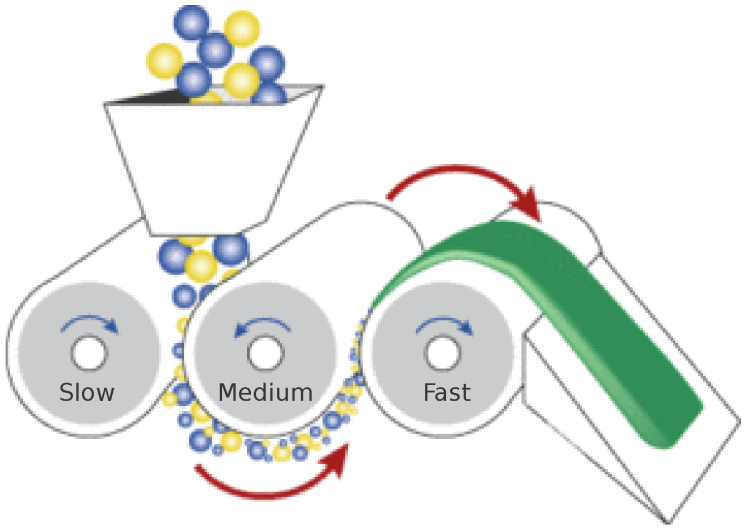

Figure 2.7: Principle of operation of a triple roll mill; typical speed ratio of the slow-medium-fast cylinders is 1 to 3 to 9 (adapted from [46])

The gaps between the roller can be set as low as few microns for electronically controlled models [46], resulting in a particle size below $1\,\mu\mathrm{m}$. This technique is particularly suitable for the preparation of viscous suspensions and has been applied to the preparation of thermosetting CNT composites by using high loadings of filler [35] or viscous media, such as vinyl ester monomer [42].

Two types of ultrasonication have been used for the preparation of nanocomposites. In bath sonication a container of CNT suspension is placed in a water tank, which walls oscillate at 50 kHz. The water bath conveys the waves to the sample, where cavitation, which is the formation and collapse of low-pressure bubbles, breaks the agglomerates. In horn sonication the tip of a horn is immersed in the suspension and oscillates at 20 kHz, creating localised, high-energetic cavitation [44, 47]. A solvent can be used to lower the viscosity of the suspension and form more bubbles and, therefore, increase the efficiency of sonication. The solvent needs to be removed in a later stage. It should be noted that creation of defects in the CNT structure caused by horn sonication in methylene chloride has been reported [48].

Melt mixing is a dispersion technique specific to thermoplastic composites: the melt

polymer containing the filler is forced to flow in the heated barrel of a single- or double-screw extruder [2]. The shear applied between the screws and the walls of the barrel causes the dispersion of CNTs. The quality of dispersion depends on the type and quality of the as-produced nanotubes as well as on the processing conditions of the melt [40, 49]. Melt mixing is an easily scalable method that is already common in industry for the preparation of polymers blends.

Examples of the modification of the carbon nanotube structures to improve dispersion are: growth of aligned CNTs, chemical functionalisation of the surface and use of molecules sitting on the surface of the nanotubes, i.e. surfactants or polymers acting as surfactants. Aligned CNTs such as the ones shown in figure 2.8 can be synthesised using injection-CVD or other special synthesis methods. Because of minimal mechanical entanglement they are much easier to disperse than normal CNTs.

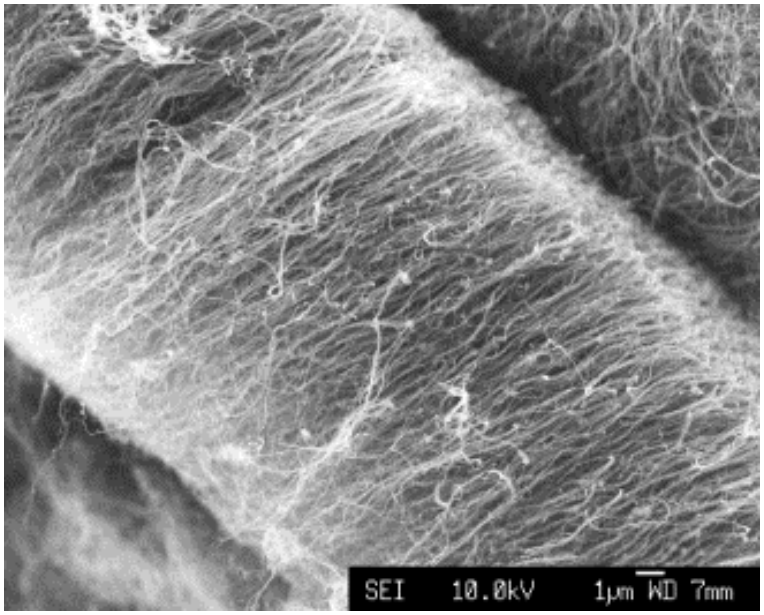

Figure 2.8: Aligned MWNT growth by catalytic carbon vapour deposition [30]

Functionalisation is a term that encompasses a series of chemical treatments, usually carried out in strong acid and oxidising conditions, to attach functional groups to the CNT sur-

face. These groups, typically -OH, can be then used as reactive sites to add specific molecular groups to the surface, producing carbon nanotubes with a controlled chemistry and polarity. The increased compatibility between the newly created surface and the polymer facilitates the process of dispersion [37, 50]. Since the modification of the surface perturbs the π electron delocalisation of the outer layer of a nanotube, a major drawback of functionalisation is the loss of electrical conductivity of the nanotube [45]. Surfactants and compatibilisation polymers use a similar approach, but the surface modification is based on non-covalent bonding. Using the appropriate surfactant, the "solvated" tubes become compatible with the polymer and disperse more easily in the matrix [51].

2.4 Conductive CNT nanocomposites

Carbon nanotubes, because of their physical properties such as high intrinsic electrical conductivity and high aspect ratio, are interesting as conductive fillers for the preparation of conductive polymeric nanocomposites [2, 13, 25–27]. Bauhofer and Kovacs have reviewed the recent developments in the field [1].

Coleman *et al.* [52] were the first to report the percolating behaviour of carbon nanotube composites. The theoretical value of percolation threshold for spherical particles is 16 vol%, whereas for particles of aspect ratio of 1000, typical of MWNT, it is about 0.07 vol%[2]. Several publications reported experimental values close to this figure, as shown in figure 2.9a. Figure 2.9b shows the experimental values of composite conductivity versus CNT loading for different types of nanotubes. Composites based on non-entangled MWNT and SWNT have conductivities higher than composites based on entangled MWNT. This is mainly due to their regular structure, which is less prone to electron scattering and increases dispersibility. The results reporting high percolation threshold values in figure 2.9a and low conductivity at

[2]corresponding to 0.16 wt %: MWNT density $\simeq$ 1.8 g/ml

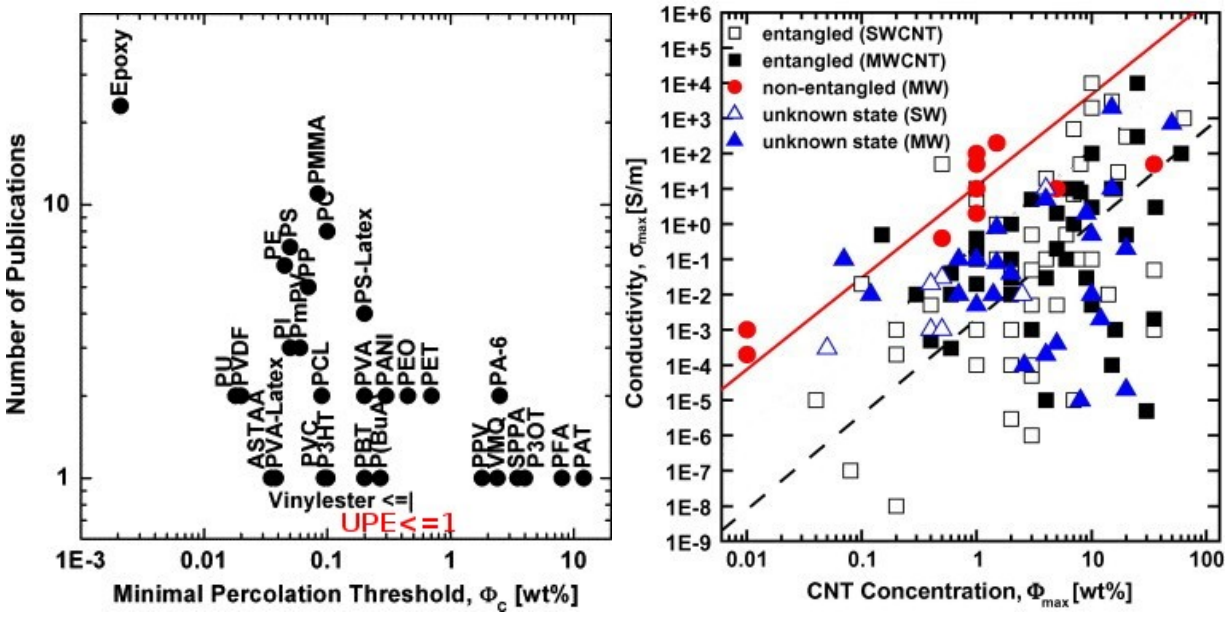

Figure 2.9: Comparison of the electrical properties of polymeric CNT composites [1]: percolation threshold (a) and maximum conductivity (b). Lines denote the percolation of specific types of nanotubes: non-entangled multi-walled nanotubes (solid) and entangled multi-walled nanotubes (dashed).

high CNT concentration in figure 2.9b and, can be attributed to poor CNT dispersion in the preparation of the material.

A random distributions of filler particles does not lead to the highest nanocomposite conductivity. The conductivity can increase when individually suspended particles are allowed to re-agglomerate during the preparation of the nanocomposite. The phenomenon was first observed by Schueler *et al.* [17] exploiting the reagglomeration of carbon black in epoxy systems to achieve percolation threshold of just 0.06 vol%. Similar behaviour has been observed for entangled MWNT in epoxy [29, 41] and vinyl ester [42] systems, with percolation thresholds lower than 0.1 wt%, well below the values predicted by theory. Thresholds lower than 0.01 wt%, which is the best performance ever achieved by any kind of a conductive composite, have been reached using aligned MWNT [30] and SWNT [31] in epoxy.

Only two scientific papers have been published so far reporting increased electrical conduc-

tivity of unsaturated polyester matrices by the addition of carbon nanotubes. Kimura *et al.* [53] reported on the electrical percolation at the loading of 1 wt% for entangled MWNT in unsaturated polyester resin. Recent work from Vera-Argullo *et al.* [39] reported on the electrical properties nanocomposites of aligned MWNT in unsaturated polyesters, showing a percolation threshold below 0.1 wt %.

A selection of the works published in the field of carbon nanotubes composites that are particularly relevant to this study is listed in table 2.3.

Table 2.3: Selection of relevant published works on CNT nanocomposites
Acronyms and symbols: single-walled nanotubes (SWNT), entangled multi-walled nanotubes (e-MWNT), aligned multi-walled nanotubes (a-MWNT), amino-functionalised entangled multi-walled nanotubes (NH2-MW), unsaturated polyester resins (UPE), vinyl ester(VE), poly(phenyleneethynylene) (PPE), polystyrene (PS), polycarbonate (PC), percolation threshold (ϕ_c).

Filler	Matrix	Dispersion method	Properties	Ref.
e-MWNT	epoxy	solvent bath sonication high shear mixing	$10^{-2} S/m$ @ 0.2 wt%	[43]
e-MWNT	epoxy	masterbatch high shear mixing	$\phi_c = 0.02\, wt\%$	[41]
e-MWNT	epoxy	masterbatch triple roll mill	$\phi_c < 0.1\, wt\%$	[32, 35]
a-MWNT	epoxy	high shear mix	$\phi_c = 0.0025\, wt\%$	[29, 30, 33, 34]
SWNT	epoxy	solvent bath sonication	$\phi_c = 0.005\, wt\%$	[31]
a-MWNT	UPE	high shear mixing	$\phi_c < 0.1\, wt\%$	[39]
e-MWNT	UPE	triple roll mill	< Strength	[54]
NH2-MW	UPE	triple roll mill	> Strength @ 5 wt%	[54]
e-MWNT	PS	solvent horn sonication	+25% Strength +42% Modulus @ 1 wt%	[44]
e-MWNT	VE	triple roll mill	$\phi_c < 0.1\, wt\%$	[42]
e-MWNT	PC	melt mixing	$\phi_c < 0.5\, wt\%$	[40]
SWNT	PPE	solvent mixing	$\phi_c < 0.1\, wt\%$	[55]

2.5 Applications of electrically conductive composites

Electrically conductive composites based on carbon black, graphite, carbon fibres and amorphous carbon are nowadays standard materials [56]. These composites usually require high filler loadings, often above 20 wt% to achieve the conductivity desired, which compromises the mechanical, aesthetic and rheological properties of the material. As shown in figure 2.9, nanocomposites based on CNTs can achieve the same electrical properties with filler loading typically below 1 wt%, without compromising the general characteristic of the material.

One of the first industrial applications of CNT composites has been the substitution of carbon black-based material as *electrostatic dissipating materials* [57]. This application requires materials with conductivity between 10^{-9} and $10^{-2}\,\mathrm{S/m}$ to avoid the accumulation of electrostatic charge. Applications range from fuel lines to aircraft wings. Carbon black has been successfully substituted by CNT in the formulation of thermoplastic composites for fuel lines in the automotive sector, allowing the conservation of the polymer mechanical properties, thus a consistent weight saving compared to the use of carbon-black as conductive filler[57].

Electrostatic discharge protection (EDS) requires conductivities above $10^{-1}\,\mathrm{S/m}$ to protect the internal circuits of electronic equipment from a voltage surge. Also called anti-static materials, they work by carrying away the electrostatic current generated by the discharge. Anti-static paints based on metallic particles are available on the market, but are heavy and costly. A nanocomposite skin on top of the housing of electronic equipment would allow meeting the EDS requirements with minimal costs and added weight. CNT nanocomposites used as matrices in processes such as RTM and pultrusion would allow the direct production of anti-static components.

The principal utilisation of *electromagnetic interference shielding* materials is to protect from electromagnetic interference with a frequency above 30 MHz [58]. This means isola-

ting the external electromagnetic noise out of an enclosure or preventing the emission of noise from malfunctioning equipments. Shielding is based on the generation of an induced current on the surface of the material, which cancels the external magnetic field. Although the shielding effect is not only related to the DC conductivity, but also to the internal structure of the conductive network of filler particles, a conductivity above $10^{-2}\,\mathrm{S/m}$ is essential. Shielding is a standard requirement in aircrafts, electronic components and hospitals, but also relevant for new applications such as suppression of mobile phone signals in defined areas, prevention of eavesdropping of Wi-Fi networks and protection from the so-called electrosmog [59]. The current technology uses metallic meshes, housings and tiles as well as coatings or electroplated enclosures, which implies additional cost and weight in a manufactured part. Paintable coatings, based on carbon black and graphite, are commercially available for the protection from electrosmog [60].

One of the first industrial applications of CNT composites has been the manufacturing of electrically conductive automotive parts for *electrostatic painting*. Electrostatic painting is used to produce coatings for corrosion protection or aesthetic purposes. Two variants of electrostatic painting are possible; powder coating, in which the part is sprayed with an electrostatically charged powder; and electrocoating, in which the part connected to an electrode is dipped in a water-borne paint. In electrocoating a moving rack immerses the parts into a

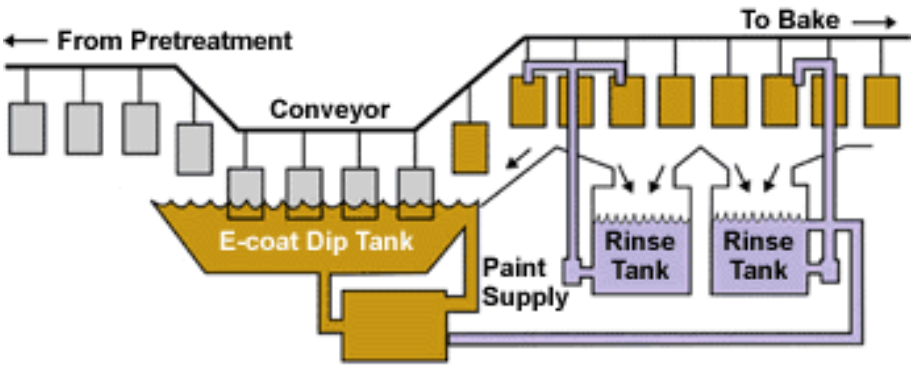

Figure 2.10: Typical Electrocoat system [61]

bath, achieving a highly automated, high throughput and continuous process, as illustrated in figure 2.10. Electrostatic painting is typically used for conductive, metallic parts with a minimum conductivity of $10^{-4}\,\mathrm{S/m}$ [62]. Plastic parts can also be painted via the application of a conductive primer, such as a suspension of nickel in organic solvents, which is not cost effective for most applications [63]. Applying the process directly to plastic parts would allow on-line processing, time and costs saving and would prevent colour mismatch between parts coated using different techniques. Hyperion Catalysis® pioneered the development of electropainted automotive parts made of thermoplastic CNT composites [57].

Electroplating is an application similar to electrocoating in which a conductive part is immersed in a galvanic cell and coated with a thin layer of metal, such as copper, chromium, or zinc. The final applications include aesthetic metal finishing, high-performance electromagnetic shielding and manufacturing of rotogravure printing rollers. Electroplating requires a level of conductivity in the order of $10^{-1}\,\mathrm{S/m}$ and a homogeneous conductivity of the surface of the part to produce an even layer of metal.

Lightning protection is a major concern in the design of aircrafts and wind turbines, especially for structures based on composite materials [64]. A lightning strike generates ac currents of up to $2 \cdot 10^5$ A, which discharge on the surface of the part through the minimum impedance path, causing structural damage and sparking. Current lightning protection of composite structures relies on dissipating the current along a low impedance pathway, such as a metallic mesh embedded into the composite. Using CNT nanocomposites as structural material would allow the current to be dispersed directly by the material, thus using a larger area and reducing structural damage. Filling fasteners connections and gaps with conductive CNT-adhesives would prevent the formation of sparks and the consequent risk of fire and explosion.

Resistance heating [56] is based on the generation of heat by a current I passing through

Figure 2.11: Testing of lightning protection systems on a wind blade [65]

a resistance R:

$$P = I \cdot V = \frac{V^2}{R} = I^2 \cdot R \tag{2.9}$$

Applications range from portable heating devices to heating of buildings and from de-icing aircraft wings to heating moulds for the manufacturing of thermosetting composites. The voltage and current that is possible to apply is limited by the power source used, therefore requiring a conductivity in the order of $10^{-1}\,\mathrm{S/m}$ to obtain optimal heat generation. Boyce components first introduced a composite based on carbon nanofibres for the resistance heating of composite structures and tooling moulds [66].

Conductive composites at low carbon nanotubes loading are investigated for making *transparent conductors* [67]. The actual technology is based on indium tin oxide (ITO), a material with a conductivity in the order of $10^{2}\,\mathrm{S/m}$ and transparency of about 95% over the whole visible spectra, but faces challenges due to the high cost of indium and the need of a highly flexible material for the manufacturing of OLEDs (organic light-emitting diode).

Transparent CNT composites would find applications such as transparent electrodes in solar cells, field emitting devices and OLEDs.

Table 2.4 is a summary of the application described, with the corresponding minimum conductivity required.

Table 2.4: Industrial applications of electrically conductive composites.

Application	Minimum σ [S/m]
Electrostatic dissipating	10^{-9}
Electrostatic painting	10^{-4}
Electromagnetic interference shielding	$> 10^{-2}$
Electrostatic discharge protection (EDS)	10^{-1}
Electroplating	10^{-1}
Resistance heating	10^{-1}
Transparent conductors	$>10^{1}$
Lightning protection	$> 10^{1}$

2.6 Dielectric spectroscopy

Broadband dielectric spectroscopy is a technique used to study the electrical and electronic interactions of matter with an electromagnetic field, encompassing frequencies from 10^{-6} to 10^{12} Hz. The response to an AC electric field arises from the phenomena of reorientation of dipoles, creation of induced dipoles and electrical conduction, allowing the investigation of the physical processes taking place in the sample. The range 0.1 to 10^8 Hz is commonly used for the analysis of polymers, investigating the dielectric material properties in the form of dielectric permittivity $\varepsilon^\star$ or complex impedance $Z^\star$ [68].

Maxwell's equations describe the interaction of the electromagnetic field with matter. The electrical displacement $\bar{D}$ due to the application of a small electric field ($\bar{E} < 10^6\, Vm^{-1}$) is expressed by:

$$\bar{D} = \varepsilon^\star \varepsilon_0 \bar{E} \tag{2.10}$$

where the constant ε_0 is the dielectric permittivity of the vacuum and $\varepsilon^\star$ is defined as the dielectric function of the sample. If a periodic electric field is applied, $\varepsilon^\star$ is a complex function of the angular frequency $\omega = 2\pi\nu$, which can be expressed as follows:

$$\varepsilon^\star(\omega) = \varepsilon'(\omega) - i\varepsilon''(\omega) \tag{2.11}$$

where ε' and ε'' are the real and imaginary part of the dielectric function, respectively. The dielectric function $\varepsilon^\star$ is typically used to represent the behaviour of dipoles. Other representations which are more suitable to observe electrical conduction are complex impedance ($Z^\star$), complex electrical modulus ($M^\star$), complex conductivity ($\sigma^\star$) or complex resistivity ($\rho^\star$). Complex impedance is defined as:

$$Z^{\star}(\omega) = \frac{1}{i\omega\varepsilon^{\star}C_0} \tag{2.12}$$

$$Z^{\star}(\omega) = Z'(\omega) - iZ''(\omega) \tag{2.13}$$

where C_0 is the capacitance of the empty cell. Another electrical unit commonly used to describe conductive systems is the AC conductivity $\sigma(\omega)$, which is the module of the complex conductivity $\sigma^{\star}(\omega)$:

$$\sigma(\omega) = |\sigma^{\star}(\omega)| \tag{2.14}$$

$$\sigma^{\star}(\omega) = i\omega\varepsilon_0\varepsilon^{\star}(\omega) \tag{2.15}$$

Impedance spectroscopy is often used to create models of the physical processes with an idealised electrical circuit. These equivalent circuits comprise resistances R, representing the ability of the material to dissipate the energy of the electric field and capacitances C, representing the ability of the material to store the energy of the electric field [69].

Polarisation mechanisms and Equivalent Circuit models

The dielectric function of the material, in its real and imaginary parts, arises from polarisation phenomena, e.g. dipole orientation and electrical conduction [69–71]. A polymeric material has permanent dipoles, such as polar groups, in the polymeric chains. Induced dipoles arise from the distortion of the neutral distribution of electronic clouds due to the electric field and mechanisms of ionic and electronic conduction.

Induced dipoles react to changes in the electric field in a very short time scale, faster than 10^8Hz, falling out of the typical analytical range of impedance spectroscopy. Since this polarisation mechanism does not involve any molecular movement it does not dissipate

energy and is denoted by a single capacitor in the equivalent circuit modelling (C_1 in figure 2.13).

The orientation of permanent dipoles (i.e. polar molecular groups) in a viscous medium, such as an uncured thermoset, implies dissipation of the energy supplied by the electric field, as well as storage of a part of the energy in the oriented configuration (see figure 2.12). It

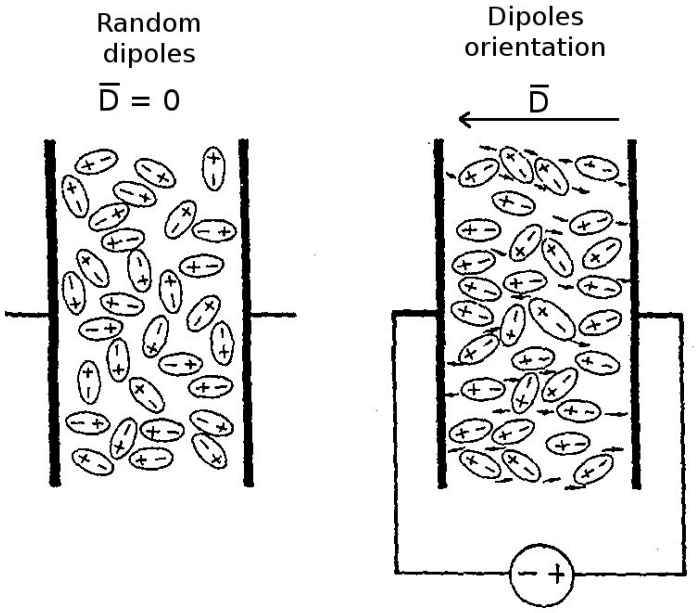

Figure 2.12: Orientation of dipoles in the presence of an applied electric field (adapted from [72])

is then represented in the equivalent circuit as a capacitance and a resistance in series (C_2 and R_2 in figure 2.13). Each $R - C$ series represents a single relaxation mechanism (Debye relaxation) with a relaxation time $\tau = RC$. The characteristic relaxation time of molecular group reorientation is in the order of $10^{-6}\,\mathrm{s}$ in the liquid state, covering the high frequency end of a typical impedance spectrum (see figure 2.16). A comprehensive treatment of Debye and non-Debye relaxations in materials can be found in [68, 73].

Both conduction mechanisms in a polymeric system are dissipative phenomena; electronic conduction dissipates energy by Joule heating and ionic conduction implies dissipation of energy due to the movement of ions in viscous media, as shown in figure 2.14. Conduc-

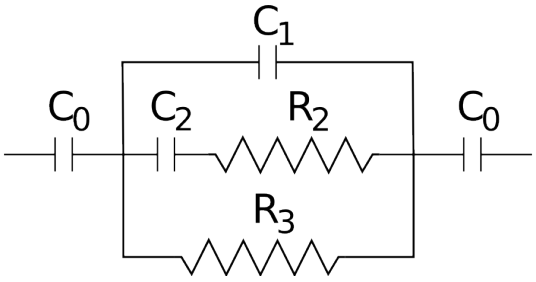

Figure 2.13: Equivalent circuit for the modelling of an homogeneous polymeric system [70]

tion mechanisms in polymers are therefore represented by a pure resistance (R_3 in figure 2.13). Since this resistance is connected in parallel with the capacitances C_1 and C_2, each conductive mechanism can be also be described by a characteristic time $\tau = RC$.

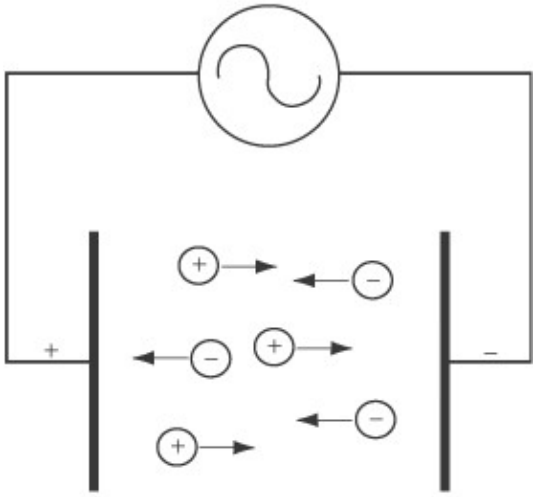

Figure 2.14: Movement of ions in the presence of an applied electric field [71]

An additional mechanism of polarisation observable in polymeric systems arises from the separation of charges at an interface, which can be either an inner boundary layer or the surface of the measuring electrode, as shown in figure 2.15. Interfacial polarisation at inner boundaries, the so-called Maxwell-Wagner-Sillar polarisation, is the polarisation at the internal interfaces between components of an inhomogeneous materials, such as a composite [73]. This polarisation can be modelled as a parallel $R - C$ circuit in series with the other components of the circuit. An extensive treatment of the dielectric properties of inhomogeneous

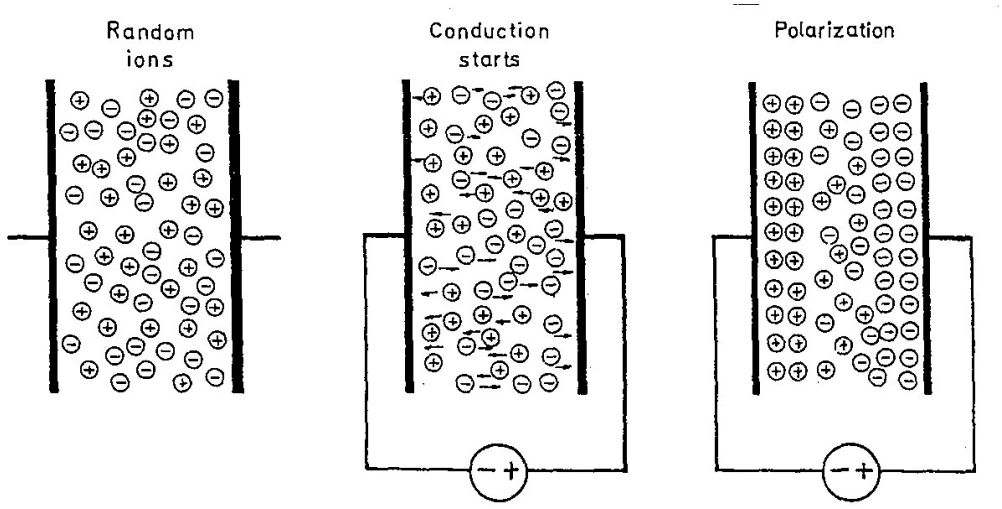

Figure 2.15: Electrode polarisation in the presence of an applied electric field [72]

materials can be found in [70]. Migrating charges cannot cross the interface while electrons can, which creates a double layer. In the impedance spectroscopy of polymers, electrode polarisation is a parasitic effect that disturbs the observation of other dielectric mechanisms. The creation of the double layer at the electrode surface, modelled by C_0 in the equivalent circuit of figure 2.13, is a slow-changing phenomenon and affects the low-frequency end of the impedance spectra (see figure 2.16).

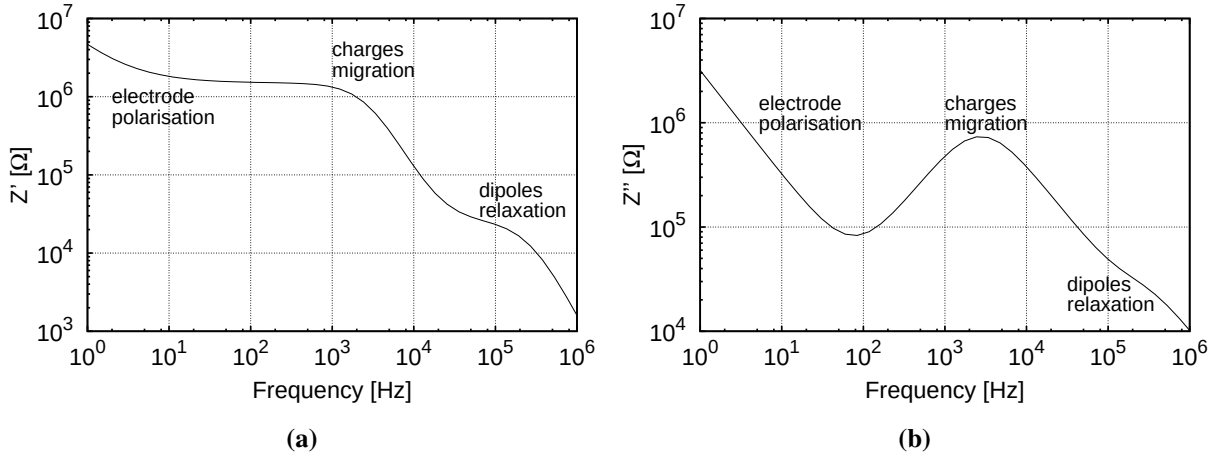

Figure 2.16: Illustration of the real (a) and imaginary (b) parts of the impedance spectra of a thermo-setting resin (adapted from [74]).

Ambiguous circuits

Analysing impedance spectra by means of equivalent circuits has an inherent source of ambiguity: multiple circuits can give exactly the same impedance response, as shown in the example of figure 2.17. Since the circuits are interchangeable in the fitting of experimental data, some specific criteria should be used to guide the selection of a circuit [70]: one should seek indications from previous knowledge and studies of the physical processes involved, if available. Analogies between the mathematical description of the model and the physical description of the phenomena should be regarded as good indications; selection should be based on the criterion of simplicity.

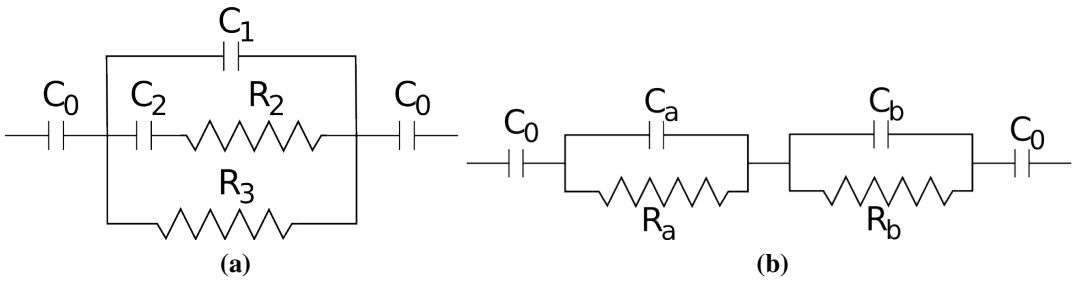

Figure 2.17: Two different representations of the same equivalent circuit: (a) Maxwell (b) Voigt

Model fitting with genetic algorithms

The fitting of an experimental impedance spectra to an equivalent circuit model requires the solution of an error minimisation problem. This can be carried out using genetic algorithm, which is an optimisation technique inspired by the principles of evolutionary biology [75, 76]. The method has been applied to the cure monitoring of thermosetting resins inverse problems in [77].

The value of each parameter of the model, within a predefined range, is encoded in a

binary string of a chosen number of digits (5 in the example).

$$\begin{aligned} 100 \leq R \leq 1000 \qquad & \text{binary} \\ R = 100 \quad \longrightarrow \quad & 00000 \\ R = 1000 \quad \longrightarrow \quad & 11111 \\ R = 627 \quad \longrightarrow \quad & 10110 \end{aligned}$$

The combination of the five parameters in a single binary string is called individual.

$$\underbrace{01001}_{R_b} \; \underbrace{10010}_{R_i} \; \underbrace{01010}_{C_b} \; \underbrace{11001}_{C_i}$$

The first generation is composed by a predefined number of randomly chosen individuals. The quality of each individual of parameter (fitness) is determined by the result of an objective function defined at the beginning of the problem ($S_{individual}$). and the fitness function of each individual is evaluated using equation 4.12. The value of $S_{individual}$ determines its probability of being selected as a parent for the next generation, which promotes the propagation of "good" genome. The individuals of the second generation (offspring) are generated from two individuals of the first generation (parents) by swapping the digits at a random point of the binary string (crossover recombination).

$$\begin{aligned} \text{parent A} \qquad & \text{offspring A} \\ \texttt{0001011110101110} \quad \Rightarrow \quad & \texttt{00010111}010110100 \\ \text{parent B} \qquad & \text{offspring B} \\ 1010110101101 00 \quad \Rightarrow \quad & 10101\texttt{10101110} \end{aligned}$$

Subsequently, each offspring is subjected to mutation: each digit of an offspring has a set

probability of being flipped, from 0 to 1 or from 0 to 1.

$$\begin{aligned} \text{before mutation} &: 0o0101110101110 \\ \text{after mutation} &: 0\imath0101110101110 \end{aligned}$$

The best solutions of of a generation (elite) are copied directly to the next generation without undergo crossover recombination. The best solution after a set number of generation is the result of the search.

Dielectric cure monitoring

Monitoring the cure of thermosets with dielectric spectroscopy can be approached with different techniques [69, 76]. In this study we focus on the cure monitoring based on migrating charge polarisation.

The signal at intermediate frequencies of the impedance spectrum of a curing resin is dominated by migrating charges, which can be isolated from the other dielectric mechanisms present, such as dipolar relaxations and electrode polarisation. This isolated migrating charge

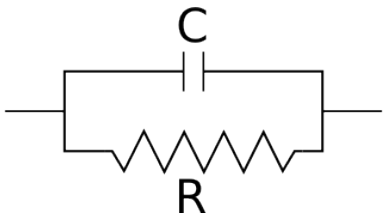

Figure 2.18: Equivalent circuit model of migrating charges in a curing thermosetting system

signal has been modelled by the simplified equivalent circuit model of figure 2.18. R denotes the energy loss correlated with the movement of migrating charges in a viscous media; C

represent the induced dipoles on the systems. Such circuit is mathematically described by:

$$Z' = \frac{R}{1+(\omega RC)^2} \tag{2.16}$$

$$Z'' = \frac{\omega R^2 C}{1+(\omega RC)^2} \tag{2.17}$$

The value of R can be extracted via graphical analysis[3] or data fitting of the impedance spectra. Knowing the geometry of the cell used for the measurement, the value of resistivity ρ can be calculated as

$$\rho = R \cdot f(S, L) \tag{2.18}$$

where $f(S, L)$ is a geometrical factor, equal to S/L for a parallel plate configuration. Cure monitoring is based on the following empirical equation that correlates the resistivity ρ with the degree of cure α:

$$\frac{\alpha}{\alpha_m} = \frac{\log(\rho) - \log(\rho_0)}{\log(\rho_m) - \log(\rho_0)} \tag{2.19}$$

where α_m is the final degree of cure; ρ_0 and ρ_m are the resistivities of the system at the beginning of cure and at the end of the reaction. Figure 2.19 shows the comparison of the degree of cure measured by DSC with the dielectric monitoring using equation (2.19). The dielectric cure monitoring technique is becoming used commercially as an on-line process control system for the composite industry and it has been used to investigate the electrical properties of CNT composites [21, 78]. The use of the technique to monitor *in-situ* the cure of CNT nanocomposites is a new research application of the method.

[3]The corresponding peak in the imaginary impedance graph has a maximum which is located at a frequency $\omega_{max} = (RC)^{-1}$ and imaginary impedance $Z''_{max} = R/2$.

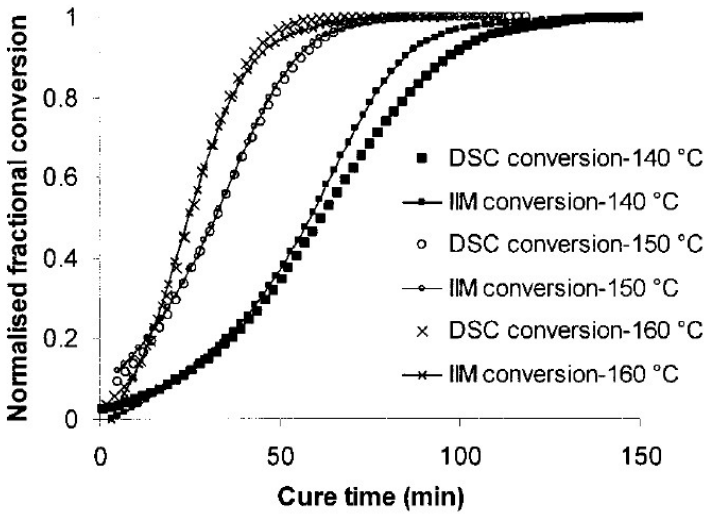

Figure 2.19: Comparison of the degree of cure measured by DSC and by dielectric measurements [77]

Chapter 3

Materials

This chapter describes the materials used for the preparation of the conductive nanocomposite. The first section covers the properties of the carbon nanotubes and gives an overview of the guidelines and regulations for the safe handling of nanomaterials. The second section covers the chemistry and the main properties of unsaturated polyester resins.

3.1 Carbon nanotubes

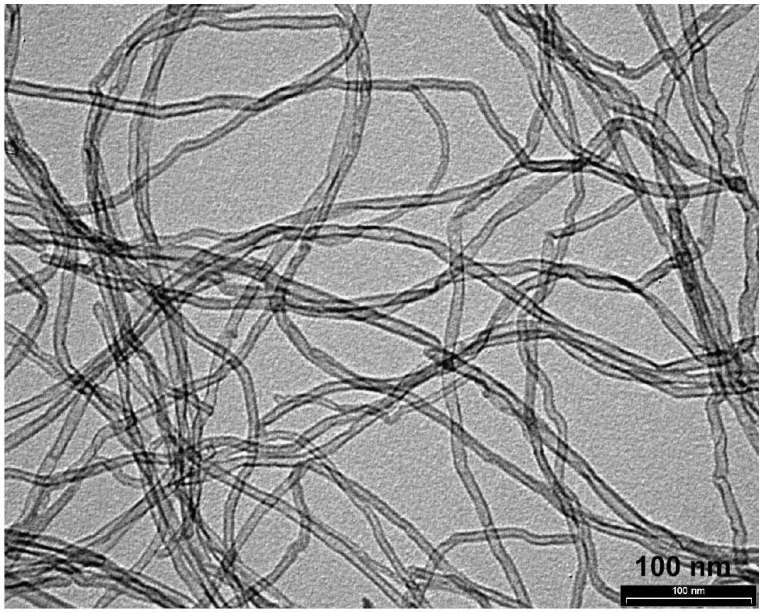

Figure 3.1: TEM micrograph of NC7000 (adapted from [79]).

The nanotubes used in this study are NC7000 (Nanocyl® S.A., Belgium), which are commercial MWNTs produced by chemical vapour deposition (CVD). The physical characteristics of the material declared by the producer are listed in table 3.1.

Table 3.1: Characteristics of NC7000 (adapted from Nanocyl® datasheet [80])

Property	Unit	Value	Method of measurement
Average diameter	nm	9.5	TEM
Length	μm	1.5	TEM
Carbon Purity	$\%$	90	TGA
Metal Oxides (impurity)	$\%$	10	TGA
Other Carbon (impurity)	$\%$	n.d.	HRTEM
Specific surface Area	m^2/g	250÷300	BET

Safe handling of nanomaterials

The application of nanomaterials in research and industry has been developing rapidly in recent years; however, the safe handling and disposal of nanomaterials is still a controversial topic. Since no specific rules have yet been established, industries and research centres involved in nanomaterial production and utilisation have to refer to guidelines and recommendations. The information is published by different regulatory bodies (e.g. British Standard Association and UK Health and Safety Executive), is frequently updated and can sometimes be contradictory. Weblogs are a good way to keep up-to-date with the new development in the field, see for example [81].

There are causes of concern about the toxicity of novel materials, which have been analysed in a report of the Royal Commission on Environmental Pollution: "Novel material in the environment: the case of nanotechnology" [82]. Their functionality is in many cases unknown and somehow unpredictable. Similarities with known dangerous materials raise the attention of the scientific and public community, as for example the resemblance between nanotubes and asbestos. The lack of scientific knowledge on health and environmental effects, route of exposure, pathways to the environment and the virtual absence of information on long-term exposure effects is also affecting the public opinion about nanomaterials [82]. The rate of development of new materials and applications outruns the rate of development of toxicological standards, which implies that the situation will not fundamentally change in the future.

As the Royal Commission report points out, the case of the nanomaterials is an example of how to deal with uncertainty. The first approach to governing the uncertainty is the "optimistic": no regulatory actions are taken until the harmful character of the material is clearly proved. The second approach is the "risk control": the use of a material is regulated, balancing costs and benefits of the limitations, if there are sound scientific reasons for concern. The third approach is "pessimistic": the use of a material is put on hold until it has been

demonstrated to be safe beyond doubt. Industrial material safety data sheets (MSDS) are an example of the optimistic approach and report nanotubes as “irritating” and “not expected to have environmental hazard” [80]; a pessimistic approach is taken by some environmentalist groups [83], which ask for a temporary moratorium on some branches of nanotechnology research.

The report of the Royal Commission points out the main issues and recommends strategies to manage the risks related to nanomaterials and novel materials. The report recommends the implementation of “early warning systems” and “codes of conduct” to anticipate and mitigate unknown harm. These consist of environmental monitoring, health surveillance of workers and establishment of rules for the safe handling to be put in place by industries and research centres.

To guide through the compilation of such voluntary codes, BSI has published the document [84]: “Nanotechnologies - Part 2: guide to safe handling and disposal of manufactured nanomaterials”. The document does not use the control of substances hazardous to health regulation (COSHH) to assess the risk of nanomaterials, because of the lack of health hazard information and exposure limits; instead all nanomaterials are classified as hazardous “unless sufficient information of the contrary is obtained”. The document also gives the first indications about exposure limits, together with a series of controls and a classification of nanomaterial bearing waste.

Safe handling of CNTs

One of the main reasons for concern in the use of nanotubes is their likeness to asbestos in terms of shape and aspect ratio. Asbestos comprises fibres that enter the human body by inhalation and stay in the lungs for a long time, causing serious illnesses and cancer. There is published evidence of nanotubes interacting with animal lung cells [85] as asbestos fibres do. However, the routes of exposure of human lungs to nanotubes are still disputed [86]. The

health and safety executive (HSE) published an information sheet on the manufacture and manipulation of carbon nanotubes [87]. Carbon nanotubes are defined as "substances of very high concern" and a set of controls is recommended:

- limit the use of dry nanotubes as far as reasonably possible: free particles are potentially more dangerous than liquid or solid suspensions
- prevent particles becoming airborne, e.g. covering the working area with cloths damped with water
- handle in an enclosed or ventilated space equipped with HEPA (High Efficiency Particulate Air) filters
- restrict access to the area to operators only
- use adequate personal protection equipment
- have an emergency procedure in place in case of accident
- use damp cloths to clean-up spillages
- use emergency respiratory protection with an assigned protection factor of 40 or more.

3.2 Unsaturated polyester resins

The resin used in this study is an isophthalic unsaturated polyester resin (UPE). Unsaturated polyesters are thermosetting resins with a relatively low cost, compared to other thermosetting resins. They are utilised for the fabrication of glass reinforced composites, gelcoats, as tooling and as casting resins [88].

The polyester chains are synthesised by condensation polymerisation of a diacid, isophthalic acid in this case, with a glycol [89]; a portion of the diacid is substituted by an unsaturated molecule, e.g. maleic anhydride, to insert unsaturations into the chain (see figure 3.2). The resulting polyester is compounded with a vinyl monomer, e.g. styrene. During cure,

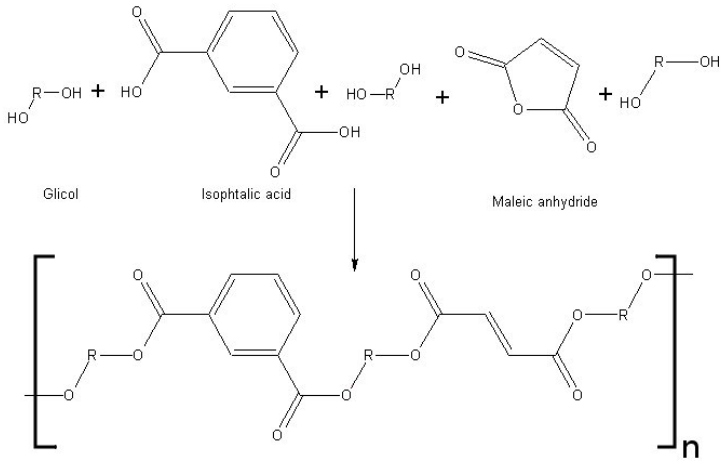

Figure 3.2: Synthesis of unsaturated polyester chains

started by a radical initiator, the unsaturations of the polyester chain cross-link with styrene to create a reticulated molecular structure (see figure 3.3). Small amounts of free radicals can

Figure 3.3: Cross-linking of unsaturated polyester resins

be generated spontaneously during storage; to prevent spontaneous polymerisation, a free radical scavenger is added to the formulation. The hydroquinone shown in figure 3.4 is a typical example of this so-called inhibitor.

The industrial standard procedure for cure [1] is to use an organic peroxide as radical initiator and a catalyst to accelerate the formation of radicals. In this study the former is methyl ethyl ketone peroxide and the latter is cobalt octanoate (see formulae in figure 3.4). The first free radicals produced by the initiator are consumed by the inhibitor rather than starting polymerisation, which results in a delay of few minutes from the addition of the initiator to the onset of polymerisation reaction. A typical cure program starts with cure at ambient temperature for typically a day, during which about 90% of the unsaturated groups cross-link

[1] In industry, the initiator is commonly referred to as “curing agent” or “catalyst” and the catalyst as “accelerator”.

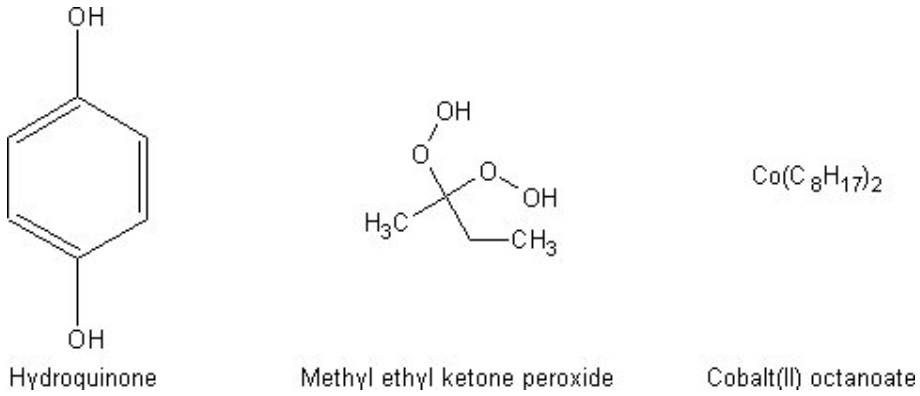

Figure 3.4: Components involved in the cross-linking of unsaturated polyester resins.

[88]. At this stage the reaction stops because of diffusion limitation due to vitrification of the resin. During the postcure phase, the resin is heated above its glass phase transition temperature[2]; because of the increased segmental mobility, the residual unsaturations can cross-link and the reaction reaches completion. Postcure improves all the mechanical properties of the resin, however, not all the industrial applications of unsaturated polyesters require postcure. A typical UPE resin shrinks up to 10 % in volume during cure. In the uncured state the molecules are held together by van deer Waals and hydrogen bonds; during cross-linking the original distance between molecules is reduced by the formation of new covalent bonds, causing the resin to shrink.

[2]typically 3 hours at 80°C

Chapter 4

Experimental techniques

This chapter lists the procedures for the preparation and characterisation of carbon nanotube filled polyester nanocomposites. The first section covers the microscopic techniques for morphological characterisation of the nanotubes and nanocomposites. Section 2 illustrates the processing techniques for the filler dispersion. Section 3 describes the newly developed techniques to monitor the filler dispersion during processing, which are detailed in chapters 6 and 7. Section 4 details procedures used for the cure monitoring of the nanocomposites and section 5 covers the determination of the electrical conductivity of the cured material.

4.1 Morphological characterisation

Optical microscopy

Liquid suspensions of CNTs

The level of dispersion of a carbon nanotube suspension was assessed qualitatively by transmission optical microscopy using a Nikon BH-2 compound microscope. The samples were prepared by placing an amount of mixture m, between 10 and 20 mg, onto a microscope glass slide. The mixture was covered with a cover slip of 16 mm diameter (d). The liquid material was uniformly spread over the whole area under the slip and analysed with objective magnification of x10, x20 or x40. The thickness t of the sample was calculated as:

$$t = \frac{4m}{\rho \pi d^2} \tag{4.1}$$

where ρ is the density of the sample[1]. All micrographs of a series had the same thickness and were acquired using identical sub-stage illumination. Dispersed carbon nanotube suspensions are observed to re-aggregate within a few minutes from sample preparation, as shown in figure 4.1; to limit this effect the micrographs were acquired within five minutes from the preparation of the slide.

Cured nanocomposites

The cured samples for transmission optical microscopy were prepared following two procedures: the glass slides were prepared before or after cure, leading to the samples shown in figure 4.2 and figure 4.3 respectively.

In the first procedure samples of mixture about 50 μm thick were formed and then cured. Twelve milligrammes of the mixture after cobalt and peroxide addition was placed onto a

[1] approximated to the density of the uncured resin of $1.1 \mathrm{g/ml}$

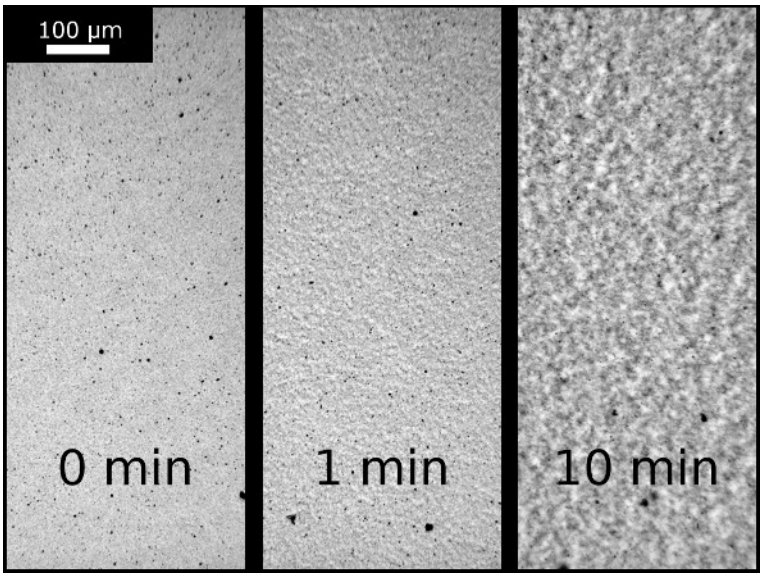

Figure 4.1: Spontaneous re-aggregation of carbon nanotubes in liquid suspension after the preparation of the optical microscopy sample

glass slide and covered with a glass slip. The slides were oven-cured following the same thermal program used for the bulk nanocomposite.

The second procedure was to slice the nanocomposite after curing. To obtain a thickness of 1 μm the sample was sliced with a Reichert-Jung Ultracut E microtome and a 45° glass blade. The blade was lubricated with distilled water to avoid the slices rolling on themselves (see figure 4.3a). To obtain a thickness of about 100 μm the slicing was carried out with a Buehler Isomet precision sectioning saw equipped with a diamond wafering blade. The slices prepared with both techniques were placed directly onto a glass slide for optical microscopy.

Scanning electron microscopy (SEM)

As-prepared nanotubes

Dry carbon nanotubes were prepared for SEM analysis by placing a strip of conductive tape on an aluminium stub and dipping it into the as-prepared nanotubes. The aggregates loosely attached to the tape were removed by tapping the stub on a firm surface. The sample was

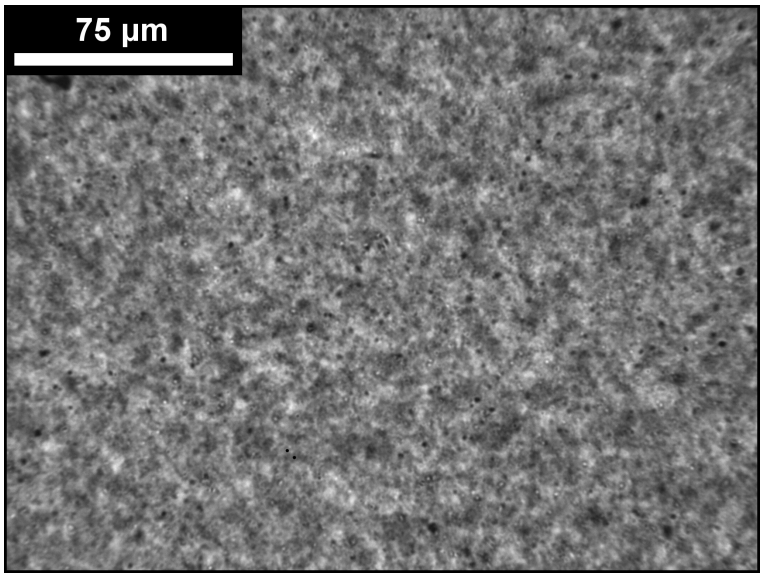

Figure 4.2: Optical micrograph of nanocomposite: $45\mu\mathrm{m}$ sample cured on-the-slide.

then analysed with a SFEG-SEM (FEI XL30) using a through-lens-detector (TLD), working distance 5 mm, acceleration voltage 15 kV and spot size[2] 3.

Cured nanocomposite

Samples of the nanocomposite for SEM analysis were prepared by cryofracture. A specimen with a notch was immersed in liquid nitrogen for five minutes and fractured immediately after. The resulting fragments, with the fractured surface facing up, were glued on an aluminium stub using conductive silver paste (Electrodag® 1415M). A layer of gold about 10 nanometres thick sputtered over the whole stub made the sample conductive to allow imaging. The samples were analysed using TLD at a working distance of 5 mm, spot size between 2 and 3 and acceleration voltage of 20 kV.

[2]diameter of the beam of electrons that scans the sample

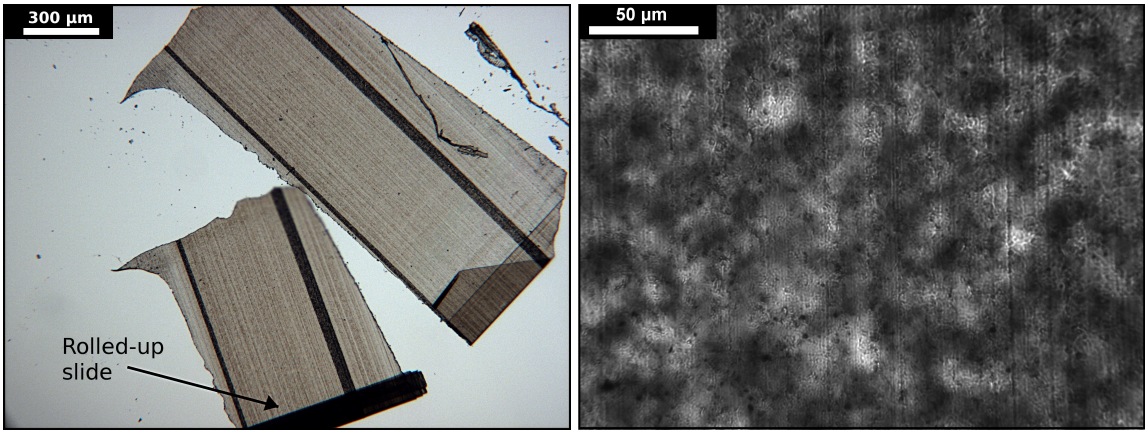

(a) (b)

Figure 4.3: Example of the optical micrographs of cured nanocomposites sliced with different techniques: $1\,\mu\mathrm{m}$ thick microtomed slice (a) and $100\,\mu\mathrm{m}$ thick sectioning saw slice (b).

Transmission electron microscopy

As-prepared nanotubes

About two milligrammes of nanotubes placed in a 50 ml beaker of distilled water were sonicated with an ultrasonic bath at 800 W power, 50 kHz, for 30 seconds. During the sonication a TEM copper grid was repeatedly immersed in the water suspension to collect some of the nanotubes on the grid. After complete water evaporation, the sample was analysed in a Philips CM20 scanning TEM using an acceleration voltage of 120 kV and spot size 1. Images captured on films were developed in-house and electronically acquired at 300 dpi using an HP N8460 scanner and a transparent media adaptor.

Cured nanocomposite

The cured material was microtomed to a thickness of 70 nm using a Reichert-Jung Ultracut E microtome equipped with a 45° diamond blade. The slices mounted on a copper grid were analysed directly at an accelerating voltage of 120 kV and using spot size from 1 to 5.

Charge contrast imaging

Figure 4.4: CNT/UPE sample for SEM contrasting charge imaging. Stub diameter 25 mm.

Samples were prepared by curing the nanocomposite *in situ*: a layer of 100 to 200 μm of the curing mixture was "painted" onto an aluminium stub and oven cured following the temperature program used for the bulk nanocomposite (see figure 4.4). The specimens were analysed with the SFEG-SEM using TLD at a working distance of 4 mm, spot size between 4 and 6 and acceleration voltage of 14 kV.

4.2 Dispersion of carbon nanotubes

Safety notes

These notes describe the main health and safety considerations for the operations described in this section:

- *Dry carbon nanotubes should be considered hazardous materials. Restrict the access to the working area and wear adequate gloves, lab coat and respiratory mask. Damp cloths surrounding the handling area and adequate area ventilation prevent the particles becoming airborne. In case of spillage the nanotubes can be collected with a damp cloth. Procedures for the disposal of the nanotube contaminated waste are available in [84].*

- *Styrene is a flammable, toxic and possible human carcinogenic substance; unsaturated polyester resins contain styrene. Wear a respiratory mask rated for solvent and use adequate ventilation.*
- *There is a risk of mechanical entrapment when operating a triple roll mill. Keep clear of the rotating rolls, maintain the equipment lubricated and ensure that cooling water is circulating while operating.*
- *Horn sonicator produces noise and vibrations. Operate the unit in a suitable sound enclosure and wear hearing protection. Do not touch any oscillating surface.*

Triple roll milling

Figure 4.5: Preparation of nanotube/styrene masterbatch by triple roll milling

Triple roll milling was used to prepare a masterbatch containing about 5 wt% of carbon nanotubes in styrene. The following procedures refer to the preparation of the masterbatch with a triple roll mill with adjustable roller speed and manual gap adjustment, as shown in figure 4.6.

CNTs and styrene were compounded with a mechanical stirrer at 250 RPM for 30 minutes to prepare a suspension at 3.5 wt% loading. The preliminary mixing produces a paste-like

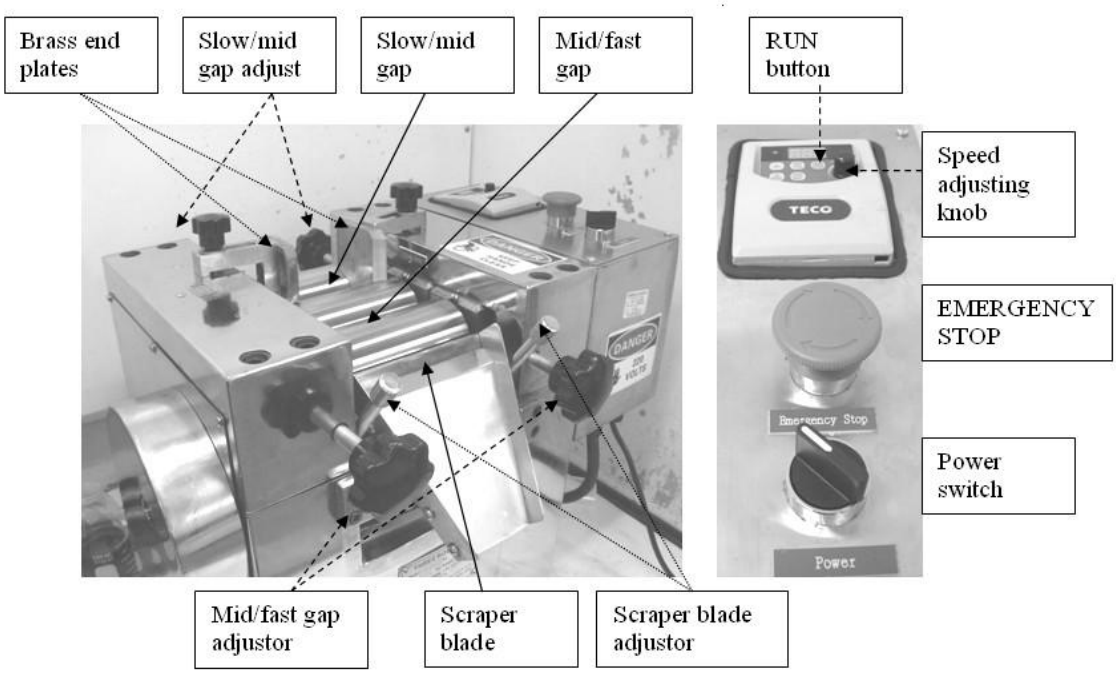

Figure 4.6: Torrey Hill Technology® Lab Model triple roll mill

suspension by breaking the bigger nanotube aggregates. The resulting suspension is then run through the triple roll mill three times. The first run is carried out at 20 rpm and medium roller gaps, to coarsely reduce the agglomerate size. The material is then triple roll milled other two times, increasing the rotational speed to 50 rpm and setting the medium-fast gap to the minimum distance that allows the material to flow. The slow-medium gap must be decreased accordingly to the medium-fast gap, to avoid overloading the faster roller.

Masterbatch loading measure

The rollers are water cooled throughout the production of the masterbatch. However, 25 to 35% of the initial styrene evaporates and brings the CNT loading from the initial 3.5 wt% to about 5 wt%. A gravimetric analysis of the CNT content was used to measure the actual loading of the final masterbatch. A thermo-gravimetric analyser (TGA) would be the instrument of choice. In its absence the measurement was carried out using a DSC cell

and an analytical scale. 20 to 30 milligrams of masterbatch were accurately weighed in a non-hermetic aluminium pan with a pinhole in the lid to allow venting of styrene vapour. The loaded pan was placed in the DSC, using a purging flux of nitrogen of 20 ml/min and a temperature ramp from ambient to 150°C at 5°C/min, where the sample was kept for 20 minutes before cooling. To guarantee complete evaporation the program was repeated until no further evaporation was observed by DSC (an endothermic peak in the heat flow signal). The loading of the masterbatch is calculated as follows:

$$[CNT\%] = \frac{m_{final}}{m_{initial}} \cdot 100 \tag{4.2}$$

The correctness of the measurement can be verified by integrating the overall area of styrene evaporation peaks (H_{peak}) in the heat flow signal and calculating the following:

$$[CNT\%] = \frac{H_{peak}}{MW_{styrene} \cdot \lambda_{MW\,styrene}} \cdot \frac{100}{m_{inital}} \tag{4.3}$$

where $MW_{styrene} = 104.15\,\mathrm{g/mol}$ and $\lambda_{styrene} = 43.5\,\mathrm{kJ/mol}$ are the molecular mass and the enthalpy of evaporation, respectively [90]. The measurement was repeated on at least five samples for each masterbatch, to calculate the 95% confidence interval of the measure. The measurement was rejected when the confidence interval was more than 5% of the average loading measured.

Shear mixing

The dispersion of carbon nanotubes in the resin was carried out by high shear mixing in the lab-scale setup illustrated in figure 4.7. The experimental apparatus comprises an overhang stirrer (Stuart SS10) which rotates a PTFE semicircular paddle at the maximum rate of 2000 rpm in a three-neck flask. Two different flask volumes were used: 100 and 250 ml. The

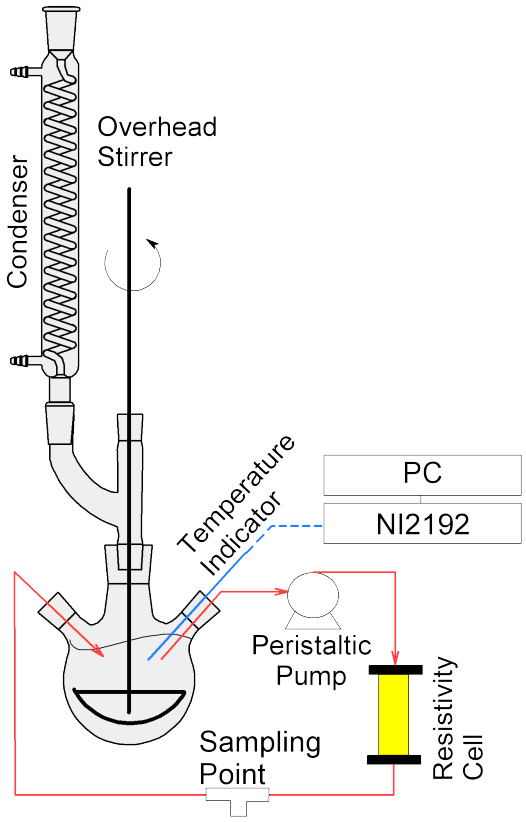

Figure 4.7: Lab-scale setup for the dispersion of carbon nanotubes in unsaturated polyester resins by high shear mixing

temperature was monitored using a type-K thermocouple immersed in the processing mixture and a water condenser was used to limit the amount of styrene evaporating[3]. A Watson Marlow 505S peristaltic pump fed the mixture to the external circulating line. Its operation is described in section *7.2*.

Horn sonication

The horn sonication of the mixture of carbon nanotubes in the resin was carried out using the setup presented in figure 4.8. A flow-through 1/2" titanium ultrasonic horn, connected at the end of the external circulating line and immersed in the processing mixture, was used to disperse the filler. The horn and the temperature probe were controlled by a Branson S-

[3]Vapour pressure of styrene at 305.5K is 0.013 bar

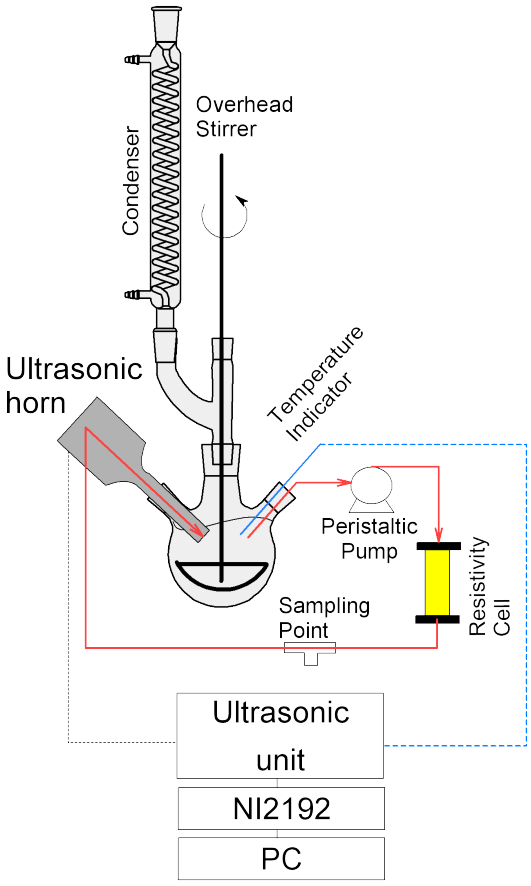

Figure 4.8: Lab-scale setup for the dispersion of carbon nanotubes in unsaturated polyester resins by horn sonication

450D Digital Sonifier®. The sonicator was operated "max temperature mode", which consist in sonicating the mixture until temperature reaches a setpoint of 51°C and suspending the sonication until temperature drops 3°C below the setpoint. The overhang stirrer was set at a rotational speed of 250 rpm. The external line was fed by a Watson Marlow 505S peristaltic pump equipped with a double-Y 1/8" silicon peristaltic pipe and rotating at the constant speed of 55 rpm, which corresponds to a flow of 10 ml/min. The ultrasonic unit was connected to a NI9219 analog-digital converter to log temperature, sonication amplitude, power and energy during processing. The sonication was stopped after a chosen level of energy (e.g. 1.5 kJ/g of mixture) had been delivered to the mixture.

4.3 Dispersion monitoring

Rheological analysis

The rheology of the material was used to monitor the level of dispersion and to compare different preparations. The measurement was carried out during processing by sampling the mixture from the sampling point of figures 4.7 and 4.8 and loading 1.35 grams of mixture onto a CVO10 rheometer. A Peltier plate kept at a constant temperature of 25°C was used and the sample was analysed as follows: cone-and-plate 4°/40 geometry, equilibration for 60 seconds, pre-shear at 100 s^{-1} for 60 seconds, equilibration for 60 seconds and then measurement of the viscosity on a shear rate scan from 0.07 to 100 s^{-1}, nine points per decade on a logarithmic scale, with a delay time of 5 seconds.

Measurement of liquid electrical resistivity

The resistance of the uncured material during mixing or sonication processing was measured with a specially designed sensor, as shown in figure 4.9. Detailed drawing of the components are given in appendix A.1.

The sensing setup comprises two copper concentric electrodes maintained in position by insulating inserts that allow the flow of the liquid suspension. The internal and external diameters of the outer electrode are $d_i = 8\mathrm{mm}$ and $d_o = 10\mathrm{mm}$, respectively; the diameter of the inner electrode is $d = 3\mathrm{mm}$ and the length of the electrodes is $L = 20\mathrm{mm}$. A type-K thermocouple inserted at a central location measures the temperature of the material entering the cell. Two silicon o-rings and four nylon studdings close the assembly to guarantee a leak-free fit. During processing a Watson Marlow 505S peristaltic pump feeds a constant stream of liquid mixture, coming from the flask containing the mixed material, to the cell. The output stream from the cell is fed back to the flask to return the liquid mixture.

The value of electrical conductivity is measured using a precision DC current source and

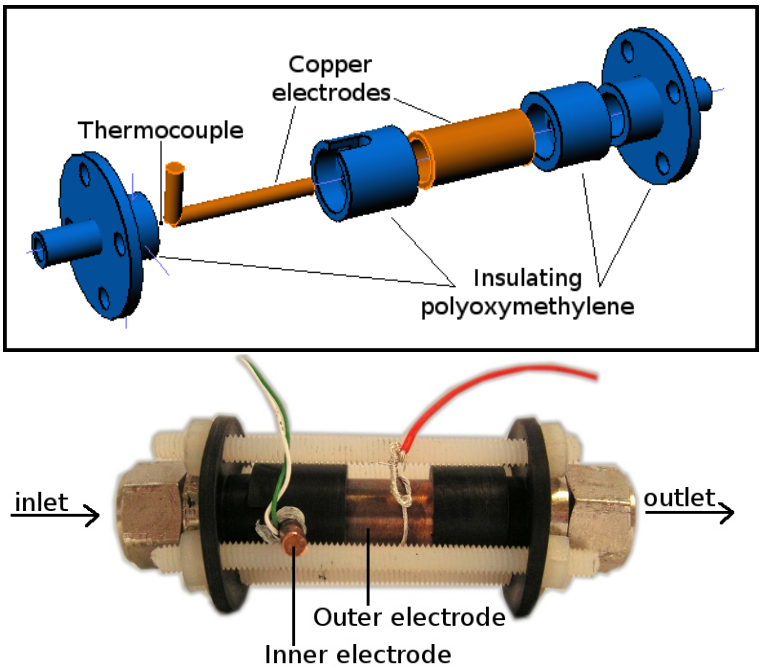

Figure 4.9: Sensor for the on-line measure of resistivity of liquid mixtures during processing

a nanovoltmeter (Keithley 6220 and 2182A, respectively). Labview software controls the two instruments and thermocouple, acquiring a resistance reading and corresponding temperature reading every 2 seconds.

The value of resistance is measured using the delta current reversal technique in order to avoid measurement bias due to thermoelectric effects [91]. This technique consists of applying a current I^+ to the sample for a predefined delay time before taking a voltage reading and calculate $R^+ = V^+/I^+$. The direction of the current is reversed and a second voltage reading is taken to calculate $R^- = V^-/I^-$. The resistance of the sample R is calculated as the average of R^+ and R^-. The maximum value of resistance that is possible to measure with this technique (R_{max}) has been found to strongly correlate with the delay time t_d, following the empirical correlation:

$$R_{max} \approx 2.5 \cdot 10^8 \, \Omega \mathrm{s}^{-1} \cdot t_d \tag{4.4}$$

The data of each section of the thermal cycle, ascending or descending, are used to cal-

culate the parameters of the following temperature-resistance relation [92]:

$$R = R_0 \exp\left(-\beta\left(\frac{1}{T} - \frac{1}{T_0}\right)\right) \tag{4.5}$$

where R is the resistance measured at temperature T (in K), R_0 is the resistance at a reference temperature T_0 and β is a coefficient. The conductivity of the liquid mixture σ_0 is calculated using the value of R_0 calculated at the reference temperature of 300 K as follows:

$$\sigma_0 = \frac{\ln\left(\frac{d_i}{d}\right)}{2\pi L R_0} \tag{4.6}$$

Fitting of data by equation 4.5 was carried out using the VBA for Excel subroutine reported in appendix A.2.

4.4 Cure monitoring

DSC

The degree of conversion of the cross-liking reaction was measured by differential scanning calorimetry using a DSC2920 (TA instruments®). The uncured resin or the uncured nanocomposite was mixed with initiator and catalyst. About 5 mg of such mixture were accurately weighed in an aluminium pan. The pan was placed in the DSC cell and analysed using the cure temperature program of the corresponding nanocomposite (see section 3.2). If the curing program do not include a postcure phase, an isotherm of three hours at 120°C was added at the end of such program. The post-processing of the experimental data was carried out using TA Data Analysis software. The area resulting from the integration of the exothermic peaks

of the heat flow signal was used to calculate the degree of conversion χ at a certain time t as:

$$\chi(t) = \frac{\int_0^t dH_R}{\int_0^\infty dH_R} \tag{4.7}$$

assuming the completion of reaction after three hours at 120°C ($t = \infty$).

Impedance spectroscopy

Dielectric spectroscopy has been used in this study to monitor the evolution of the conductive network of the nanotubes during cure. The sensor (GIA sensors, Pearson Panke) used to measure the ac response of the composites during cure is shown in figure 4.10.

Impedance measurements were performed using a Solartron SI 1260 frequency response analyser. The instrument communicated with a computer via an IEEE-USB interface. The commercial dielectric sensors used comprise an assembly of interdigitated copper electrodes, printed with a spacing of 200 μm on a thin polymeric film. The sensor was immersed in a glass tube containing the liquid resin and the glass tube was placed in a hollow copper cylinder, surrounded by heating elements controlled by a Eurotherm 2408 temperature controller. A control thermocouple (Type K) was placed in an opening on the wall of the hollow cylinder. A second thermocouple was placed in the glass tube in order to record the actual thermal profile followed by the resin. Typical measurements were performed in the frequency range between 1 Hz and 10 MHz, measuring five frequencies per decade on a logarithmic scale.

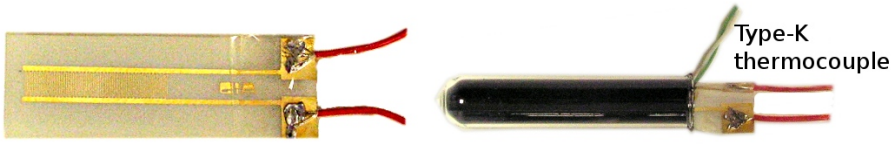

Figure 4.10: Dielectric sensor (left) and its positioning in the curing sample (right)

Time interpolation of impedance data

Each frequency sweep takes 3 minutes and 20 seconds to scan from 10^7 to $1\,\mathrm{Hz}$. The time lapse implies that fast changing phenomena can negatively affect the quality of the results. In order to mitigate this effect, the data for each spectrum were synchronised by interpolation of the R and C values as follows:

$$\bar{t} = \frac{t_{1,k} + t_{n,k}}{2} \tag{4.8}$$

$$\bar{R}_i = \frac{R_{i,k}\left(t_{i,k+1} - \bar{t}\right) + R_{i,k+1}\left(\bar{t} - t_{i,k}\right)}{t_{i,k+1} - t_{i,k}} \tag{4.9}$$

$$\bar{C}_i = \frac{C_{i,k}\left(t_{i,k+1} - \bar{t}\right) + C_{i,k+1}\left(\bar{t} - t_{i,k}\right)}{t_{i,k+1} - t_{i,k}} \tag{4.10}$$

where t is the time and i denotes the frequency of the measurement; $i = 1$ is the first and n the last point of the sweep; k denotes the consecutive number of a sweep. The interpolation was carried out using the VBA for Excel subroutine reported in appendix A.3.

Genetic algorithm fitting

Equivalent circuit modelling has been used for the interpretation of experimental impedance data. The circuit of figure 4.11 is described in terms of impedance as follows:

$$\begin{aligned} Z^*(\omega) &= Z'(\omega) - jZ''(\omega) \\ Z'(\omega) &= \frac{R_b}{1 + \left(\omega C_b R_b\right)^2} + \frac{R_i}{1 + \left(\omega C_i R_i\right)^2} \\ Z''(\omega) &= \frac{\omega C_b R_b^2}{1 + \left(\omega C_b R_b\right)^2} + \frac{\omega C_i R_i^2}{1 + \left(\omega C_i R_i\right)^2} \end{aligned} \tag{4.11}$$

Here Z^* denotes the complex impedance of the circuit, Z' and Z'' are the real and imaginary part of impedance respectively. C_b and R_b denote the capacitance and resistance of

the bulk material, C_i and R_i are the capacitance and resistance of the interfaces, and ω is the angular frequency.

The four parameters of the equivalent circuit model are estimated for each set spectrum during the cure of the nanocomposite using a genetic algorithm technique (see section 2.6). The settings of the genetic algorithm used in this study are listed in table 4.1. The VBA for Excel code[4] used for the search is listed in appendix A.4.

Table 4.1: Parameters of the genetic algorithm used for the estimation of equivalent circuit parameters

Binary string length	164 digits
Number of individuals	199
Number of generations	100
Selection operator	roulette wheel
Mutation probability	0.05

The estimation is performed using genetic algorithm to minimise the following objective for each frequency sweep:

$$S\left(R_b, C_b, R_i, C_i\right) = \sum_{i=1}^{n} \frac{\left|\overline{Z}\left(\omega_i\right) - Z\left(\omega_i\right)\right|^2}{\left|\overline{Z}\left(\omega_i\right)\right|^2}\ ,\ \tau_b \leq \tau_i \tag{4.12}$$

Here $\overline{Z}$ and Z denote the experimental and model impedance respectively, ω_i the frequency of measurement i. An additional constraint is used to ensure that the objective function is defined only when the characteristic time corresponding to the bulk sub-circuit ($\tau_b = R_b C_b$) is less than the characteristic time of the interfaces sub-circuit ($\tau_i = R_i C_i$). The introduction of this constraint remedies problems related to the non-uniqueness of solution caused by the use of two identical sub-circuits in the equivalent circuit model. Solutions that are significantly different (more than 20% in impedance terms) from the previous step are rejected. The estimation is then repeated until a solution within the acceptable limits is

[4]adapted from a code described in [77]

found or for a maximum of 50 repetitions. The assumptions underlying this treatment are that values of the parameters obtained in the previous sweep are good a priori estimates for the inverse solution in the current step and that interfacial relaxation occurs at relatively low frequencies.

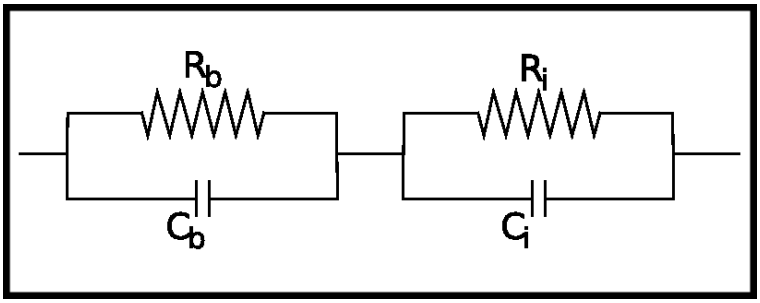

Figure 4.11: Equivalent circuit for the fitting of the impedance spectrum of a CNT nanocomposite

Figure 4.12 shows an example of an impedance spectra fitted with the model of equation 4.11 using the genetic algorithm.

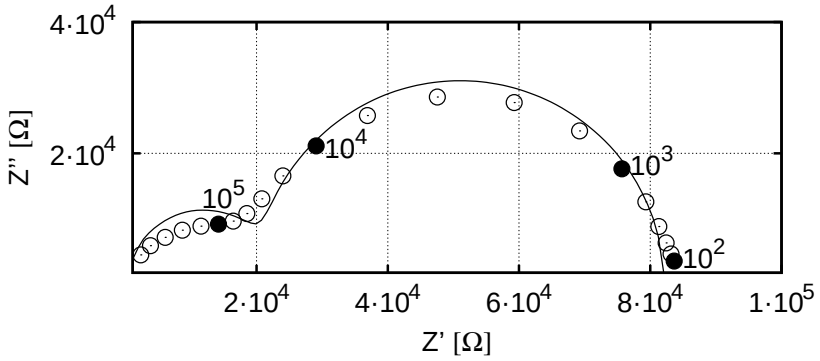

Figure 4.12: Comparison of experimental (circles) and model (solid line) impedance of an impedance spectra

4.5 Measurement of the electrical properties of cured materials

The DC electrical properties of the cured resin and nanocomposites were determined by a two-point contact measurement. The two parallel faces of a 4 mm thick cylinder of cured material of 8 mm diameter were painted with a suspension of silver in methyl isobutyl ketone (Acheson Electrodag® 1415M), as shown in figure 4.13. After complete evaporation of the

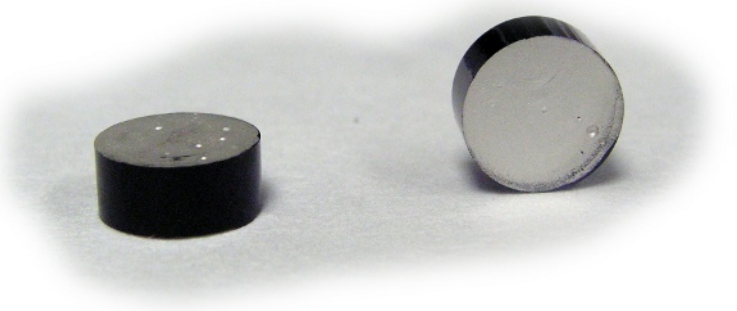

Figure 4.13: Samples used for the determination of DC resistivity

solvent the value of resistance was measured at 20°C. The neat resin, which has a conductivity below $10^{-8}\,\mathrm{S/m}$, was characterised using a Keithley® electrometer model 6517A. The nanocomposites, which have conductivity above $10^{-8}\,\mathrm{S/m}$, were characterised with a combination of a DC precision current source (Keithley® 6220) and a nanovoltmeter (Keithley® 2182A) using the three-point delta current reversal technique described in section 4.3. The volume resistivity ρ and conductivity σ of the sample were calculated as follows:

$$\rho = R \cdot \frac{\pi d^2}{4t} \tag{4.13}$$

$$\sigma = \frac{1}{\rho} \tag{4.14}$$

Chapter 5

Micrographic characterisation of carbon nanotubes and thermosetting nano-composites

This chapter covers the microscopical characterisation of the materials used and prepared in this study; it also includes an account of the advantages and the limitations of the different techniques used. Sections 1 and 2 cover the characterisation of the as-grown nanotubes and of the nanocomposite, respectively. Section 3 is a critical overview of how the information provided by single characterisation techniques is combined to address the specific aspects of the preparation of a conductive nanocomposite.

5.1 As-received CNT

Figure 5.1 shows SEM micrographs of as-grown nanotubes at x1000 and x10000 magnifications. The NC7000 carbon nanotubes present a characteristic morphology: the micron-sized

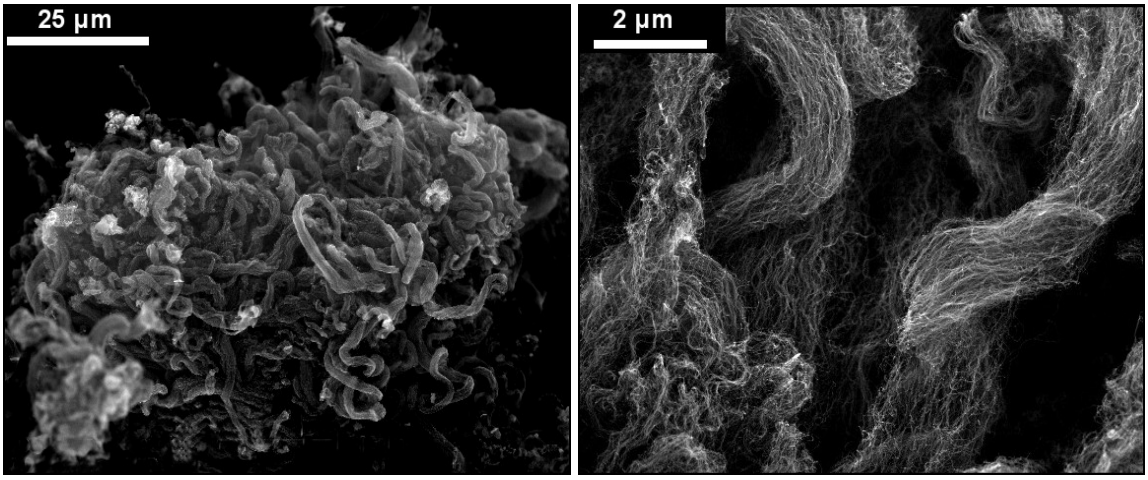

(a) **(b)**

Figure 5.1: SEM micrographs of as-prepared uncoated nanotubes

clusters of about 100 μm, such as the one illustrated in 5.1a, are assemblies of rope-like aggregates of nanotubes. Each of these elongated rope-like aggregates appear longer than ten micrometres and about 2 μm thick. Figure 5.1b shows the internal structure of the aggregates, which comprise thousands of nanotubes grown in the same direction. Although the superstructure is directional, the nanotubes forming the rope-like aggregates are wavy and entangled. TEM imaging of the as-grown nanotubes is presented in figure 5.2. At this level of magnification the waviness and entanglement of the nanotubes are clearly visible.

Precise measuring by SEM of the CNT diameter requires resolution and magnification higher than the limits of the instrument used in this study. This has not therefore been carried out. In the entangled state shown in SEM and TEM micrographs it is difficult to find the extremities of a nanotube to measure the particle length. The contrast and resolution of TEM micrographs allows image analysis to measure the diameter of the nanotubes: 11.2$\pm$0.6 nm.

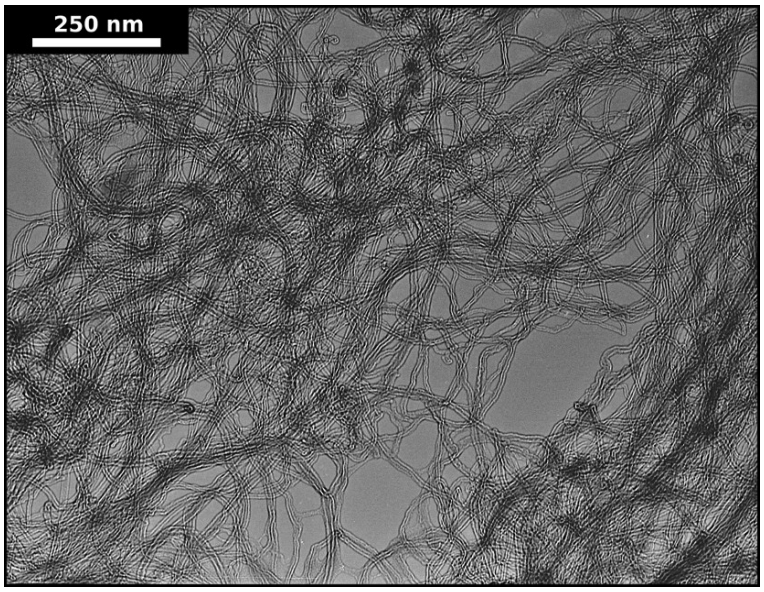

Figure 5.2: TEM of as-received NC7000 nanotubes

Longer sonication time in the preparation of the TEM sample may result in less dense assemblies of nanotubes and facilitate the measure of the CNT length. However, this has not been done because long sonication times are likely to damage and break the nanotubes, as reported in [48]. The declared values of diameter and length have been used for the calculations carried out in this study.

5.2 CNT nanocomposites

Optical microscopy

Liquid suspensions

The transmission optical microscopy observation of liquid suspensions, of the evolution of dispersion by triple roll milling and high shear mixing at 1000 rpm is presented in figure 5.3. The dispersion of the filler in the host resin is indicated by the decrease of aggregate size and by darker micrographs, due to lower overall light transmission through the samples.

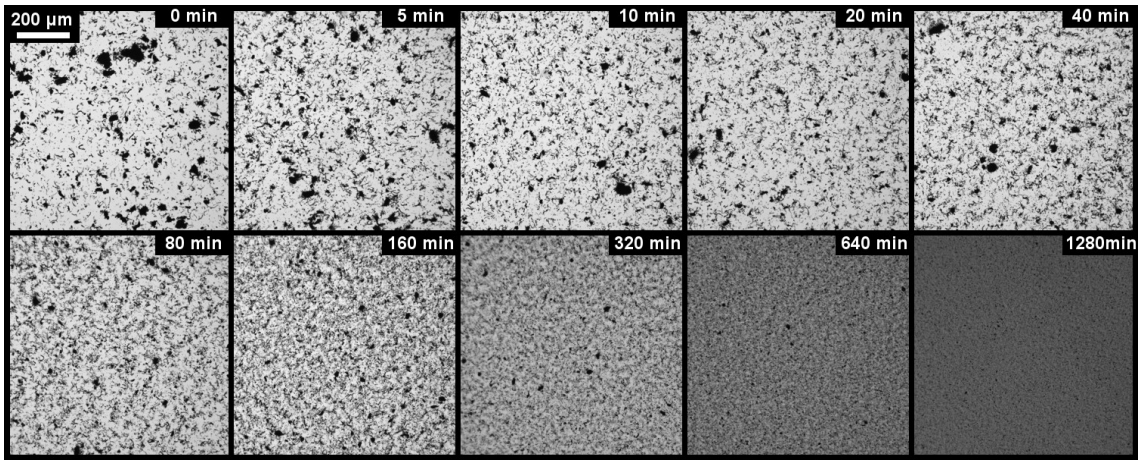

(a)

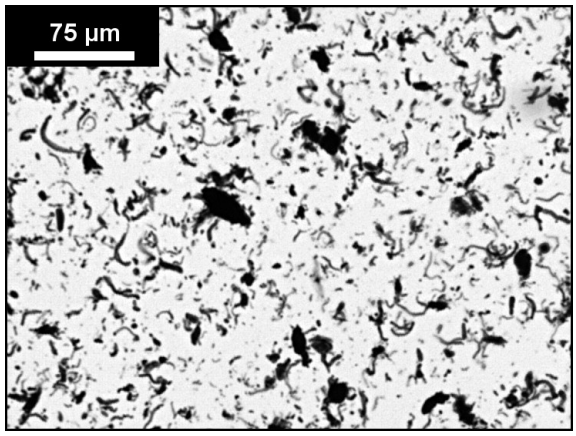

(b)

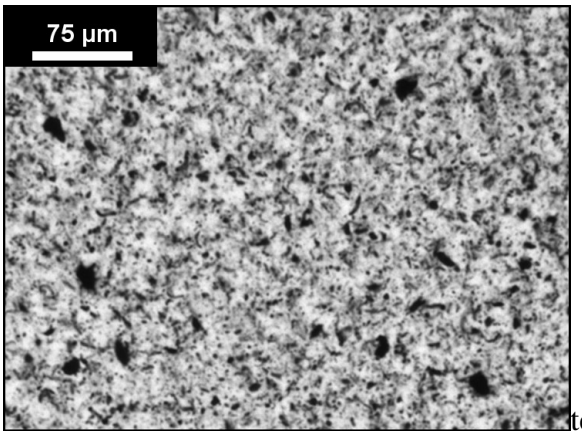

(c)

temperature

Figure 5.3: Optical microscopy of NC7000/UPE mixtures in the liquid state, at increasing high shear mixing processing time. Detail of the micrographs after 10 minutes (c) and after 320 minutes (d). CNT loading 0.10 wt%, specimens thickness 45$\pm$5 μm.

Figure 5.3b shows the state of dispersion at the beginning of the process, where two types of CNT structures are observed: aggregates in the order of tens of micrometres in more than one dimension, which correspond to the clusters of figure 5.1a, and smaller, elongated structures about 10 μm long and few micrometres thick, corresponding to the rope-like aggregates of figure 5.1b. Clusters and agglomerates are surrounded by clear resin. Figure 5.3c shows the state of dispersion after 320 minutes of high shear mixing: less than ten big clusters and rope-like aggregates are still visible, but the rope-like aggregates are shorter than at the

beginning of the process. The surrounding matrix is "cloudy", suggesting the presence of individual nanotubes suspended in the resin that decrease the amount of light passing through the sample.

Cured nanocomposites

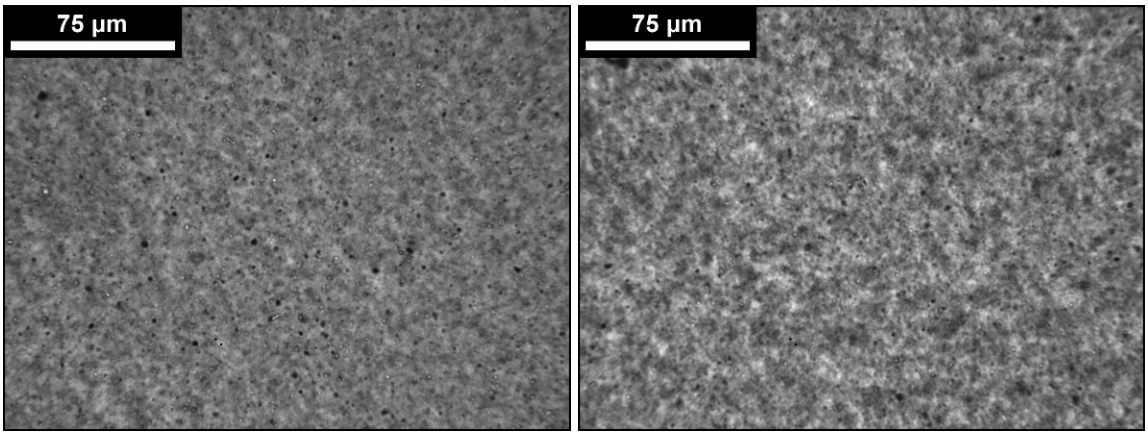

Figure 5.4: Optical microscopy of nanocomposite before (a) and after (b) cure. Preparation of the cured sample on the glass slide was followed by oven cure (see section 4.1). CNT loading 0.125 wt%, shear mixing dispersion, specimen thickness $45\pm5\ \mu m$.

The optical micrographs of the state of dispersion of a nanocomposite before and after cure are compared in figure 5.4. A more inhomogeneous pattern is observed for the cured sample, when compared to the uncured sample. This suggests that re-aggregation of individually dispersed particles happens during cure. The spontaneous re-aggregation of carbon nanotubes has been observed in a non-curing mixture, as shown in figure 4.1. A comparison with the few original aggregates of CNTs still present suggests that the structures form as a consequence of the electrostatic attraction between initially separated nanotubes, resulting in somewhat loosely packed aggregates of carbon nanotubes.

Scanning electron microscopy

Figure 5.5a shows the SEM micrograph of a NC7000/UPE composite. The appearance of the fracture surface is non uniform and fragmented. The formation of an irregular surface makes the visualisation of the CNT aggregates difficult and limits the effectiveness of SEM for the characterisation of this specific system. Higher magnification imaging, as the one

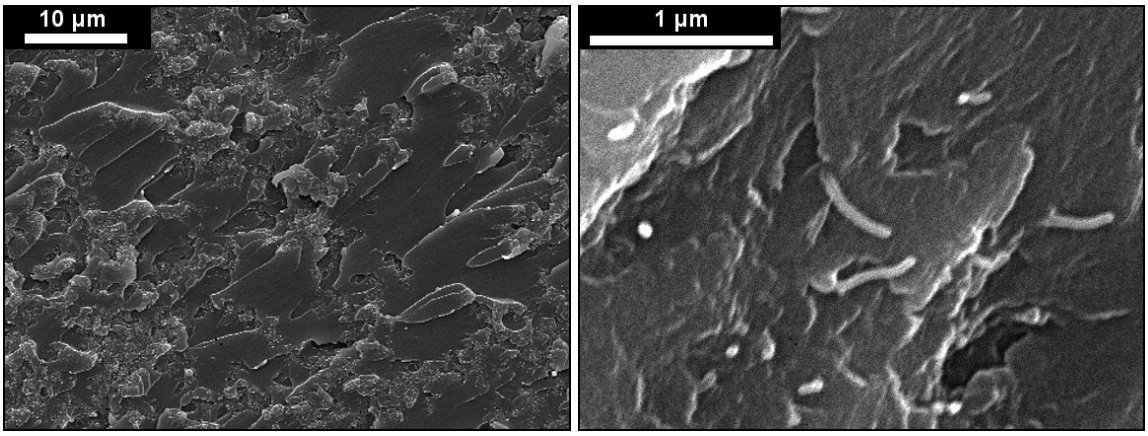

(a) **(b)**

Figure 5.5: SEM micrographs of 0.25 wt% CNT nanocomposite prepared by horn sonication.

shown in figure 5.5, reveals the presence of individual nanotubes partially sticking out of the surface. These individual nanotubes confirm the achievement of dispersion at the nano-level, as suggested by optical microscopy observations.

Transmission electron microscopy

Figure 5.6 shows the TEM micrographs of a nanocomposite. The images have lower contrast than the image of the as-received nanotubes of figure 5.2, due to the presence of the polymeric matrix surrounding the filler particles. The poor contrast and the characteristic of the microscope used affect the quality of the micrographs obtained. Only a small portion of the micrographs obtained was useful for characterising morphology and distribution of the nanotubes. The area covered in the figure presented here is 0.26 μm^2. Few long and several

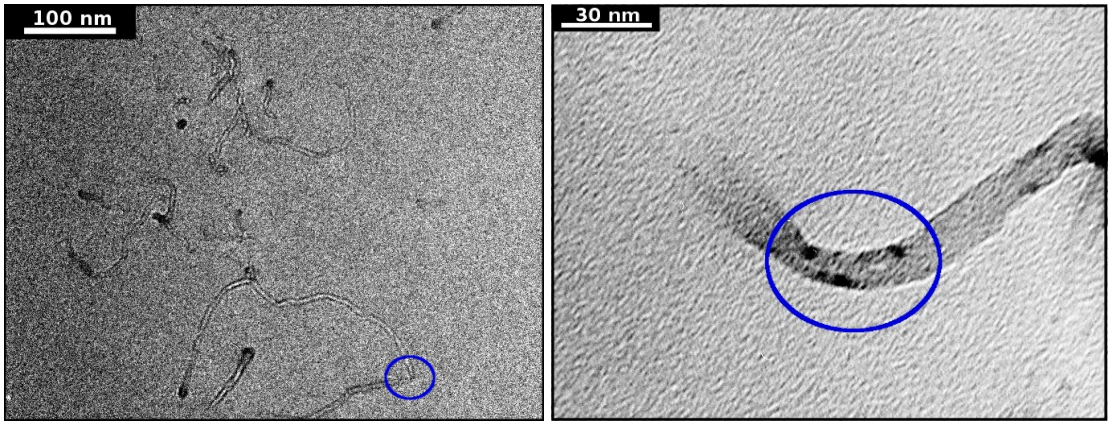

(a) **(b)**

Figure 5.6: TEM micrograph of 0.25 wt% CNT nanocomposite prepared by horn sonication, magnification (a) x125 000 and (b) x450 000. The circles denote possible points of buckling.

short nanotubes or fragments of nanotubes are visible in the lower magnification micrograph of figure 5.6a.

The average particle length observed is in the order of few hundreds of nanometres, considerably smaller than the 1.5 μm declared by the producer. This length reduction is attributed to the preparation of the specimen by ultramicrotomy and therefore is not indicative of length reduction by processing: the nanotubes sitting entirely within an 80 nm thick slice are visible as a whole, but the nanotubes crossing between are cut into shorter fragments. The diameter, measured by image analysis of the image shown, was 7.7$\pm$0.8 nm. However, the contours of the nanotubes are weakly contrasted and only a few nanotubes can be measured, adding uncertainty to the measurement. This can explain the difference with the diameter value observed in figure 5.2. Defects in the CNT structure have been observed, such as the possible buckling indicated by a circle in figures 5.6a and b.

Charge contrast imaging

Charge contrast imaging is a technique for the imaging of the nanotubes embedded in a nanocomposite [93]. An example of the results obtained in this study is shown in figure 5.7. The

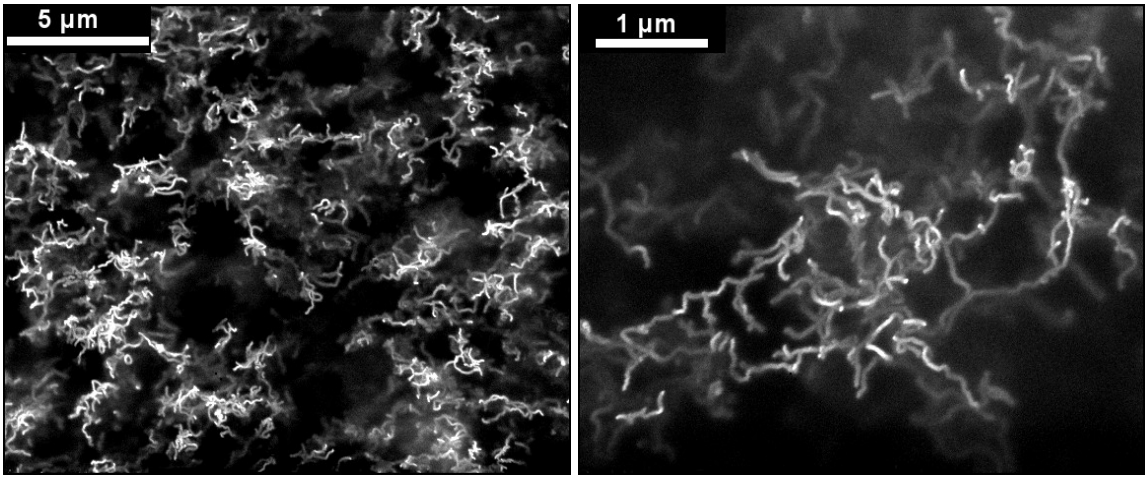

(a) **(b)**

Figure 5.7: Charge contrast imaging of unsaturated polyester nanocomposite. CNT loading 0.10 wt%, dispersion by shear mixing.

dispersion at the micro-scale is illustrated by the low magnification micrograph of figure 5.7a: the distribution of the nanotubes is not uniform, with agglomerates forming spatial structures of a few micrometres. The boundaries between agglomerates are not clearly defined, indicating a network of carbon nanotubes formed by interconnected aggregates. Nanotube-rich aggregates and resin-rich areas among them are considerably different in brightness. High magnification micrographs, such as the one presented in figure 5.7b, reveal the arrangement of the nanotubes in the cured nanocomposite. The aggregates are assemblies of loose nanotubes suspended in the resin matrix. The nanotubes appear to be more wavy than in the as-grown state characterised by SEM and TEM in figures 5.1b and 5.2. A precise assessment of the dimensions of each individual particle is not possible, but the tube length can be estimated to exceed 1 μm. This value, which is in good agreement with the length of 1.5 μm declared by the producer, suggests little or no reduction of the particle length during processing. The charging phenomena that are the basis of the imaging result in "swelling" of the appearance of nanotubes by several nanometres, precluding a precise measurement of the particle diameter using charge contrast imaging.

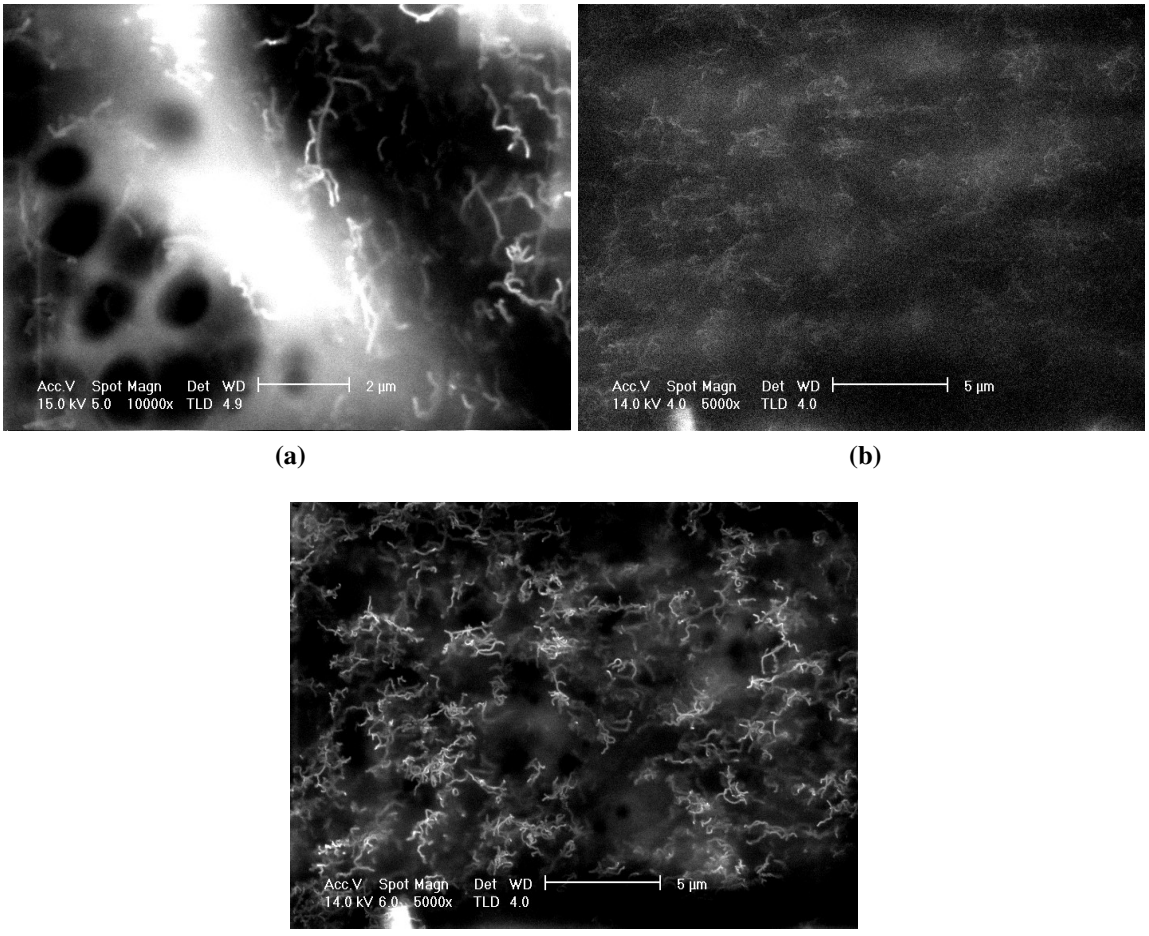

(a) **(b)**

(c)

Figure 5.8: Effect of spot size adjusting on charge contrast imaging of CNT/UPE composites: sample damage (a) and comparison of imaging at spot size 4 (b) and 6 (c) of the same sample area.

Excessive electron doses can damage the area under investigation, as shown in figure 5.8a, especially at high magnification and with samples with low intrinsic material conductivity. The damage can be avoided using smaller spot size, which leads to higher definition but lower nanotube-resin contrast, as the comparison of figures 5.8b and c illustrates. The spot size at each magnification level was adjusted to find the best combination of contrast and definition without damaging to the sample. A minimum electrical conductivity above $10^{-3}\,\mathrm{S/m}$ is needed to have the characteristic sample charging that allows imaging; nanocomposites with

conductivity below this level result in micrographs as the one shown in figure 5.9, where overall sample charging interferes with the charge contrast imaging.

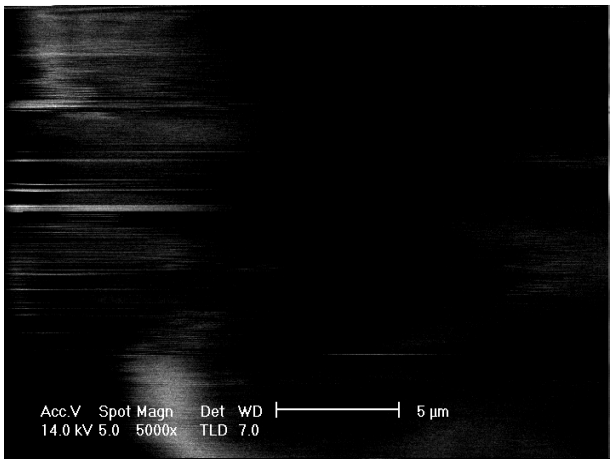

Figure 5.9: Example of overall sample charging affecting the quality of the charge contrast imaging of a composite with conductivity $10^{-3}\mathrm{S/m}$, CNT loading 0.075 wt%.

5.3 Discussion

The length of the CNT observed by charge contrast imaging is consistent with the value declared by the producer, suggesting that the aspect ratio of the nanotubes is not reduced by the particular processes of dispersion adopted (see section 4.2). There is evidence of CNT damage from processing, such as the buckling shown in figure 5.6b, the high CNT waviness shown in figures 5.6a and 5.7 and the diameter reduction measured from TEM micrographs. However, the reliability of these observation is limited by their qualitative character and by technical difficulties, such as the low contrast of TEM imaging of the nanocomposite. Confirmation of the hypothesis of damage [28] would require further investigations based on high resolution microscopy such as HR-TEM.

The dispersion of the filler particles in the matrix, monitored via optical transmission microscopy, illustrates the mechanism of dispersion during processing. The dimension of the residual aggregates of nanotubes and the amount of optical light transmitted from the sample

provides information on the dispersion quality of a mixture. Processing by shear mixing takes 1280 minutes to reach the so-called 'optically dispersed' level of dispersion (see section 2.3). The carbon nanotubes, which are initially present as sub-millimetric clusters, are broken into rope-like aggregates; subsequently, these rope-like structures de-aggregate to form the individually suspended nanotubes. The hierarchical evolution of dispersion echoes the structures of the as-prepared nanotubes. It can be inferred that the structure of the dry nanotubes affects the mechanism of dispersion and should be taken into account in the selection of the nanocomposite processing route. SEM and TEM characterisation, used to visualise individual carbon nanotubes embedded in the resin matrix, confirm dispersion at the nano-level.

The irregular surface obtained by cryofracture limits the ability of SEM characterisation of CNT/UPE nanocomposites to visualise the structures of nanotubes formed curing cure, as previously reported for CNT/epoxy systems [30, 31]. SEM characterisation using the charge contrast imaging technique has been used to study the morphology of the filler at the micro and nano-level. As suggested by the comparison of optical micrographs of the cured and uncured material, after cure the filler particles form loose structures of re-aggregated CNTs, such as the one illustrated in figure 5.7b. These spatial structures of re-aggregated carbon nanotubes are interconnected, forming the complex structure of CNT-rich aggregates and resin-rich interphase shown in figure 5.7a. The network of carbon nanotubes, which extends throughout the whole nanocomposite, is the physical entity responsible for the conduction of electrons in the nanocomposite.

Chapter 6

Monitoring dispersion of carbon nanotubes in a thermosetting polyester resin

This chapter[1] concerns the initial steps in the preparation of carbon nanotube containing nanocomposites of an isophthalic unsaturated polyester resin, prior to cure. The rheological behaviour of the liquid samples was monitored as a function of the level of energy introduced via ultrasonic horn mixing and was related to microscopic observations. Online sampling is coupled with off-line viscosity measurements. These are compared with online measurements of electrical resistivity of the mixture, in terms of the relative suitability of these techniques for real-time monitoring of nanofiller dispersion in the liquid mixtures. The shear thinning parameter, N, derived from fitting Carreau's model to the shear dependent viscosity data, appears to provide a good quantitative indicator of the state of nanotube dispersion in the sample.

[1] adapted from [94]

6.1 Materials and Methods

Sample preparation

The thermosetting polyester matrix was an isophthalic unsaturated polyester resin with a styrene content of 30 wt%, produced by Scott Bader Co. Ltd. The resin was modified by the addition of 0.25 wt % of multiwalled carbon nanotubes (MWCNTs) (Nanocyl®7000).

The liquid CNT/resin pre-polymer mixtures were prepared by triple roll milling and horn sonication, using the setup illustrated in figure 4.8. Experiments were performed using a 150 ml flask, setting the overhang stirrer at 250 rpm and using 20, 55 and 100 W ultrasonication power input levels. The treatment duration was adjusted to reach a set amount of energy input, namely 1.5 kJ/g of mixture. It should be noted that the power and energy input refer to that delivered by the ultrasonic horn rather than to the actual amount absorbed by the liquid nanocomposite. As the geometry and boundary conditions of the system are identical in all experiments, and the specific heat capacities of the materials investigated also do not vary widely, it is assumed that the ratio of energy absorbed to energy delivered remains relatively constant [47].

Sampling and Rheology analysis

During the sonication process samples were collected for rheological measurements. A Bohlin CVO rheometer with 4°/40 mm cone and plate geometry was used in steady shear mode, at 25°C, and with a sample size of 1.35 ± 0.01 g of material. After 2 minutes of 100 s^{-1} pre-shear and 1 minute of stabilisation, a scan of viscosity against shear rate was performed, from 0.1 to 100 s^{-1}. The relationship between the shear rate and the viscosity was fitted using the general Carreau viscosity model [95–97],

$$\eta = \eta_\infty + (\eta_0 - \eta_\infty)\left(1 + \lambda^2\gamma^2\right)^{-N} \tag{6.1}$$

Here λ denotes a relaxation time, and N a shear thinning exponent. Both are fitting parameters that describe the relationship between the viscosity η of the pre-polymer and the shear rate γ. η_0 and η_∞ are the limiting viscosities, at very low and at very high shear rates respectively.

The fitting was performed using a least-squares method with the generalized reduced gradient method implemented in Microsoft Excel [98].

Liquid electrical resistivity measurements

The electrical resistivity of the liquid sample was measured online, following the procedure described in section 4.3. The resistivity of the sample was given by:

$$\rho = \frac{2\pi L R_0}{\ln\left(\frac{r_0}{r_i}\right)} \tag{6.2}$$

Here R_0 is the corrected resistance, L denotes the sensing length (20 mm), r_0 is the internal radius of the outer cylinder (4mm) , and r_i the radius of the inner rod (1.5mm).

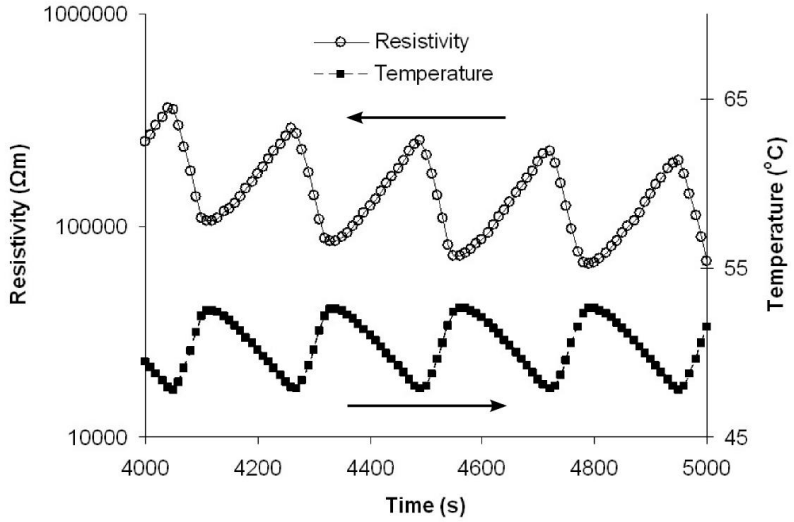

Figure 6.1: Temperature and resistivity profile during sonication

A typical thermal profile during ultrasonication is shown in figure 6.1, alongside the corresponding resistivity measurements. As the resistivity is highly sensitive to the instantaneous temperature, a correction was introduced to remove the effect of temperature changes using equation 4.5. The reference temperature, chosen within the window of varition of temperature (see figure 6.1), was 51°C.

6.2 Results and Discussion

Evolution of Rheological parameters: off-line measurements

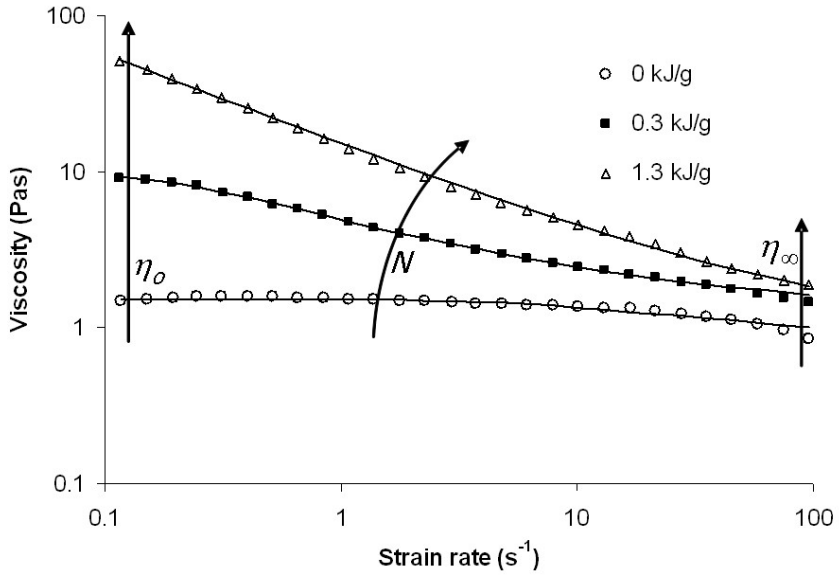

Figure 6.2: Viscosity as a function of strain rate at various ultrasonication energies during the treatment at 55 W

Figure 6.2 is a plot of the shear viscosity of the CNT/polyester pre-polymer mixture, against strain rate in the 0.1 to 100 s^{-1} range. Representative plots are presented for samples that have undergone horn sonication at 55 W to total energy input levels of 0.3 and 1.3 kJ/g (specific

energy referred to a gram of sample mixture) and these are compared with a hand-mixed control sample. Referring to the parameters of the Carreau model (eq. 1), the absolute values of the low shear rate viscosity, the high shear rate viscosity and the shear thinning parameter all increase across the entire measurement frequency range as more sonication energy is delivered to the system. The change in the shear thinning nature of the liquid mixtures is the most pronounced, with N increasing from 0.0046 to 0.207 and 0.317 in the samples (before sonication, at sonication energy 0.3 kJ/g and at sonication energy 1.3 kJ/g respectively).

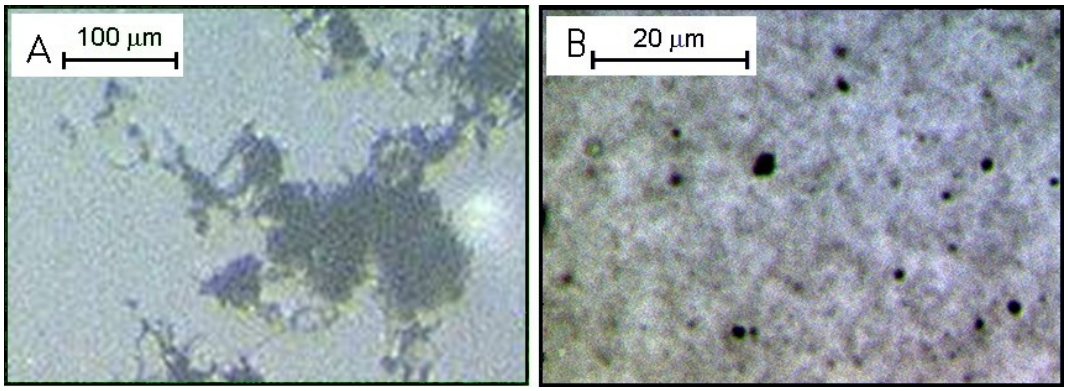

Figure 6.3: Liquid state optical transmission micrographs of (A) the untreated material and; (B) the material after 1.55 kJ/g sonication at 55 W

This is an expected effect of the improved dispersion of the CNTs in the mixtures [32, 50, 99–101], as evidenced by the presence of large nanotube clusters in the control sample (figure 6.3a) and the absence of such large aggregates in the sample that had been horn-sonicated to 1.3kJ/g level (figure 6.3b).

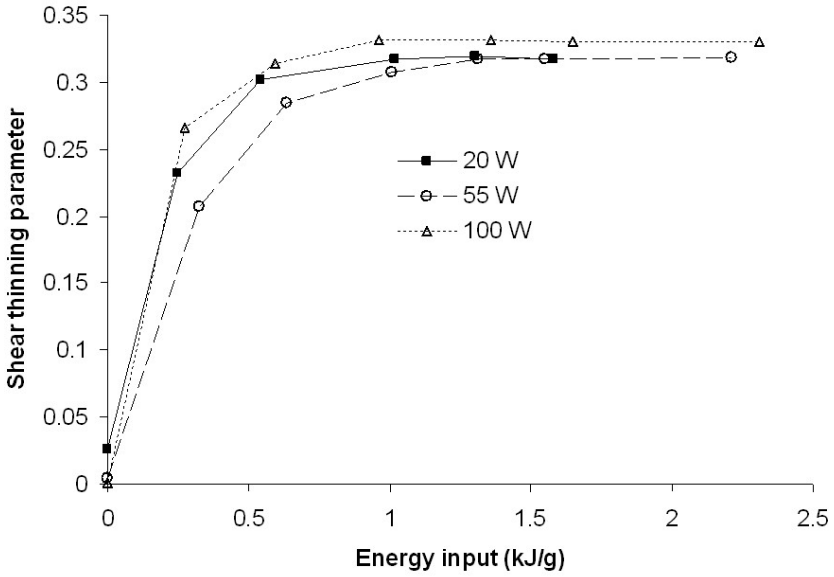

dipolar

Figure 6.4: Evolution of shear thinning parameter N during ultrasonication

In terms of sensitivity and robustness the shear thinning parameter proves preferable to the other parameters and thus has been chosen as a qualitative measure of the level of dispersion in further experiments, which were designed to evaluate the effect of the sonication power. Figure 6.4 shows how the shear thinning parameter N changes in response to different total energy inputs, delivered at three different ultrasonication power levels, namely 20, 55 and 100 W. The value of N rises rapidly, from close to zero in the unsonicated samples, up to energy input of about 0.6 kJ/g, and then it changes only gradually, reaching a limiting value of just over 0.3 in highly sonicated samples. The ultrasonication at 20 and 100 W appears to be more efficient than at 55 W. This could be a real result, suggesting a complex interplay between energy input and mechanisms of energy absorption. However, it is just as likely that the sonication efficiency is highly influenced by the exact positioning of the ultrasonic horn within the mixing vessel [47]. Given the limited number of experiments reported here, it is not possible to make this judgement. Nevertheless, the variations between the shear

thinning parameter vs ultrasonication energy curves obtained at the different power levels are relatively small, indicating that energy is the main controlling factor of the dispersion process.

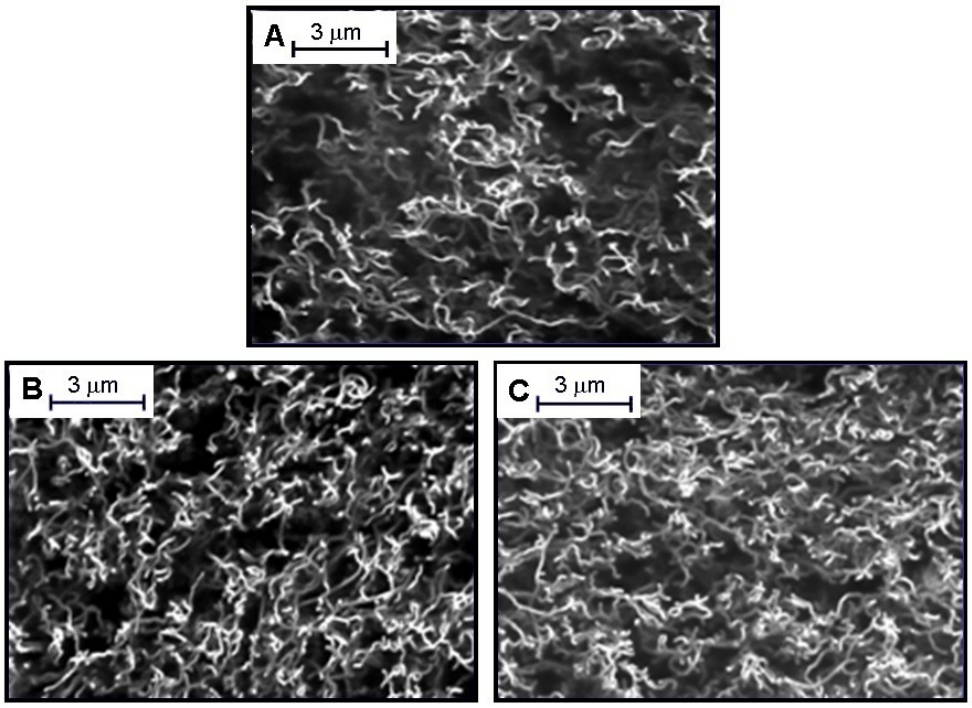

Figure 6.5: Charge contrast imaging SEM of cured samples. The liquid mixtures have been sonicated at 55 W to different energy input levels: (A) 0.32 kJ/g (B) 0.63 kJ/g (C) 1.55 kJ/g. The significant apparent depth of focus is a consequence of the charging phenomenon [102].

Charge contrast imaging scanning electron microscopy examination of corresponding cured specimens shows a clear initial increase in the quality of the dispersion, up to sonication energy input of 0.6 kJ/g. Above this level the CNTs appear evenly distributed in the material and it becomes difficult to perceive any further change (see figure 6.5).

Electrical Resistivity Monitoring: online measurements

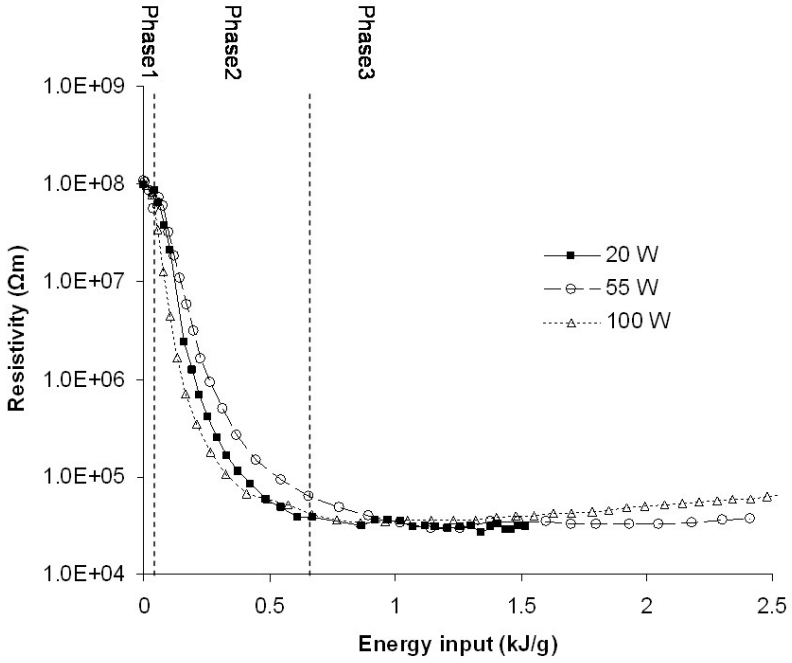

Figure 6.6: Evolution of resistivity during ultrasonication

The indication of the dispersion quality changes through the sonication process are corroborated by the accompanying changes in the DC electrical conductivity of the samples. The order of the resistivity against energy input curves in figure 6.6 is out of sequence with the increasing power level, as observed previously in figure 6.4. The changes in resistivity can be interpreted in terms of the development of a percolating system [18]; the microstructure of the sample changes from a few large isolated clusters of CNTs to predominantly separate individual nanotubes and a few smaller remaining clusters. As a consequence of the sonication, the number of individual conductive particles increases and the resistivity decreases slowly in the early stage of the process (phase 1 in figure 6.6). Once the concentration of dispersed filler reaches the electrical percolation threshold, the resistivity drops sharply (phase 2), by three to four orders of magnitude. Any further improvement in the dispersion contributes only very slightly to the effectiveness of the conductive network and the resistivity levels off

to a final value (phase 3). The resistance of the material sonicated at the highest power level (100 W) exhibits a slow upward drift in the latest stages of the process. This could be an indication of eventual damage to the nanotubes by some form of "oversonication".

The electrical measurements give the same qualitative indication of the changes in the dispersion of the CNTs in the polyester resin as that provided by the viscosity measurements. The online nature of the electrical measurements is an added attraction. However, as mentioned previously in section 2.4, there is a need for the instantaneous temperature correction in order to obtain reliable data.

6.3 Conclusions

The results of this study demonstrate the potential use of rheological properties as a metric of dispersion of carbon nanotubes in liquid polyester pre-polymer. Shear thinning is identified as the parameter with the greatest sensitivity to variations in dispersion state, combined with a high level of robustness in parameter estimation. The technique requires sampling and off-line measurement of viscosity over a range of strain rates. The duration of the procedure is in the range 5- 10 min, which makes it acceptable for use in the context of industrial scale quality control.

The evolution of electrical resistivity during ultrasonication treatment closely follows the results obtained by rheometry. Measurement of resistance provides the means for online dispersion monitoring in the case of conductive nanofillers and as such it presents an opportunity for quality control in the processing of nanocomposites. However, electrical behaviour can be influenced by other phenomena such as detail of nanoparticle network formation that may hinder the correlation with the state of dispersion.

Chapter 7

Measurement of dispersion of carbon nanotubes in thermosets during processing

This chapter[1] presents the development of a sensor for the on-line monitoring of carbon nanotube dispersion during nanocomposites processing. The method is based on the measurement of the electrical conductivity of the liquid mixture. The quality of filler dispersion, as evaluated using transmission optical microscopy of liquid samples collected at various mixing times, is compared with the evolution of the value of conductivity during processing. Results from the preparations of nanocomposite based on unsaturated polyester and epoxy matrices are reported, with filler loading ranging from 0.05 to 0.3375 wt%. The results show that the progress of dispersion is marked by a rise of the conductivity of the liquid and the attainment of the final level of dispersion corresponds to a levelling off of the value of conductivity. A quantitative index characterising dispersion is proposed based on the on-line measurement of the conductivity of the suspension.

[1] adapted from a paper submitted to *Measurement Science and Technology*

7.1 Introduction

The assessment of the dispersion quality of a nanocomposite is typically based on the microscopical characterisation of the material, using techniques such as optical microscopy, SEM or TEM. However, these approaches have several limitations; they are labour-intensive, time-consuming, especially if based on the analysis of cured samples, and investigate only small portions of the material. A further limitation is the off-line character of these metrics, which is prone to systematic errors due the sample preparation; typical examples of this are the length reduction of CNTs observed in TEM due to the preparation of the sample by ultra-microtoming and the spontaneous re-aggregation of CNTs during the cure of thermosetting nanocomposites [29].

7.2 Materials and Methods

The carbon nanotubes used in this work are Nanocyl®7000. Two commercial thermosetting matrices have been tested: an unsaturated polyester resin (UPE, Scott Bader limited) and a low viscosity epoxy resin (LY564, Huntsman). The two resins have been selected to have similar viscosity and density at room temperature: 1.2 to 1.4 Pas and 1.1 g/ml respectively.

The dispersion of the nanotubes was carried out using a combination of triple roll milling and shear mixing, as described in section 4.2. Processing was carried out on 150 grams of mixture at a stirrer speed of 1000 rpm and a temperature controlled between 25 and 30°C.

The measurement of the electrical conductivity of the liquid mixture was carried out as described in section 4.3.

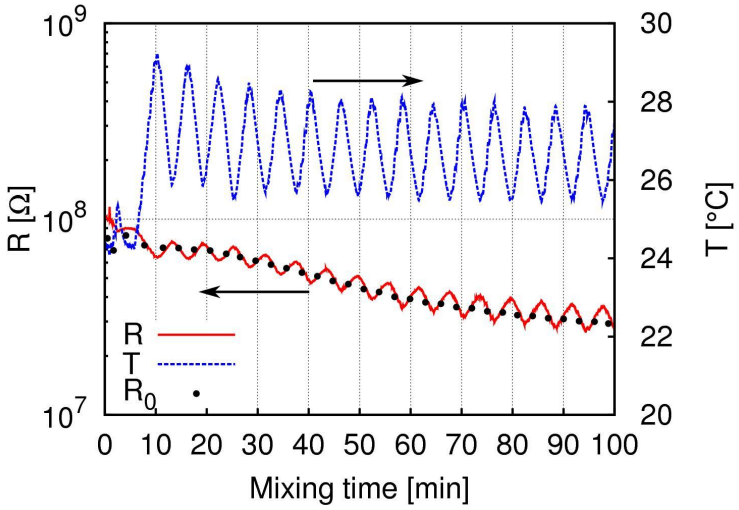

Figure 7.1: Raw data of temperature (dotted line) and resistance (solid line) as measured using temperature modulation during the mixing (0.10 wt% CNT/UPE). • denotes the resistance at the reference temperature, calculated using equation (4.5).

The temperature of the material flowing into the cell is controlled by a heating element wrapped around a portion of pipe mounted between the pump and the cell. A Eurotherm 2408 controller was used to generate a modulation of temperature in the cell from 25 to 28°C at the rate of $1°\mathrm{C}/\mathrm{min}$. Figure 7.1 is an example of temperature modulation and the corresponding resistance measurements.

7.3 Results and Discussion

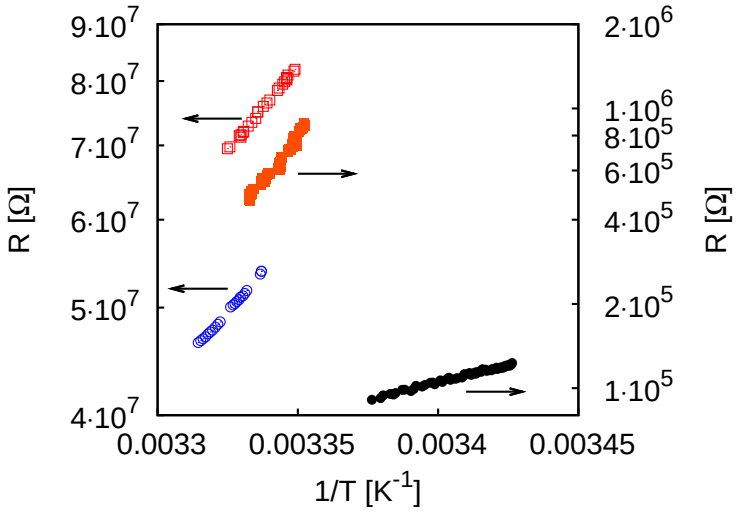

Figure 7.2: Plot of resistance vs. temperature for 0.05 wt% CNT/UPE after 20 minutes (□) and 600 minutes (○) of mixing time; 0.3375 wt% CNT/epoxy after 20 minutes (■) and 600 minutes (●) of mixing time.

The value of conductivity has been calculated assuming validity of equation (4.5). Figure 7.2 shows the experimental data at the beginning and at the end of the process for UPE and epoxy suspensions of carbon nanotubes. The linear character of these logarithmic plots is indicative of the validity of the model chosen.

Optical micrographs of liquid samples, collected at different mixing time, are illustrated in figure 7.3.

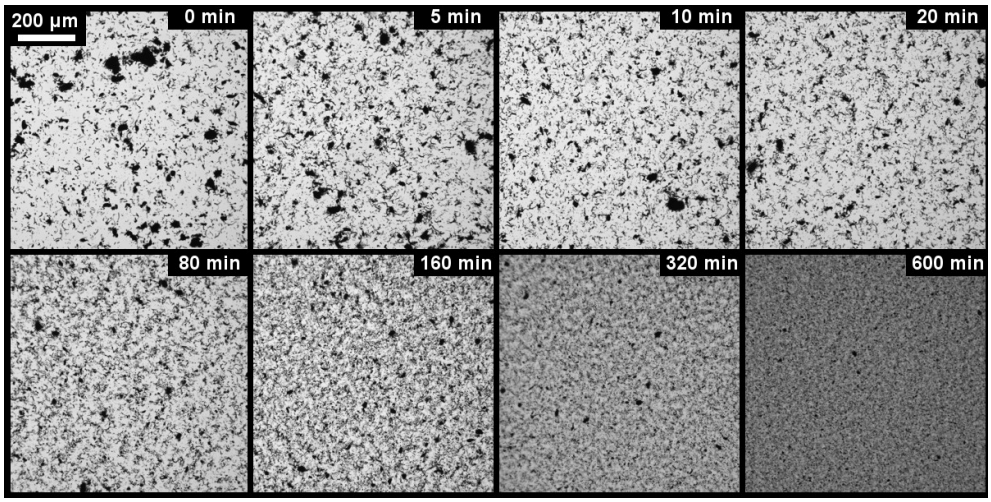

Figure 7.3: Transmission optical micrographs of liquid samples at different mixing times (0.10 wt% CNT/UPE)

The action of shear mixing on the dispersion of the filler can be observed as two separate effects. The first is the change in the dimension of the primary aggregates, shown as dark areas. At the beginning of processing there are many aggregates with a maximum dimension of several tens of micrometres; after 600 minutes very few aggregates are bigger than ten micrometres. The second noticeable effect is the variation in overall light transmission of the sample. What appears as a clear background of a heterogeneous sample in the first micrograph becomes a grey background of a more homogeneous sample in the final micrograph. Both effects can be justified by a larger number of nanotubes leaving the aggregates to become individually suspended in the resin matrix, i.e. by an improved level of dispersion.

The evolution of conductivity during the processing for the nanocomposite shown in figure 7.3 is illustrated in figure 7.4 (0.10 wt% loading curve). The value of conductivity, plotted in logarithmic scale, rapidly increases during the first 50 minutes of processing. At this time the rate at which conductivity raises starts to decrease, finally levelling off after about 200 minutes. After 200 minutes little or no increase is noticeable up to the end of the experiment. The noise of the measurement is negligible in the first part of processing, but becomes significant after 300 minutes when the value of conductivity has levelled off.

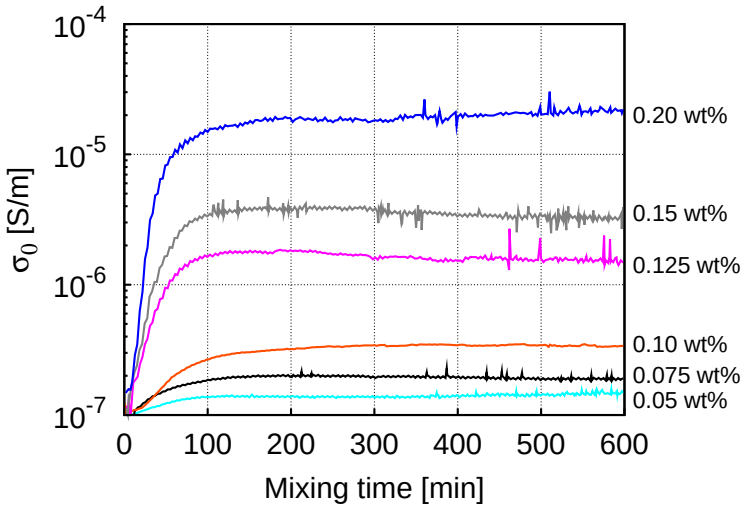

Figure 7.4: Comparison of the liquid conductivity during high shear mixing of different CNT loadings in UPE resin

Figure 7.4 also compares the dispersion of different CNT loadings into UPE resin. The trend described for the 0.10 wt% loading is valid in all loadings: an initial fast increment of conductivity increase is followed by a levelling off at about 200 minutes, with a more noticeable level of noise during the final section of processing.

The final part of the experiments indicates the existence of secondary effects; slow drops of conductivity, visible after the levelling off, are observable in particular for the 0.075, 0.125 and 0.15 wt % samples. This effect can be attributed to styrene evaporation; the slow drop of conductivity was observed in cases where the temperature of the mixture in the flask approached 30°C. The temperature of the flask builds up as a consequence of shear, in particular for high filler loadings due to the high viscosity of the mixture. Although the use of a water condenser reduces styrene evaporation to a minimum, a small degree of evaporation is inevitable and its effect is noticed at long mixing times.

The final conductivity of the liquid mixture increases with filler loading. This effect is smaller at low loadings and more pronounced at higher loading; for example, the value of final conductivity doubles from 0.05 to 0.10 wt % but gains one order of magnitude from

0.10 to 0.15 wt%. This behaviour is indicative of a general power law relation.

The qualitative assessment by microscopy, shown in figure 7.3, correlates well with the trends shown in figure 7.4. The initial raise of conductivity corresponds to the reduction of aggregate dimensions due to CNT dispersion. The levelling off of the liquid conductivity corresponds to the observation of an almost complete dispersion by optical microscopy. The dimension of the aggregates at 320 minutes decreases only slightly by the end of the experiment. This small change, which is probably hindered by the effect of styrene evaporation, is beyond the sensitivity of the measurement system in the specific setup. It should be noted that the extent of styrene evaporation is linked to the surface-to-volume ratio of the processing setup, which is high for small, lab-scale setups as the one described here. Monitoring of preparation of CNT/UPE composites on a bigger scale would be intrinsically less disturbed by this effect.

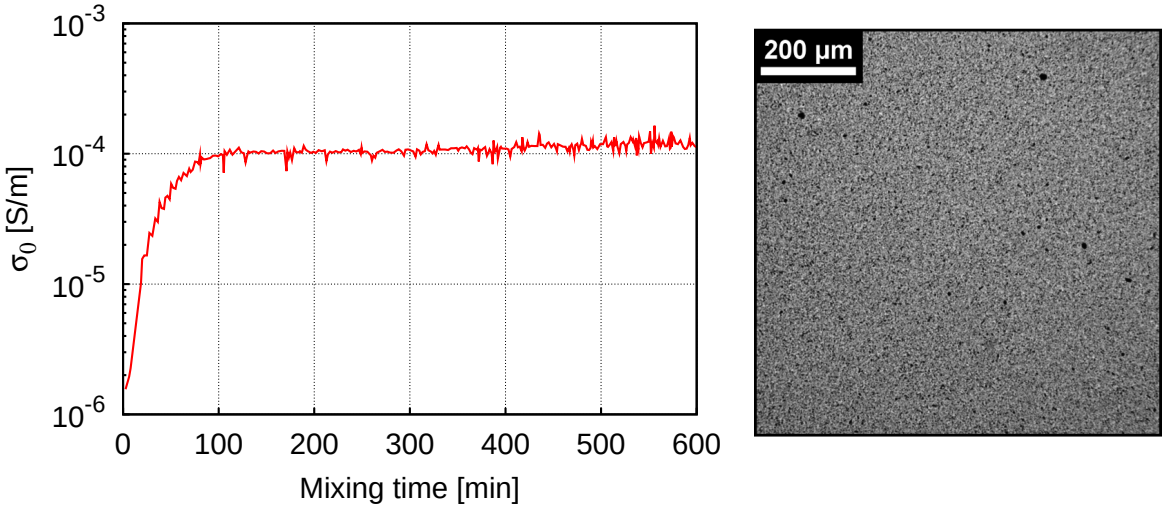

Figure 7.5: (a) Liquid conductivity during high shear mixing of 0.3375 wt% CNT in epoxy resin and (b) corresponding optical micrograph after 600 minutes of high shear mixing

Figure 7.5a shows the on-line liquid conductivity during the dispersion of 0.3375 wt% of carbon nanotubes in epoxy. The behaviour is consistent with the observation for the un-

saturated polyester matrix; after a fast initial grow, conductivity increase slows down and tends to level off at about 150 minutes. Unlike CNT/UPE composites, styrene evaporation is not disturbing the measurement and the conductivity rises slightly even after 200 minutes, up to 600 minutes, indicating a further slight improvement of dispersion. This hypothesis is supported by the presence of few residual aggregates of carbon nanotubes at the end of the process, observable as dark areas in figure 7.5b. The level of noise, which is higher than for the experiments carried out with the unsaturated polyester matrix, is attributed to the higher nanotube loading and the corresponding high conductivity of the suspension. The value of input current of $10^{-8}\mathrm{A}$ was selected to optimise sensitivity at the beginning of dispersion. Conductivities in the range of $10^{-4}\mathrm{S/m}$ cause the voltage output to drop below the optimal range, thus increasing the noise-to-signal ratio.

The quality of the measurement can be improved by increasing the current input to its optimum value during the experiment, leading to a less noisy voltage response over the whole experimental range. The need of temperature modulation and temperature-resistance correction can be removed by operating the sensor at constant temperature, resulting in the direct measurement of R_0 and instantaneous evaluation of the liquid conductivity.

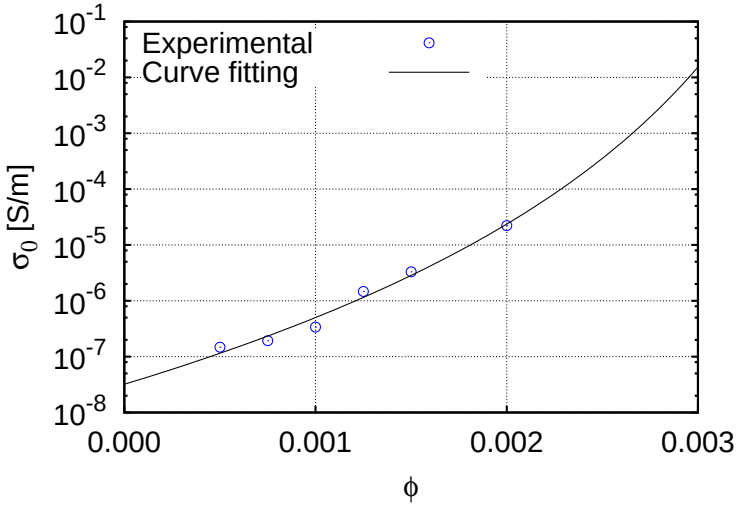

Figure 7.6: Final conductivity of CNT/UPE mixture fitted by equation (7.1). Fitting parameters: $\sigma_i = 3.20 \pm 0.96 \cdot 10^{-8}\mathrm{S/m}$, $\phi_c = 0.00406$, $s = 9.72 \pm 0.66$.

Figure 7.6 shows the data of conductivity at the end of processing for different CNT loadings. Several models are available for the description of the conductivity of nanocomposites, such as power law equation, Bueche's equations and general effective media equations. These models have been reviewed in [18]. The two exponents phenomenological percolation equation (TEPPE) [21] has been chosen, as it models the conductivity of the systems over the whole range of loading, below and above percolation. A simplified version of the TEPPE (equation 2.5) has been used to fit the data of figure 7.6:

$$\sigma = \sigma_i \left(\frac{\phi_c}{\phi_c - \phi} \right)^s \tag{7.1}$$

where ϕ is the weight fraction of filler in the composite, ϕ_c is the percolation threshold, σ is the conductivity of the composite at the end of processing, σ_i is the conductivity of the isolating component (the resin matrix) and s is the critical exponent.

An "electrical dispersion index" has been defined as follows to quantify the dispersion of a carbon nanotube suspension:

$$EDI = \frac{\ln(\sigma) - \ln(\sigma_0)}{\ln(\sigma_\infty) - \ln(\sigma_0)} \tag{7.2}$$

where σ is the conductivity of the suspension, σ_∞ denotes the conductivity of an ideally dispersed suspension and σ_0 the conductivity of a fully undispersed mixture. The value of EDI ranges from 0 to 1, indicating a completely undispersed and dispersed suspension, respectively. The calculation of EDI for real systems requires the estimation of the two case-limit conductivities; given the low filler loading σ_0 can be approximated as the conductivity of the pure resin σ_i; σ_∞ can be estimated by the conductivity σ_f at the end of the process, if the level of dispersion achieved is sufficiently good.

$$E \approx \frac{\ln(\sigma) - \ln(\sigma_i)}{\ln(\sigma_f) - \ln(\sigma_i)} \tag{7.3}$$

For preparation below the percolation threshold, the value of σ_f can be predicted by equation (7.1) as follows:

$$E \approx \frac{\ln(\sigma) - \ln(\sigma_i)}{s \ln\left(\frac{\phi_c}{\phi_c - \phi}\right)} \tag{7.4}$$

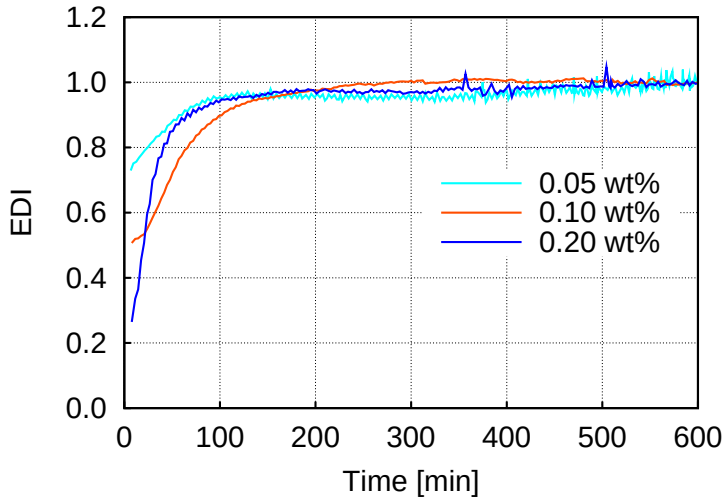

Figure 7.7: Electrical dispersion index during the processing of CNT/UPE suspensions

Figure 7.7 shows the evolution of the dispersion index for the data of figure 7.4; only three loadings are shown for clarity. The starting value of EDI is a decreasing function of filler loading. The dispersion index increases, to approach the unity at about 200 minutes processing time.

The initial value of EDI represents the level of dispersion achieved by hand mixing, which is closer to the final state of dispersion when the filler loading is low. The constant time needed to level off suggests that the dispersion the nanotubes is independent of the loading, i.e. a certain amount of shear is needed to break an agglomerate and form individually suspended nanotubes, regardless of the total number of agglomerates in the suspension. The drift of EDI after 200 minutes is attributed to styrene evaporation. The behaviour of EDI for the 0.10 wt% loading at the beginning of processing, which seems anomalous in comparison to the other two loadings, is reflecting a small difference in processing: a rotational speed of 250 rpm was

used for the first 20 minutes, then increased to 1000 rpm. This point, which is not noticeable using the conductivity representation of figure 7.4, demonstrates the potential advantages of using the dispersion index as a representation of dispersion for process control.

7.4 Conclusion

Microscopy results in only a qualitative assessment of carbon nanotube dispersion during the preparation of thermosetting nanocomposites. Electrical liquid conductivity, measured using a coaxial sensor, is a tool for on-line, quantitative assessment of CNT dispersion. The progress of dispersion is observed as a conductivity increase and the attainment of the final level of dispersion is marked by a levelling off of conductivity at the end of the process. The calculation of the electrical dispersion index proposed in this work would allow the direct comparison of different loadings, temperatures, resin matrices and dispersion techniques.

The measurement described here is a tool for assessing on-line the level of dispersion during the processing of thermosetting nanocomposites. This technique can be used for the development, optimisation and scale-up of nanocomposite processing, with the potential of offering a quantitative metric of dispersion quality. Limitations of the proposed method that have not been addressed in this study include the noise-to-signal ratio, the requirement for temperature modulation and the interference of styrene evaporation. Although the scope of this work has been limited to the preparation of thermosetting nanocomposites by high shear mixing, the scope can be extended to other dispersion techniques and matrices, including thermoplastics.

Chapter 8

Dielectric monitoring of carbon nanotube network formation in curing thermosetting nanocomposites

This chapter[1] focuses on the monitoring of a carbon nanotube network during the cure of unsaturated polyester nanocomposites by means of electrical impedance spectroscopy. A phenomenological model of the dielectric response is developed using equivalent circuit analysis. The model comprises two parallel RC elements connected in series, each of them giving rise to a semicircular arc in impedance complex plane plots. An established inverse modelling methodology is utilised for the estimation of the parameters of the corresponding equivalent circuit. This allows a quantification of the evolution of two separate processes corresponding to the two parallel RC elements. The high frequency process, which is attributed to carbon nanotube aggregates, shows a monotonic decrease in characteristic time during the cure. In contrast, the low frequency process, which corresponds to inter-aggregate phenomena, shows a more complex behaviour explained by the interplay between conductive network development and the cross-linking of the polymer.

[1] adapted from [103]

8.1 Introduction

Recent work in the authors' group [104] examined the dielectric response of epoxy/CNT nanocomposites during cure; when the addition of nanoparticles induces a conductive response, impedance generally increases as cross-linking advances . As in the case of pure thermosets, this behaviour can be attributed to mobility limitations imposed on the charge carriers by the progress of cure [105]. However, in cases where an epoxy matrix has been reinforced with SWNT, the frequency corresponding to the conductive mechanism of the system increases with the progress of cure [78]. This type of behaviour, which has also been observed in thermoplastics filled with nanotubes when melts are allowed to recover from a shear deformation, has been attributed to re-aggregation of carbon nanotubes [49, 106].

8.2 Materials and Methods

The resin used was an isophthalic unsaturated polyester (UPE) in a typical formulation that contains inhibitors, and it is cured by the addition of radicalic initiator and catalyst. This material cross-links by addition polymerisation between polyester chains and the vinyl group of styrene, which in this study was carried out at 40°C for 10 hours. The nanocomposite prepared contains between 0.05 and 0.15% by weight of filler dispersed by a combination of shear mixing and horn sonication, as described in section 4.2.

Impedance measurements during cure were carried out as described in section 4.4. The measurements were performed in the frequency range 10 Hz and 1 MHz for the unfilled resin and 100 Hz and 1 MHz for the nanocomposite. Five frequencies per decade were swept on a logarithmic scale. The experimental setup and the measurement procedure are described in detail in section 4.4.

8.3 Experimental results

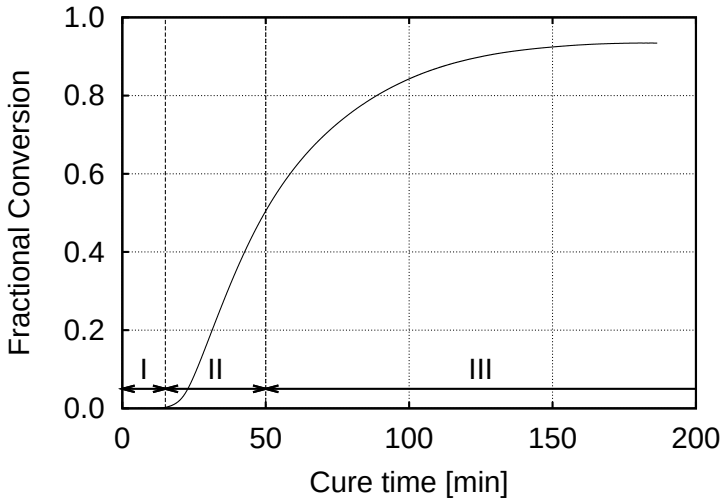

Figure 8.1: Differential scanning calorimetry results: Degree of cure evolution with time for the isothermal cure at 40°C, CNT loading 0.10 wt%

Calorimetry results for the sample containing 0.10 wt% of carbon nanotubes are illustrated in figure 8.1. The cure kinetics behaviour is characteristic of a radical-initiated addition polymerisation. The rate is negligible up to about 15 min at the cure temperature. This corresponds to the time during which radicals produced are consumed by the inhibitor (stage I in the graph). The reaction rate is maximised at about 50 min (stage II). After that the reaction slows down significantly and the degree of cure levels off after 150 min (stage III). The maximum degree of cure reached is 93%, as a consequence of diffusion limitations imposed on the cure reaction after vitrification.

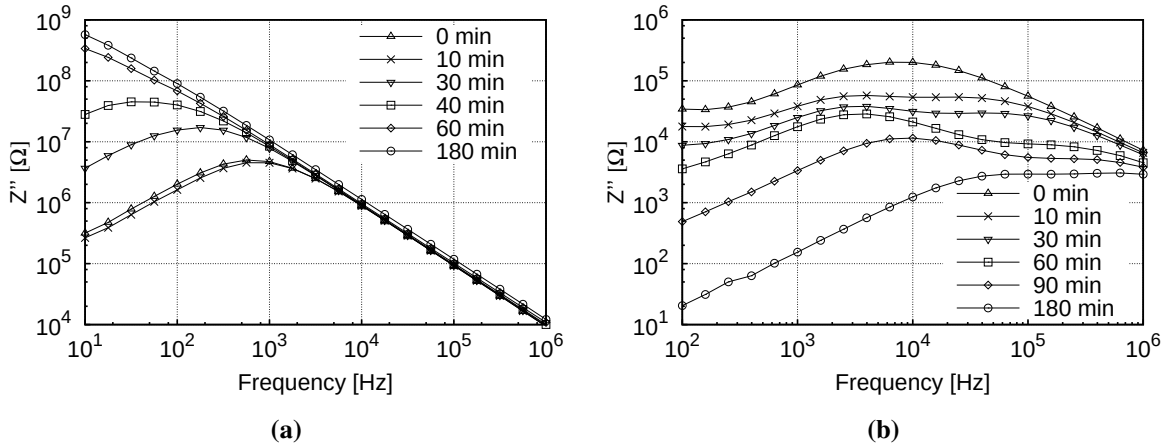

Figure 8.2: Evolution of imaginary impedance spectrum during the cure: (a) pure UPE (b) 0.10 wt% CNT/UPE composite.

The results of impedance spectroscopy for the pure resin are illustrated in figure 8.2(a). The imaginary impedance spectrum is characteristic of the existence of a mechanism of charge migration which is manifested as a peak at frequencies in the range 100 Hz to 10 kHz [105, 107]. A dipolar relaxation mechanism, which is often manifested as a secondary peak or knee at higher frequencies [105], is also present but cannot be discerned clearly in a logarithm plot. The imaginary impedance at the beginning of cure peaks at approximately 500 Hz and 5 $\mathrm{M}\Omega$. With the progress of cure the imaginary maximum increases and shifts to lower frequencies, e.g. its value is about 50 $\mathrm{M}\Omega$ and its position 20 Hz after 40 min. After some 60 min the peak moves outside the experimental window of observation. This behaviour is typical of curing thermosets and is attributed to the mobility limitations imposed on charge carriers as the viscosity of the material increases with cross-linking.

The evolution of the imaginary impedance spectrum of the nanocomposite during the cure is illustrated in figure 8.2(b). The behaviour observed is noticeably different from that of the pure polyester. The initial imaginary impedance spectrum has a peak which is significantly broader than that observed in the neat resin. The peak value decreases by more than one order of magnitude with the addition of nanotubes, as a result of the high conductivity of the

filler. Furthermore, the evolution with time is distinctly different in the nanocomposite. The spectrum moves towards lower impedance, while the broad peak resolves into two separate peaks. Both peaks move to higher frequencies as the cure progresses. Thus, the low frequency peak moves from an initial position of about 2 kHz and a level of approximately 100 $\mathrm{k}\Omega$ to a frequency of 10 kHz and a level of 10 $\mathrm{k}\Omega$, whilst the high frequency peak shifts from about 10 kHz and 100 $\mathrm{k}\Omega$ to 500 kHz and 5 $\mathrm{k}\Omega$ after 90 min. This behaviour is indicative of the existence of two mechanisms which are related to the behaviour of the nanoparticles rather than that of the matrix.

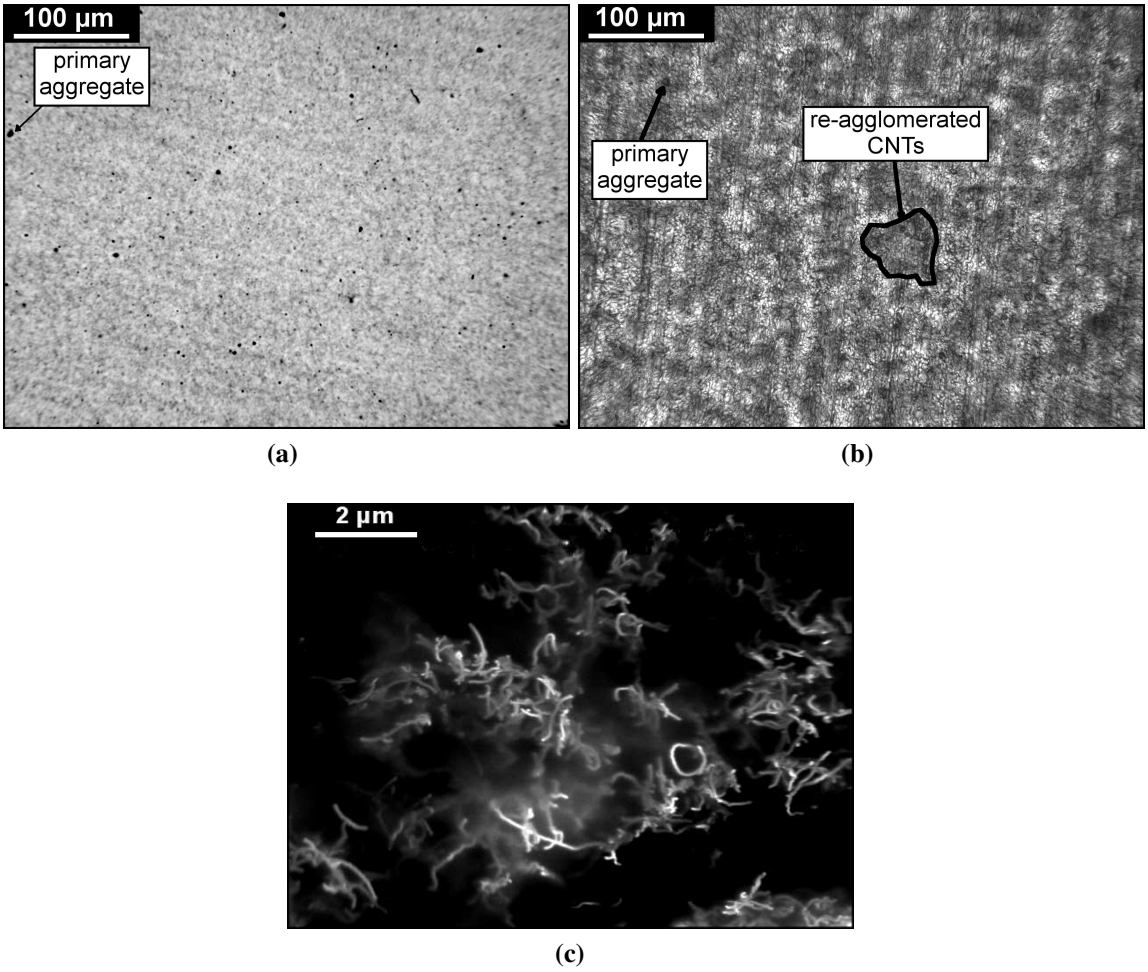

(a) **(b)**

(c)

Figure 8.3: Micrograph of 0.10 wt% CNT/UPE composite. Optical transmission microscopy of (a) liquid uncured material; (b) fully cured material. (c) Charge contrast imaging SEM of fully cured nanocomposite.

Figures 8.3(a-b) show the microstructure of the nanocomposite before and after cure, respectively. Prior to cure a slight degree of re-aggregation can be observed. This differs from undispersed primary aggregates, which appear as small dark areas with a size of about 2 to 10 μm. Some areas are more optically transparent, but the limits of nanotube-rich regions are not well defined. The microstructure of the cured nanocomposite differs significantly, comprising two different types of regions: (i) low transmission areas, which are in the range of 10-100 μm, are rich in nanotubes and cover about 50-70% of the surface; (ii) areas of relatively low nanotube content with high optical transmission. During the process of cure some process of re-aggregation of initially well dispersed carbon nanotubes occurs. The existence of loose aggregates of carbon nanotubes is evident in contrasting charge scanning electron micrographs of the cured composites, as shown in figure 8.3(c).

8.4 Modelling of impedance response

The heterogeneous structure of the nanocomposite observed in microscopy comprises resin-rich regions that are expected to have properties closer to those of neat polyester and filler-rich regions with relatively higher conductivity. The impedance spectra of the system with nanotubes show two mechanisms. These differ significantly from the single mechanism of the neat resin in terms of absolute value, characteristic frequency and evolution during the cure. The impedance response of the composite material is dominated by the behaviour of the conductive loose aggregates of nanotubes and the resin-rich areas acting as interfaces among them. The behaviour of the system can be modelled by the simplest form of the 'brick-layer' equivalent circuit used for the simulation of the behaviour of polycrystalline ceramics [70, 108, 109]. The equivalent circuit, illustrated in figure 8.4(b), comprises two parallel RC sub-circuits connected in series. In the context of the bricklayer model these are assumed to represent the bulk resistance and capacitance (b) and the behaviour of interfaces (i). The bulk

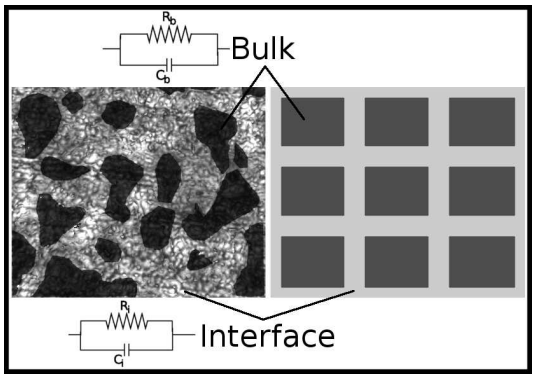

(a)

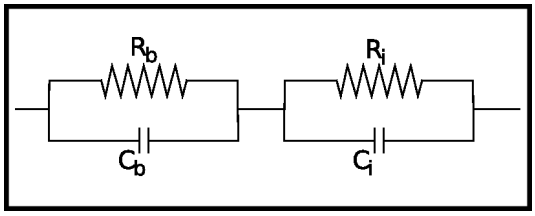

(b)

Figure 8.4: (a) Schematic of structure of aggregated nanotubes and associated bricklayer model (b) corresponding equivalent circuit.

sub-circuit is expected to result in a relatively higher characteristic frequency, with interfaces occupying the low frequency part of the spectrum. The four parameters of the equivalent circuit model are estimated for each set spectrum during the cure of the nanocomposite following the procedure described in section 4.4.

Figure 8.5 illustrates a complex impedance plane plot obtained after about 60 min in the cure. The two semicircles in the experimental data point to the presence of the two mechanisms that are represented by the parallel RC sub-circuits of the model. It can be observed that the two experimental arcs are decentralised and slightly depressed. These are typical of non-Debye type behaviour with distributed relaxation times usually observed in disordered materials and modelled using an equivalent circuit incorporating constant phase elements [70]. The model utilised in this study is limited to an ideal RC behaviour to allow a more robust estimation of the evolution of parameters by minimising the number of parameters and their interrelationships.

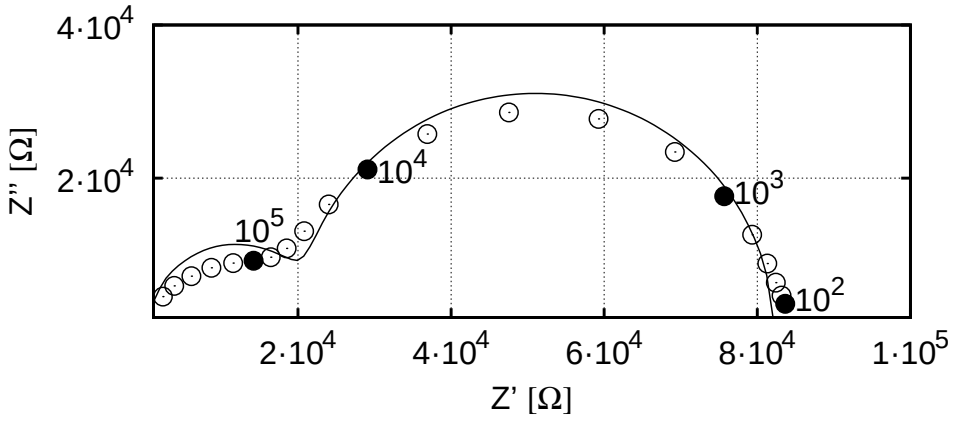

Figure 8.5: Equivalent circuit analysis of curing nanocomposite impedance response: comparison of experimental and model response at 60 min in the cure in the form of complex impedance plane plots; ∘ represent the experimental data, solid line represents model results and • denote selected frequencies (given in Hz).

The results of parameter estimation are illustrated in figure 8.6. The evolution of the conductive network can be separated in three different stages, corresponding to the stages of reaction measured by DSC (figure 8.1). Stage I corresponds to the first 15 minutes of the experiment, during which the degree of conversion is negligible; the interphase shows an increase of capacitance (C_i) and a drop of resistance (R_i), whilst the capacitance of the bulk (C_b) remains approximately constant and the corresponding resistance (R_b) decreases steadily. Stage II corresponds to the time between the onset of curing to approximately the point of maximum rate of reaction; the capacitances C_i and C_b remain essentially constant, while the behaviour of the two resistances is remarkably different. The two resistances tend to level off at about 35 minutes, at which point they separate: R_i increases and R_b drops sharply. Reaction continues in stage III, reaching a steady state after about 150 minutes; C_i decreases slightly and C_b remains constant; R_i and R_b decay, levelling off at similar final values.

The evolution of characteristic times for composites with different CNT loadings is shown in figure 8.7. The value of characteristic time at the end of cure is lower at higher filler

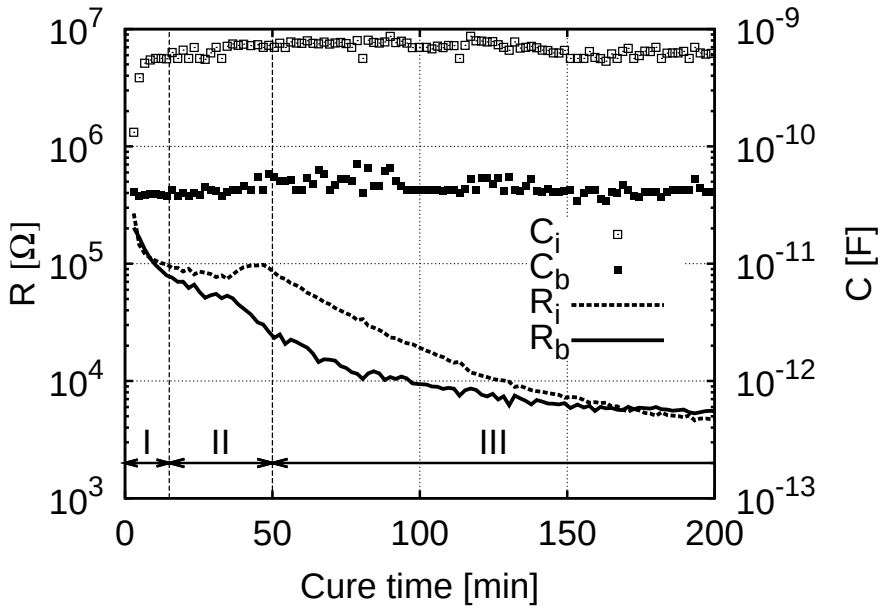

Figure 8.6: Evolution of the four parameters of the equivalent circuit versus cure time. Composite containing 0.10 wt% of CNT.

loading. The characteristic times of the interphase, shown in figure 8.7(a), start at similar values and then separate during cure. The peak of conductivity observed at about 50 minutes at 0.05 wt%, moves to shorter time and lower intensity with increasing CNT loading. The characteristic times of the bulk phase at the three loadings studied (figure 8.7b) are well separated from the beginning of cure.

8.5 Discussion

The results of impedance measurements during the cure of pure polyester and nanocomposites show different behaviours. The pure resin has the response usually observed in curing thermosets, i.e. the existence of a conductive mechanism due to charge migration that is affected by the increasing viscosity of the material as it cures. In contrast, the response of the nanocomposite is dictated by re-aggregation of nanotubes occurring after the end of the process of dispersion. Several models can be used to describe the AC response of a conduc-

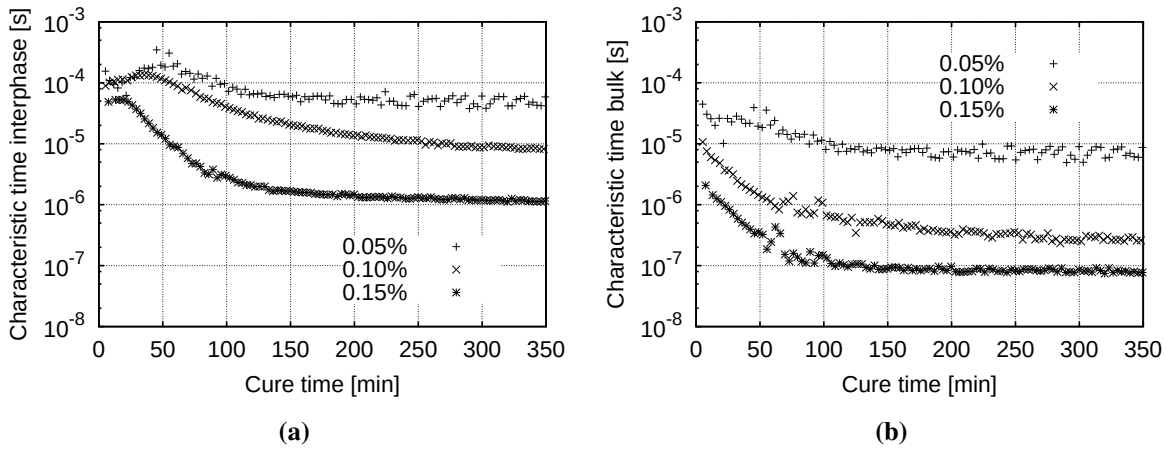

Figure 8.7: Comparison of the evolution of characteristic times in CNT/UPE composites at different loadings: (a) interphase between aggregates and (b) bulk of the aggregates.

tive/insulating matrix composite, such as the effective media Maxwell-Wagner equation, the two exponent phenomenological percolation equation and the bricklayer model [21, 110–112]. The bricklayer model with two RC sub-circuits in series, previously used for polycrystalline ceramics [108, 113], has been selected in this study for its ability to separate bulk and interphase contributions and to monitor their changes during cure. The choice is based on the heterogeneous morphology of the nanomaterial observed by microscopy. This morphology is represented schematically in figure 8.8.

The evolution of the parameters of the equivalent circuit model during the cure of the nanocomposite is influenced by changes in both the geometry of the conductive network and in the resin properties. The initial sharp increase of the interfacial capacitance reflects the generation of interfaces during the formation of aggregates, which in turn become richer in filler, leading to lower resistance. When cure begins, the increase of resin resistivity is manifested as a temporary increase in the resistance of the resin-rich component (R_i). However, the more evident effect of cure on the conductive network is a continuous drop of R_b as well as R_i during the progress of reaction, leading to final values of more than one order of magnitude lower than those at the beginning of cure.

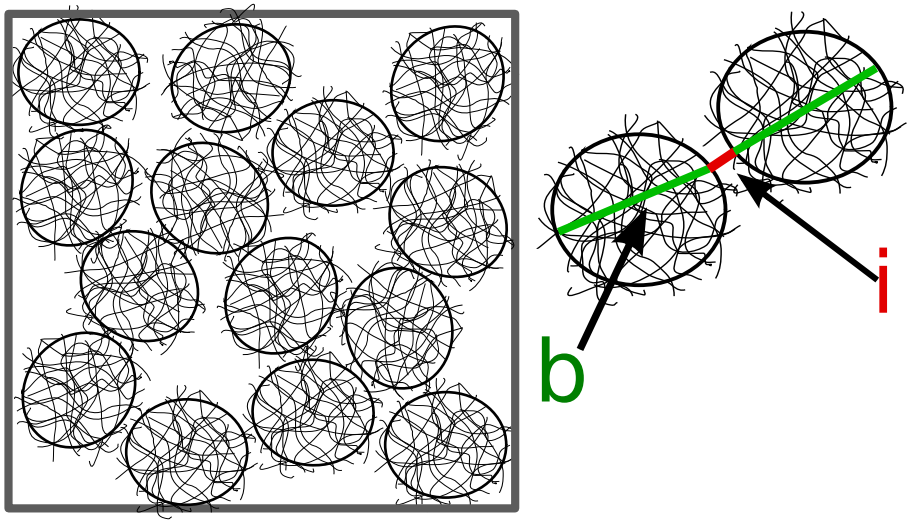

Figure 8.8: Schematic of carbon nanotube network in insulating thermosetting resin during and after secondary aggregation. Arrows indicate nanotube-rich areas (b) and resin-rich layers (i).

The values of resistance and capacitance of the equivalent circuit are influenced by geometrical factors as well as by material properties. Calculation of the characteristic time corresponding to each of the sub-circuits allows elimination of some of the effects related to geometry. Figure 8.7 shows the evolution of the characteristic time of the two sub-circuits during the cure. The sequence of the three stages described previously is repeated for all loadings, although at the lower loading scatter is higher due to the low signal/noise ratio caused by the low conductivity of the material. The characteristic time of interfaces (τ_i) is about one order of magnitude higher than that of the bulk (τ_b) for all loadings. The characteristic time of the interface sub-circuit is almost constant during the first part of cure although both the resistance and capacitance change significantly. This fact points to a pure geometrical effect occurring in the first stages of cure, during which new interface is produced. Subsequently, the characteristic time increases slightly as a result of rising mobility limitations imposed by polymerisation of the thermosetting matrix. After this point, the characteristic times of both interfaces and bulk decay until the end of the cure, showing a contribution from the reaction to the resistivity of both phases.

The characteristic times at the end of cure of both interphase and bulk decrease with carbon nanotube content. This is in agreement with the expected increase of conductivity with filler loading, typical of percolating systems. The peak of conductivity due to migrating charges mobility limitations is less evident at higher loadings, as shown in figure 8.7(a). This is due to the faster drop of interphase resistance, which causes the shifting and hindering of the peak. The separation of characteristic times of the bulk phase at the three loadings (figure 8.7b) suggests the existence of a different conductivity of the loose aggregates of carbon nanotubes. The decay of characteristic time of both components suggests that reaction affects the electrical properties of the composite, improving its conductivity. Although this effect is observed on both the bulk of the CNT aggregates and the resin-rich interphase, the latter is more significant at higher loading.

8.6 Conclusions

The investigation of the dielectric behaviour during cure of unsaturated polyester/carbon nanotube composites highlighted significant differences between the response of nanocomposites and the thermosetting matrix. The imaginary impedance spectrum of the nanocomposite shows two mechanisms, both moving to lower impedance and higher frequencies with the progress of cure. This behaviour is attributed to the re-aggregation of carbon nanotubes observed after the end of dispersion processing. This aggregation leads to heterogeneous morphology of the nanocomposite, with nanotube rich regions of size in the range of 10-100 μm. The heterogeneous morphology can be modelled by an equivalent circuit comprising two parallel RC sub-circuits, one of them representing the nanotube rich regions and the second the interphase that surround them. Parameter estimation based on a genetic algorithm was used to estimate the evolution of the parameters of the circuit during the cure. This analysis was capable of evaluating the influence of material properties changes as well as of geometrical

characteristics of the morphology. The generation of interphase induced by re-aggregation affects both elements of the corresponding sub-circuit, whilst the drop in conductivity of the thermosetting matrix influences the resistance of interfaces. The phenomenon of aggregation causes an increase in conductivity in the nanotube rich regions, which is reflected in a drop in the resistance of the bulk sub-circuit. The characteristic times of the two sub-circuits follow closely the local material response, isolating that from geometrical effects. The characteristic time corresponding to the nanotube rich regions decreases continuously, whilst that of interphase is non-monotonous due to the interplay between the changes in the electrical properties of the resin and the effect of cure on the carbon nanotubes. The characteristic time of the interphase follows the behaviour of resin, with an increasing trend up to a point which reverses in the later stage of cure. At higher filler loadings the effect of the nanotubes is dominant and only a decay can be seen.

The information obtained using this type of analysis can form the basis for on-line monitoring of dispersion/re-aggregation in the context of nanocomposites processing. The phenomenological model reported in this study can facilitate the understanding of the changes of electrical characteristics of a nanocomposite during cure, which in turn determine its final electrical conductivity. The contributions of the different components can be discerned, which can be a useful tool for control and optimisation of the cure of nanocomposites. Implementation in on-line process monitoring, e.g., RTM or pultrusion, could be applied as quality control for the industrial production of fibrous composites containing a nanocomposite matrix.

Chapter 9

Percolation threshold of carbon nanotube filled unsaturated polyesters

This chapter[1] reports on the development of electrically conductive nanocomposites containing multi-walled carbon nanotubes in an unsaturated polyester matrix. The resistivity of the liquid suspension during processing is used to evaluate the quality of the filler dispersion, which is also studied using optical microscopy at the end of mixing. The electrical properties of the cured composites are analysed by AC impedance spectroscopy and DC conductivity measurements. The conductivity of the cured nanocomposite follows a statistical percolation model, with percolation threshold at 0.026 wt % loading of nanotubes. The results obtained show that unsaturated polyesters are a matrix suitable for the preparation of electrically conductive thermosetting nanocomposites at low nanotube concentrations. The effect of carbon nanotubes reaggregation on the electrical properties of the spatial structure generated is discussed.

[1] adapted from a paper submitted to *Composites Science and Technology*

9.1 Materials and Methods

The nanofiller used in this study is industrial grade of multi-walled nanotubes (Nanocyl®7000). The expected percolation threshold, calculated using the length and diameter declared by the producer in equation 2.7, is 0.43 vol% (see table 3.1). This corresponds to a value of gravimetric percolation threshold of approximately 0.96 wt% [1, 114].

The matrix used for the preparation of nanocomposites is an unsaturated polyester resin (UPE, from Scott Bader), with styrene content of 30 wt %. After the addition of cobalt and peroxide the samples were placed in an oven at 40°C for 6 hours, followed by 3 hours at 120°C to obtain full cure.

Sample Preparation

The preparation of the nanocomposites consisted of triple roll milling and high shear mixing, following the procedure described in section 4.2. Appropriate amounts of unsaturated polyester resin and masterbatch were compounded to obtain mixtures with CNT loading ranging from 0.05 to 0.30 wt %. Each sample was mixed for 420 minutes at 1000 rpm, whilst the temperature was kept between 30 and 35°C.

During processing a peristaltic pump fed the material to a coaxial flow-through cell designed to measure the resistivity of the liquid (see section 7.2). The deviations of resistance due to temperature variations were corrected by assuming an Arrhenius dependence of conductivity on temperature presented in equation 4.5 and by calculating the values of resistivity at a reference temperature of 34°C.

Electrical measurements

AC impedance spectroscopy was carried out after cure using a Solartron SI 1260 frequency response analyser. An interdigitated copper sensor (GIA sensors, Pearson Panke) was em-

bedded in the material by immersion in a glass tube containing the liquid resin, previously mixed with cobalt and peroxide. The glass tube was placed in a heated cell and cured using the thermal profile described previously. The measurements were performed after cure completion, at temperature of 40°C, in the frequency range between 1 Hz and 1 MHz measuring five frequencies per decade on a logarithmic scale. The AC conductivity σ of the sample was calculated from the real and imaginary parts of complex impedance ($Z^{\star}$) as follows:

$$\sigma(\omega) = \frac{l}{|Z^{\star}(\omega)|} \tag{9.1}$$

where ω is the angular frequency and l = 3.93 m^{-1} is the geometric constant of the sensor [115]. The DC electrical conductivity of the cured materials was determined by a two-point measurement described in section 4.5.

9.2 Results and Discussion

Dispersion of CNT

A representative example of the evolution of the liquid resistivity of a sample during processing is shown in figure 9.1. At the beginning of the process the resistivity is in the order of several $\mathrm{M\Omega m}$, and decreases slowly with mixing. After an incubation period, whose duration varies with the filler content (e.g. about 50 minutes in the sample containing 0.20 wt % CNT), the resistivity falls steeply by more than one order of magnitude. This is followed by a steady decrease until the end of the process. The sharp fall of resistivity observed during mixing can be interpreted as an effect of CNT dispersion in the liquid mixture. The downward trend in the final part of processing suggests that dispersion is not complete after 420 minutes of mixing.

Figure 9.2 illustrates the filler dispersion after processing. Higher loadings of CNTs re-

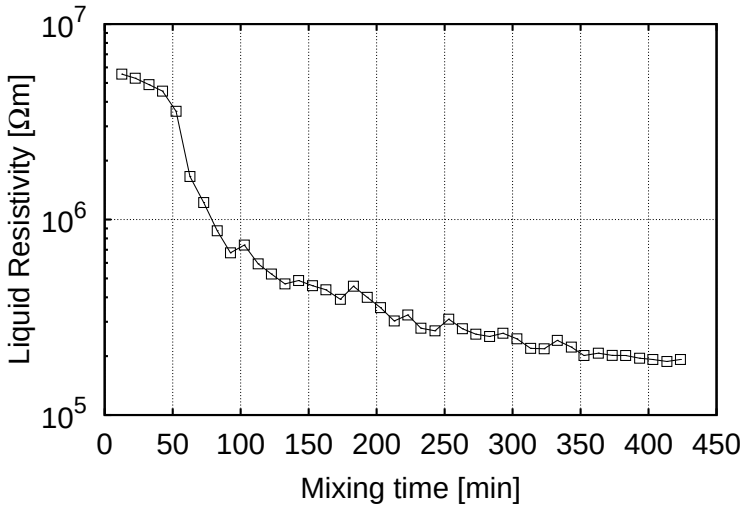

Figure 9.1: Evolution of liquid resistivity during the mixing of a composite with CNT content 0.20 wt %

sult in lower optical transmission (top row). Contrast adjustment of these images reveals the remaining clusters of undispersed nanotubes (bottom row). These appear as isolated dark particles with the size of a few microns. The micrographs have not been analysed quantitatively, however qualitative observations are possible. The total area covered by the residual clusters appears small compared to the samples before shear mixing (not shown here) and the residual area is similar between all loadings. The existence of undispersed nanotube clusters corroborates the suggestion of incomplete dispersion based on the continuous drop of liquid resistivity.

Morphology of CNT in cured nanocomposites

Figure 9.3a shows the microstructure of the cured nanocomposite. The existence of an heterogeneous structure comprising areas of high and low nanotube content is observed. The low brightness regions, corresponding to relatively higher nanotube content, cover a significant percentage of the sample area indicating the existence of aggregates of a different nature to those originally mixed with the resin. These aggregates, which are formed during the cure of

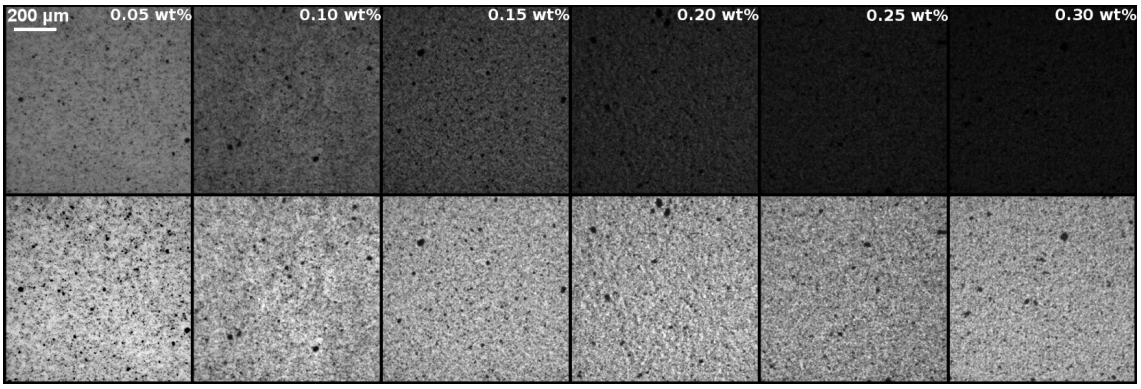

Figure 9.2: Optical micrographs of liquid nanocomposites after mixing. Top row samples are imaged using identical sub-stage illumination. Bottom row shows the same images, with contrast adjusted to reveal the clusters of undispersed nanotubes.

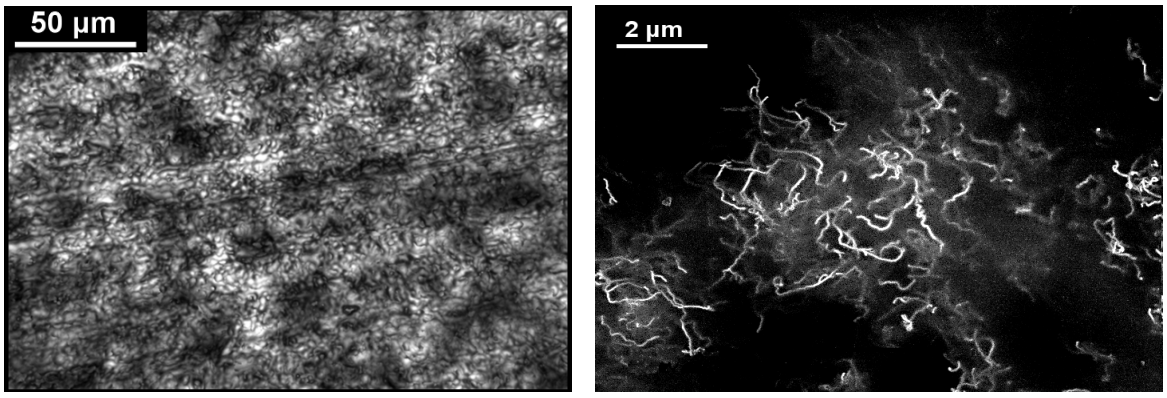

(a) **(b)**

Figure 9.3: Cured nanocomposite containing 0.15 wt % of carbon nanotubes: (a) transmission light micrograph (b) charge contrast imaging.

the material, are not as tightly packed as the original clusters. Charge contrast imaging can be used to visualise the nanotubes embedded in the resin in the proximity of the sample surface [93, 102]. Figure 9.3b is a representative example of the structure of such secondary agglomerate. Its size is about 10 μm and it comprises an assembly of loosely packed nanotubes. Since the tubes are wavy and entangled, a precise evaluation of their length is not possible. However, most of the visible nanotubes appear to be consistent with the nominal length of 1.5 μm.

Electrical behaviour

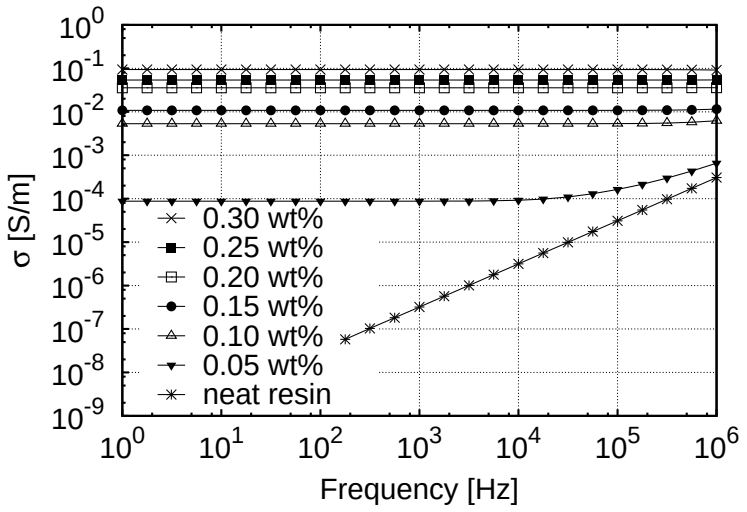

Figure 9.4: AC conductivity at the end of curing as a function of frequency for different filler loadings.

Impedance spectroscopy has been used to evaluate the AC conductivity of composites at the end of cure, as shown in figure 9.4. The neat cured resin follows a purely capacitive behaviour at all frequencies. The nanocomposite with loading of 0.05 wt % exhibits a frequency independent conductivity up to 10^4 Hz, which changes to a capacitive response at high frequencies. The nanocomposites with nanotubes loading greater than 0.10 wt % show a predominantly resistive electrical behaviour, with constant conductivity over the whole range of frequencies investigated.

The effect of filler loading on the DC conductivity of the solid composites is shown in figure 9.5a. The neat resin is an insulating material, with an electrical conductivity in the order of 10^{-12} S/m. Addition of 0.05 wt % of filler increases the electrical conductivity by eight orders of magnitude, to the value of $2.7 \cdot 10^{-4}$ S/m. Conductivity increases further with higher loading, up to $1.3 \cdot 10^{-1}$ S/m at the highest loading tested. The values of DC conductivity are in agreement with the values of AC conductivity measured by impedance spectroscopy. The nanocomposites show the characteristics of a percolating system. Conductivity at various loading has been fitted to the model of statistical percolation described by equation **??**,

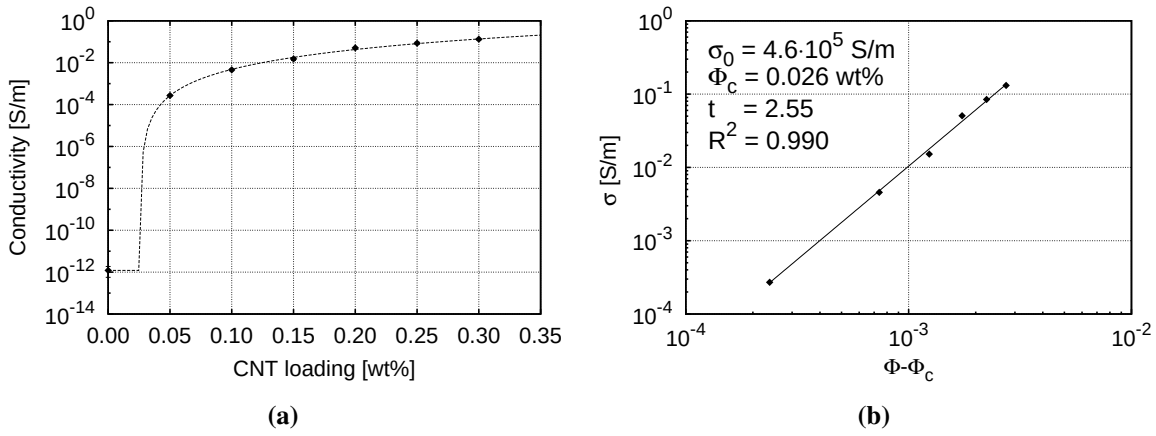

Figure 9.5: (a) DC conductivity as a function of filler loading. The dotted line denotes the fitting of experimental data using the statistical percolation model of equation (2.2). (b) Fitting of DC conductivities according to equation 2.2.

resulting in a percolation threshold of 0.026 wt % and a critical exponent of 2.55. The value of percolation threshold is significantly lower that the value predicted by statistical percolation theory (0.96 wt%). This suggest that the electrical properties of the CNT-unsaturated polyester composite are enhanced by the spontaneous reaggregation of filler particles during cure, as previously reported for CNT/epoxy systems [31].

The electrical properties of the material described in this study have been compared with the data published in literature. The percolation threshold observed compares well with the best results obtained with entangled MWNT in different polymers, i.e. epoxy, polyurethane and vinyl esters [1, 42]. The value is lower than the 1 wt% previously observed for entangled MWNT/unsaturated polyester systems and similar to the 0.1 wt% of non-entangled MWNT/unsaturated polyester systems [39]. Given the simple preparation process, the low cost of the resin and the electrical conductivity achieved, CNT/unsaturated polyester nanocomposites hold potential for the production of electrically conductive composites. The non-complete dispersion observed suggests that even better electrical properties are possible.

9.3 Conclusion

The preparation of microscopically uniform unsaturated polyester nanocomposites based on industrial grade multi-walled nanotubes has been carried out successfully using a combination of triple roll milling and shear mixing. The resistivity of the liquid composite has been measured to monitor the evolution of dispersion during processing. The on-line data showed that after an incubation period the resistivity drops more than one order of magnitude. This is followed by a gradual decrease which is attributed to the existence of residual undispersed clusters of nanotubes.

The final level of dispersion achieved was adequate to create a conductive network whilst preserving the high aspect ratio of filler particles. Well dispersed suspensions of nanotubes in unsaturated polyester form a spatial structure of agglomerates during cure which results in a percolation threshold of 0.026 wt %. The cured nanocomposite has maximum conductivity of 0.13 S/m for 0.30 wt% CNT loading.

Chapter 10

Industrial applications of CNT filled unsaturated polyester nanocomposites

The first section of this chapter is an account of the potential applications tested for the specific CNT/UPE nanocomposites developed in this work. The preparation of the nanocomposite had been scaled up to the scale of 20 kg batches, at the premises of Scott Bader Company Ltd. This scale-up exercise is described in section 2. Section 3 summarises the main results of the experimental work carried out toward the industrial exploitation of carbon nanotubes unsaturated polyesters nanocomposites. This chapter constitutes the industrially sensitive part of the thesis.

There are several motivations for using carbon nanotubes in polymers: nanocomposites can reach new performance levels, allowing new applications; nanocomposites can be more economical than the materials currently used for a specific application; they can have technical advantages over the current materials. CNT nanocomposites potential applications are investigated in many fields [116–119], mainly exploiting improved electrical and mechanical properties. In addition, some applications exploit the improvement of thermal conductivity and flame-retardant properties [62], the reduction of algae growth on marine structures [120] and the ability of health monitoring for composites structures [121].

10.1 Proof-of-concept studies for potential applications

Electromagnetic field shielding

The electromagnetic shielding effectiveness of the nanocomposites prepared in this study has been characterised[1] between 10 MHz and 1 GHz following the indications of ASTM standard D 4935-99.

A plate of nanocomposite 3 mm thick, with a carbon nanotube loading of 0.25 wt% and a volume conductivity of 0.2 S/m has been tested using the procedure described in the standard (see figure 10.1a). The results of figure 10.1b show, for most of the spectrum analysed, a higher signal transmission for the nanocomposite than for the reference sample[2]. The maximum shielding is observed at the frequency of 1 GHz, equal to -3 dB, but it was not possible to measure a value of shielding effectiveness over the whole spectrum.

In spite of a reasonably high conductivity, the electromagnetic shielding effectiveness of the nanocomposite is negligible. This can be attributed to the network of nanotubes not being able to host the induced current required to cancel the external electromagnetic field. It could

[1]The measurement has been carried out at the George Green Institute for Electromagnetic Research at the University of Nottingham, in collaboration with Professor David Thomas.

[2]A 3 mm thick specimen of mylar sputtered with gold, with an empty area for the transmission of the signal

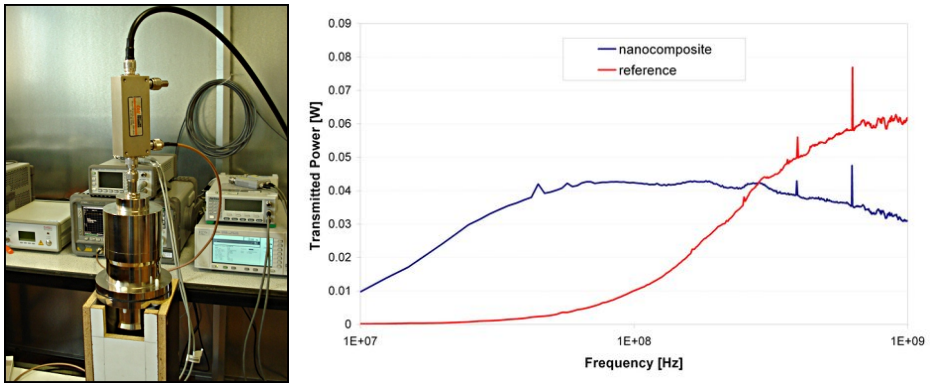

(a) **(b)**

Figure 10.1: Setup for the measurement of the EMF shielding effectiveness (a) and signal transmission of the nanocomposite sample and the reference (b).

be inferred that, although conductive, the nanocomposite has less skin effect[3] than metallic conductors, which is the phenomenom at the base of electromagnetic interference shielding as well as lighting protection. Hence, this result suggests that applications relying of surface conduction should be carefully investigated, with special regard to the manufacturing of the nanocomposite aimed at the generation of surface conductivity.

Electroplating

The nanocomposite developed in this project has been tested as a material for electroplating, specifically using acid copper deposition, which is described in detail in [122].

The electrodeposition of the 0.25 wt% CNT/UPE composites was carried out using the lab-scale setup shown in figure 10.2a. The deposition was carried out at ambient temperature, setting a Thurlby PL154 current source to a voltage of 15 V and limiting the current output to 100 mA. The solution for the deposition was 200 g/L (0.80 M) of $CuSO_4 \cdot 5H_2O$ and 60 g/L (0.61 M) of H_2SO_4 in distilled water. The anode was a high purity copper ribbon. The specimens for the electrodeposition were prepared as shown in figure 10.3. The faces of the

[3]the distribution of ac current on the surface of a conductor

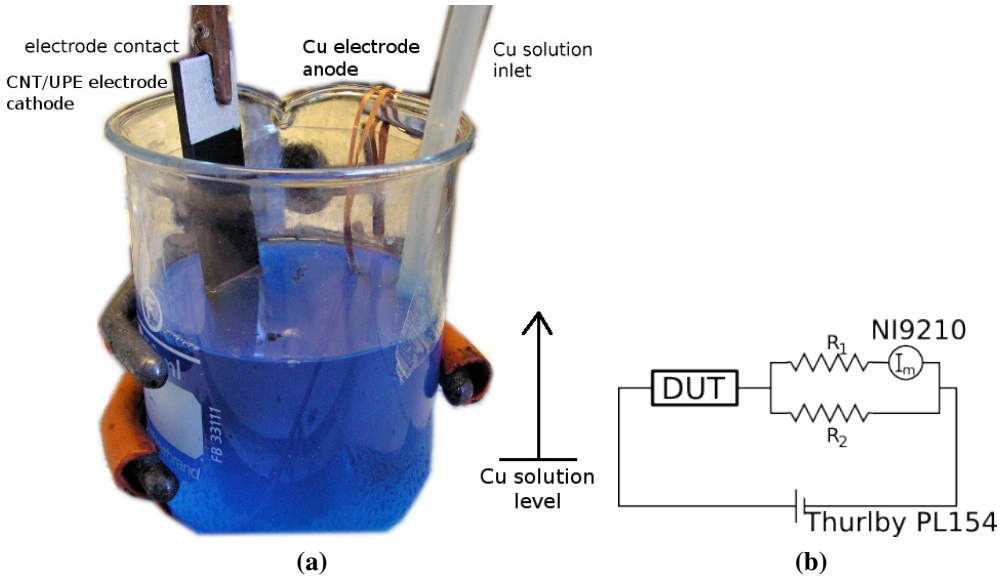

Figure 10.2: Setup for the electroplating of CNT/UPE specimens

panels were polished at 240 grit and an electric contact was painted on the specimen using a suspension of silver in methyl isobutyl ketone (Electrodag® 1415M). Araldite®420 was used to mask the area to be coated and to ensure electrical isolation from the electric contact and the solution. The level of the solution was raised gradually at a constant rate for 200 minutes to cover the surface to avoid uneven coating, as indicated in figures 10.2a and 10.3.

The current value was aquired using the circuit illustrated in figure 10.2b, which results in:

$$I = I_m \cdot \left(1 + \frac{R_1}{R_2}\right) \tag{10.1}$$

where I_m is the current measured by NI 9210 board and R_1 and R_2 are two known resistances of 1000 and 20 Ω respectively. The mass of copper deposited m_{Cu} was calculated as:

$$m_{Cu} = \frac{\int_0^t I(t) \cdot dt}{2\,\mathrm{eq/mol} \cdot 96500\,\mathrm{C/eq}} \cdot 63.546\,\mathrm{g/mol} \tag{10.2}$$

where 96500 C/mol is Faraday's constant and 63.546 g/mol is the atomic weight of copper; the factor of 2 is used to account for the number of electrons exchanged in the cathodic

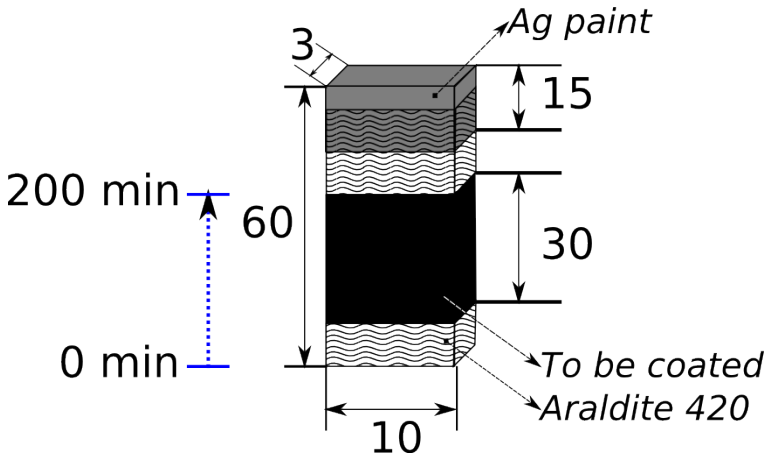

Figure 10.3: CNT/UPE specimen for the electrodeposition of copper

deposition:

$$Cu^{2+} + 2e^{-} \rightarrow Cu^{0} \tag{10.3}$$

Figure 10.4 shows a typical example of the current evolution during an electrodeposition. The current increases during the first 200 minutes while the level of the solution rises; once the area to be deposited is completely immersed, the current stabilises. The experiment is stopped when 1.6 grams of copper have been deposited.

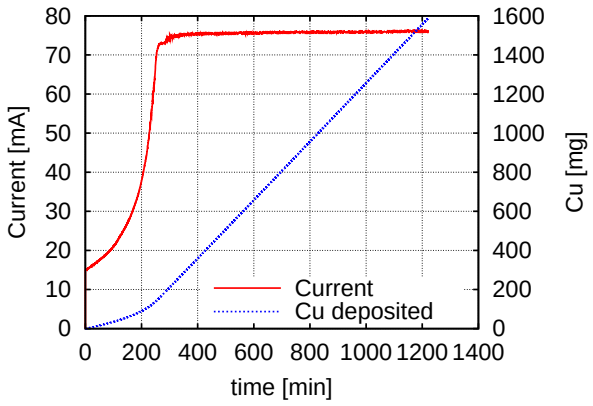

Figure 10.4: Electrodeposition of copper on a CNT/UPE specimen

The morphology of partially electrocoated samples is shown in figure 10.5. The deposition appears granular by optical microscopy and SEM reveals uncoated areas of low

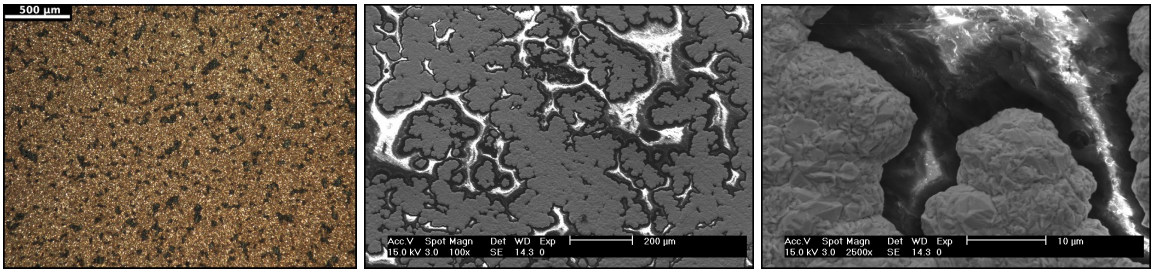

(a) **(b)** **(c)**

Figure 10.5: Electrodeposited copper: (a) transmission optical microscopy (b-c) SEM

conductivity, which are bright due to SEM charging. The formation of a continuous deposit appears to be the results of the coalescence of crystalline domains, which corresponds to the nucleation-coalescence growth mechanism described in [122].

Adhesion

The adhesion of the electrodeposited copper to the nanocomposite was evaluated by tension testing. Squares of the dimension of 25x25 mm were bonded to steel blocks as illustrated by the schematic of figure 10.6. The testing compared nanocomposites based on two resin formulations (Crystic® D3061 and Crestapol® 1210) and two level of roughness (surface finishing at 240 and 1200 grit). The results shown in figure 10.6(b), indicate that better adhesion is associated with a rougher surface and the use of Crestapol® 1210 resin.

Rotogravure cylinder prototype

To demonstrate the applicability of CNT/UPE as materials for electrodeposition, a small rotogravure cylinder has been prepared. The current technology for the preparation of polymeric rotogravure rollers consists in moulding a cyclinder of resin around a metal spine, apply a hard ceramic layer and a conductive primer [123]. The cylinder resulting for this 3-stage process is then electrodeposited with a copper layer of $500\,\mu\mathrm{m}$.

The cylinder prepared here, shown in figure 10.7, comprises an internal copper spine and

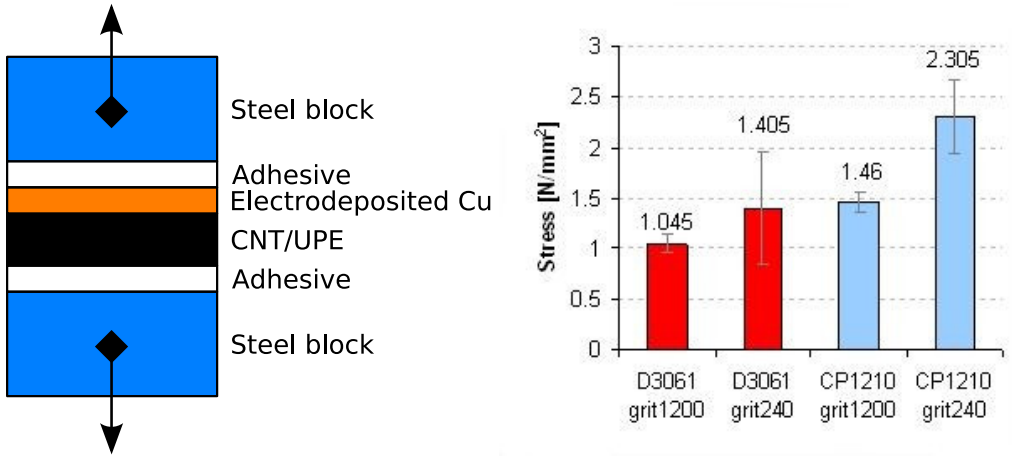

(a) **(b)**

Figure 10.6: Adhesion testing of electrodeposited copper layer: (a) schematic on the experimental setup and (b) stress at failure for the sample tested

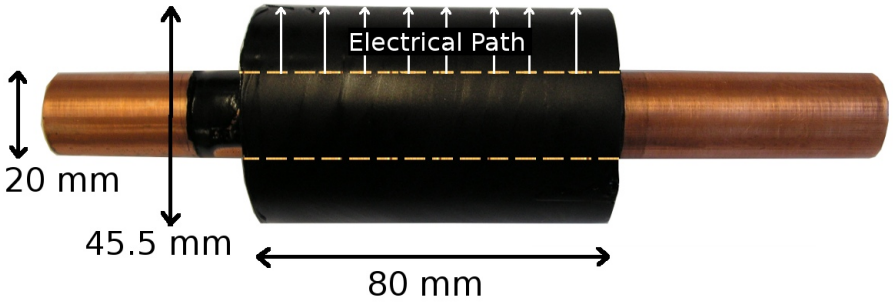

Figure 10.7: Copper coating of a cylinder of CNT/UPE

a out layer of nanocomposite to carry the current to the surface of the cylinder. 200 grams of nanocomposite were mould around the spine and sized by lathe to the desired diameter. The cylinder was electroplated in a modified version of the setup presented in figure 10.2, with the cylinder revolving in the copper solution and the current applied to the copper spine. The spine was coated with Araldite® 420 to avoid direct contact with the copper solution. The voltage was limited at 12 V and the maximum current density was 0.65 $\mathrm{A/dm^2}$; the deposition was carried out for 72 hours to deposit $500\,\mu\mathrm{m}$ of copper.

Figure 10.8 shows the cylinder at the beginning and at the end of the process of deposition. Excluding air bubbles formed during the moulding of the nanocomposite, the layer of copper

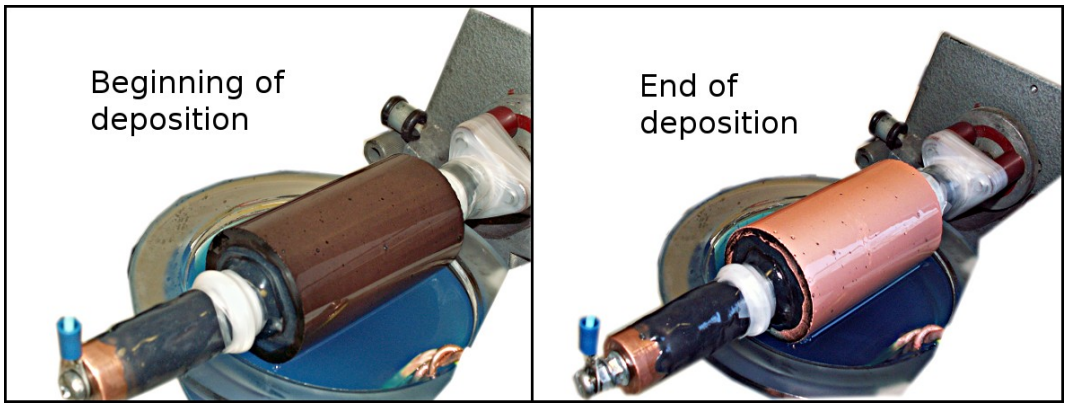

Figure 10.8: Copper coating of a cylinder of CNT/UPE

is consistent and homogeneous.

Resistance heating

Nanocomposites prepared in this study have been tested for resistance heating. The material used had a filler loading of 0.25 wt%, an electrical conductivity of 0.5 S/m. The dimension of the specimen are detailed in figure 10.9a. The two electrical connections have been painted on the specimen using Electrodag®1415M and thoroughly dried before testing. The DC voltage

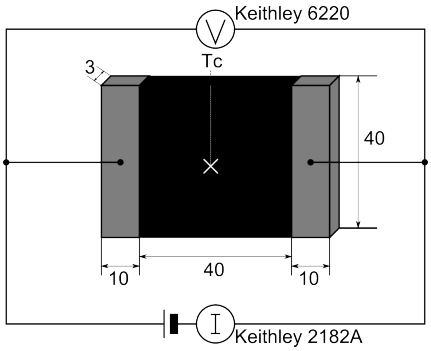

(a)

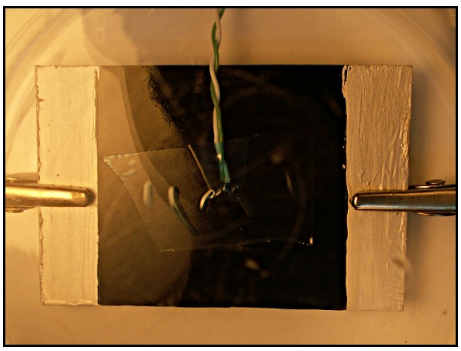

(b)

Figure 10.9: Sketch of the testing apparatus (a) and nanocomposite under testing for resistance heating (b).

and the current supplied were controlled with a combination of two Keithley® instruments (6220 and 2182A). The temperature of the sample was measured by a type K thermocouple

placed on the surface of the specimen. The assembly of figure 10.9b was positioned in a glass enclosure to minimise perturbations. The experiment was carried out varying the voltage from 0 to 70 V, allowing 20 minutes for the stabilisation of the temperature after each voltage change. The specific heating power was calculated as follows:

$$P_s = \frac{I \cdot V}{A} \tag{10.4}$$

where A=0.0016 m^2 is the area of the specimen.

As shown in figure 10.10 the heating of the specimen increases quadratically with voltage, as expected for Joule (equation 2.9). The temperature of the sample starts to increase with the application of 10 V and it reaches as much as 130°C with the application of 70 V. The specific heating power increases quadratically with voltage, but with significant point-to-point fluctuations. This is a consequence of small variations of the nanocomposite conductivity with temperature, which result from several contributions, such as the temperature-conductivity dependence of the nanotubes, the thermal expansion and the glass transition of the resin of 58°C [88].

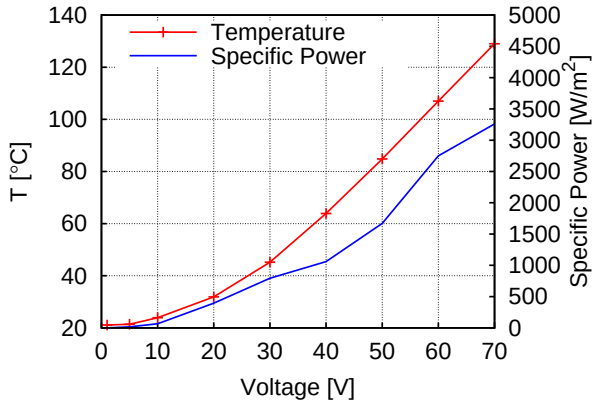

Figure 10.10: Sample temperature and specific heating power as function of the voltage applied, for the resistance heating of the specimen of figure 10.9a.

10.2 Scale-up exercise

The dispersion of carbon nanotubes in unsaturated polyester resin has been scaled up to the preparation of 20 kg batches, an intermediate step toward a final scale of 200 to 2000 kg batches. The triple roll mill used is a fixed speed, manually controlled gap machine, similar to the one used for lab scale operations (see figure 10.11a). The setup for shear mixing comprises a heavy-duty dissolver disk and a 40 lt cylindrical vessel, as shown in figure 10.11b, which creates the flow pattern of figure 10.11c. The geometry of the mixer

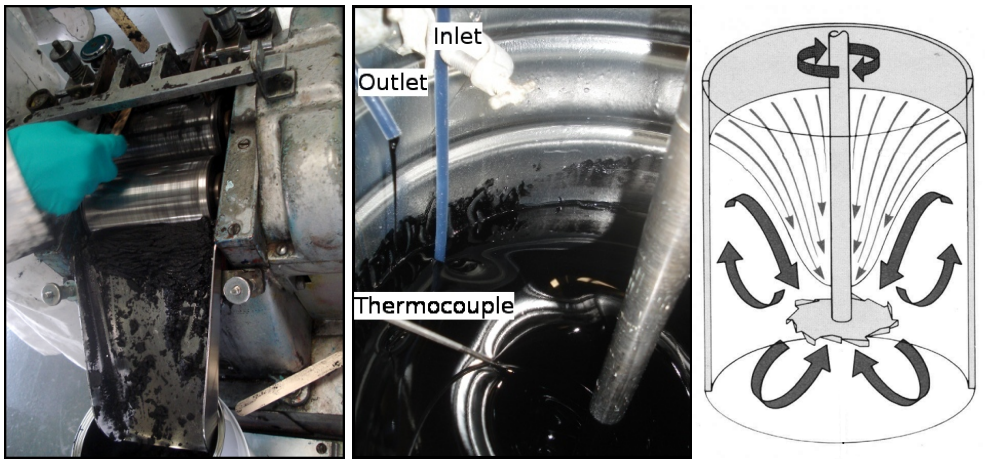

(a) **(b)** **(c)**

Figure 10.11: Preparation of a 20 kg batch of CNT/UPE: triple roll milling (a), shear mixer (b) and flow pattern of a dissolver disk in a cylindrical vessel [124] (c).

is different than the lab scale, where a semi-circular paddle spins in a round-bottom flask (see figure 4.7). The vessel used in the industrial setup is open, thus it does not allow the implementation of a styrene re-condensation system. It also dissipates heat less efficiently than the lab scale flask, due to the high volume-to-surface ratio. The higher temperature is likely to cause consistent styrene evaporation. The liquid conductivity during mixing has been monitored on-line, as shown in figure 10.12, to follow the evolution of filler dispersion by the calculation of the electric dispersion index of section 7.3.

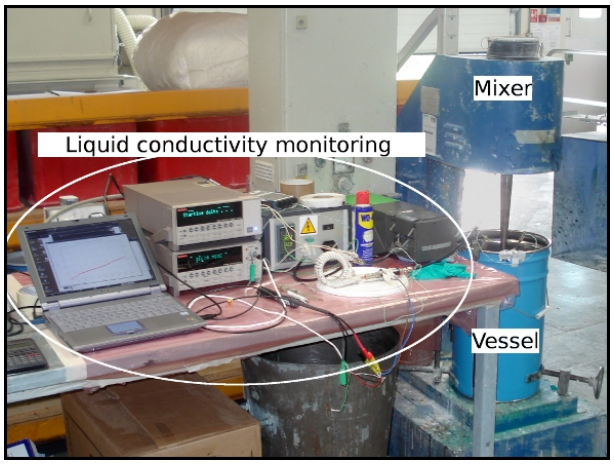

Figure 10.12: Industrial setup for shear mixing of 20 kg batches of nanocomposites

Experimental details

The masterbatch was prepared compounding 100 g of NC7000 nanotubes and 2.757 kg of styrene with a dissolver disk at 1000 rpm for 1 minute and 1500 rpm for 2 minutes (initial filler loading 3.5 wt%). The resulting paste was triple roll milled twice: the first time coarsely, to obtain a thick, uniform paste and the second time setting a small gap to reduce the aggregate dimension as much as possible.

Two approaches to the dispersion of CNTs in the resin by shear mixing have been tested, with the aim to improve the efficiency of the process.

Direct mixing approach UPE resin was added to 1 kg of masterbatch up to 20 kg of total mixture, to obtain filler loading of 0.2 wt%. The mixture was stirred with the 40 lt stirrer and vessel at standard speed, which correspond to a funnel shaped as illustrated in figure 10.13. The rotating speed was increased slightly after 110 minutes, still maintaining the standard flow pattern.

Step dilution approach UPE resin was added to 1 kg of masterbatch up to 3 kg of total mixture and stirred with a Dispermat® CA mixer, adjusting the speed between 1000 and 1700

rpm. Resin was added in steps, as reported in table 10.1, moving to the 40 litres vessel and mixer for the mixing of 10 kg or more of mixture. After 255 minutes the speed of the plant

Table 10.1: Step dilution in the preparation of 20 kg batch of mixture. The terms "standard" and "high shear" indicates the mixing modes of figure 10.13a and 10.13b, respectively.

Mixing time [min]	CNT [wt %]	Mixer	Rotational speed [rpm]
0 - 15	1.33	small	1000÷1700
15 - 40	1	small	1000÷1700
40 - 50	0.89	small	1000
50 - 120	0.85	small	1000
120 - 160	0.4	plant	standard
160 - 255	0.2	plant	standard
255 - 270	0.2	plant	high shear

mixer was increased, to create the patter shown in figure 10.13b.

(a) **(b)**

Figure 10.13: Two mixing modes: (a) "standard" with no air inclusion and (b) "high shear" with air inclusion

Results and discussion

The trial operation of triple roll milling took about 6 hours, due to the small throughput, a consistent amount of mixture and the difficulty to work with styrene. The final filler loa-

ding, measured as described in section 4.2, was 3.97±0.22 wt%. This corresponds to the evaporation of 350 grams of styrene.

Figure 10.14 illustrates the evolution of dispersion using the direct mixing approach. The dispersion of the filler increases with time, reaching a final value of EDI of 0.62, but not as promptly as during the lab scale preparation. The temperature of the mixture reaches 50°C

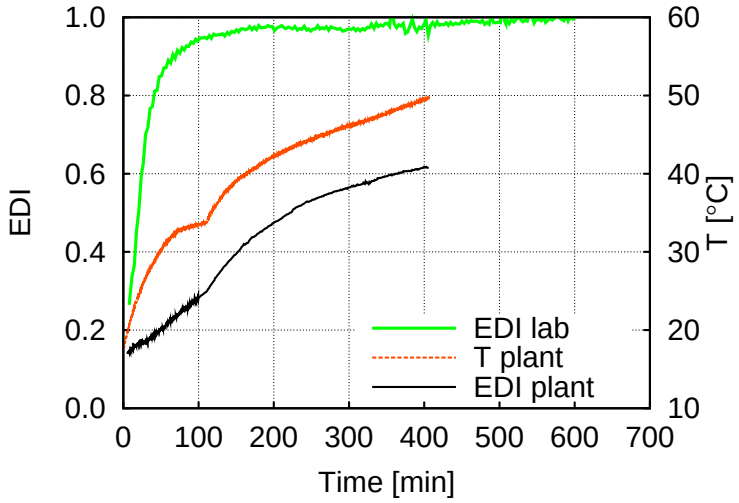

Figure 10.14: Evolution of EDI and temperature during direct mixing of 20 kg of mixture at 0.2 wt% in comparison with EDI of the lab preparation of a 0.20 wt% mixture.

during the scale-up trial, compared to the 30°C of lab processing. As a consequence 54 wt% of the initial styrene evaporates during mixing, which corresponds to 3.84 kg of styrene in total. The final conductivity of the solid composite, after compensating for the styrene lost, curing and postcuring, was $1.1 \cdot 10^{-2}$ S/m (measurement described in section 4.5). At the same loading the lab scale nanocomposite reaches $5.1 \cdot 10^{-2}$ S/m. Using the percolation data of figure 9.5b, the industrial scale preparation corresponds to a lab preparation of 0.129 wt% loading. This results in a solid conductivity efficiency[4] of 0.64, which compares well with the final value of EDI of the liquid mixture of 0.62.

The long processing time of the direct mixing approach is not industrially feasible. Step-

[4]ratio between the effective loading achieved and the total CNT loading of the nanocomposite = 0.129/0.20

dilution approach has been attempted to shorten the processing time by applying shear to concentrated, viscous mixtures, similarly to what reported in [41]. However, as shown in figure 10.15a, step-dilution is less efficient than direct mixing.

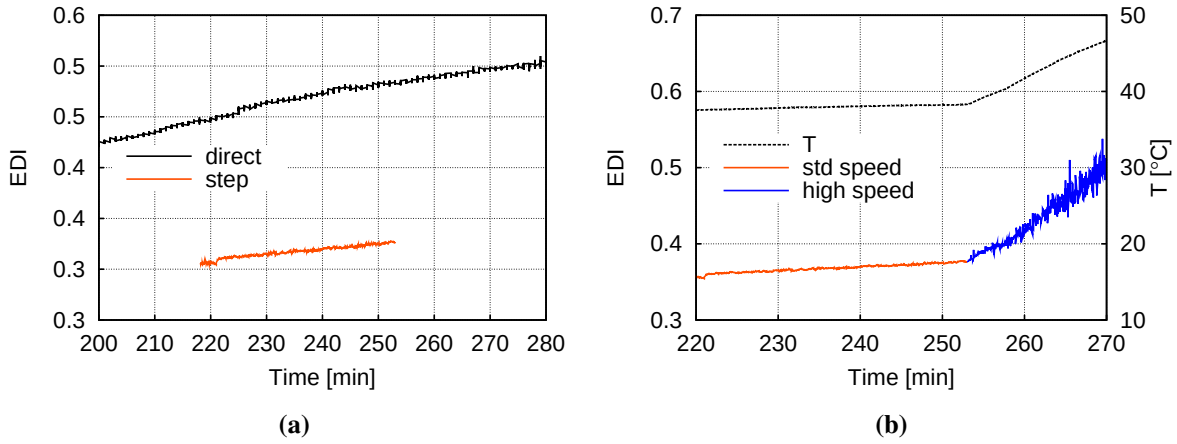

Figure 10.15: (a) Comparison of EDI by direct mixing and step dilution and (b) effect of speed in the processing of 20 kg batches of nanocomposite

The effect of high rotational speed on dispersion was tested by increasing the mixing speed above the industrial standard at 255 minutes of the step dilution trial. As illustrated in figure 10.15b, high speed mixing clearly accelerates dispersion; however, this is accompanied by a consistent temperature build-up, which is not industrially applicable for technical and health and safety reasons. The high level of noise of EDI is due to the incorporation of air in the mixture.

10.3 Conclusions

The level of conductivity of the nanocomposites prepared was sufficient for medium to high demands applications, such as copper electrodeposition and resistance heating. In spite of an electrical conductivity in the range of 10^{-1} S/m, the nanocomposite proved ineffective for shielding of electromagnetic waves, which might be attributed to the geometry of the CNT

conductive network. It can be inferred that the material should meet the requirements of less demanding applications, such as electrostatic painting, dissipation and discharge. However, the example of electromagnetic shielding suggests that electrical conductivity cannot be used as a sole criterion to support applicability. The electrical characteristics of the nanocomposite, radically different from those of metals, can play an important role in the development of applications.

The scale-up exercise served to highlight the strengths and weaknesses of the transfer of the lab-process to the industrial scale and the main processing issues that need to be addressed. In addition, the applicability of liquid conductivity dispersion monitoring to the industrial scale has been demonstrated.

Triple roll milling is scalable, but the use of styrene and the long processing time required hinder industrial adoption. To address the relevant issues, the real contribution to dispersion should be assessed. This can be done by comparing the EDI during shear mixing of triple roll milled and non-triple roll milled mixtures. Also alternative systems may be investigated, such as triple roll milling using a carrier different than styrene or ball milling of CNT/styrene suspensions.

Direct mixing is a feasible way to prepare industrial volumes of nanocomposites. However, the efficiency aspect of the process must be increased and the issue of styrene evaporation needs to be addressed. Step dilution has been already ruled out as a way to increase efficiency. Cooling of the mixture, e.g. using a water cooled vessel, and increasing the rotational speed beyond the standard speed may be a relatively easy way to address both needs.

The use of EDI in an industrial setting is a good demonstration of the potential of this technique for process control; it allows a rapid screening of the parameters affecting efficiency, e.g. the effect of rotational speed illustrated in figure 10.15b. There is also an interesting quantitative agreement between the electrical dispersion index (liquid mixture) and the efficiency of the conductivity after cure (solid composite). This suggests that EDI could

predict the electrical conductivity of the final material, which may be useful in the process optimisation.

Chapter 11

Overall discussion and Suggestions for further investigation

Chapters 5 to 10 reported results and conclusions on the individual sections of this work, namely material characterisation, CNT dispersion, dispersion monitoring, cure monitoring, conductive performance of the nanocomposites and their industrial applications.

Section 1 of this chapter combines the outcomes of these individual sections to provide an overall picture of the scientific advancements achieved and indications for the industrial exploitation of the electrical properties of the CNT/UPE nanocomposites.

The questions that still remain unanswered are listed in section 2, together with some of the possible approaches for their investigation. In addition, some of the results collected during this project inspire further investigation. What is listed is a personal, purposely non-exhaustive, account of the aspects that are worth addressing in future.

11.1 Discussion

The aim of a dispersion process is to obtain the maximum filler dispersion with the minimum damage to the filler structure. In this study dispersion has been found to correlate strongly with the processing method used. The combination of triple roll milling and horn ultrasonication leads to a good level of dispersion, as reported in figure 6.5; however, micrographic evidence of damage to the structure of the nanotubes should be taken into account (figure 5.6). The combination of triple roll milling and high shear mixing also results in a good dispersion level (see figure 5.4), but using a simpler and more industrially scalable approach. Given the non-complete dispersion of filler particles at the end of processing observed in figure 9.2, the electrical conductivity of the final nanocomposite may be further increased by refinishing of the dispersion process.

The mechanism of dispersion of the filler in the host resin has been found to be related to the structure of the as-produced carbon nanotubes, as shown in figure 5.3. The nanotubes disperse in the unsaturated polyester resin first as clusters, then as rope-like aggregates and finally as individual nanotubes, echoing the hierarchy of nanotubes, rope-like aggregates and clusters characteristic of the commercial multiwalled nanotubes used. The correlation between the morphology of the nanotubes and the mechanism of dispersion has not been investigated before. In this study the morphology of the nanotubes has been found to influence the mechanism and therefore the level of dispersion achieved, which ultimately affects the properties of the final composite. The dispersion methodology used in this study has been designed taking into account the characteristics of the nanotubes: triple roll milling helps to break the micro-structured clusters into rope-like aggregates and high shear mixing or sonication de-aggregate the ropes into individual nanotubes.

Two physical properties of the mixtures of CNTs in resin, viscosity and conductivity, have been used to monitor the dispersion of the filler during processing. The rheological approach

provides real-time assessment of dispersion by using equipment commonly available to material manufacturers composite industries and research centres. The liquid conductivity based technique uses a purpose built sensing setup to achieve on-line monitoring of dispersion. The measurement of the liquid conductivity is the basis of the calculation of the electrical dispersion index (EDI), which has been used to compare processing of mixtures at different loadings. Most of the studies published in the field of CNT nanocomposites recognise the key importance of dispersion to improve the properties of the composite, but dispersion is often assessed only qualitatively (see section 2.3). This approach is adequate for the study of the material properties, but is not appropriate for transferring nanocomposite preparations from the lab scale to the industrial scale. The methods reported in this study allow real-time monitoring of dispersion and can be valuable tools for rapid development, scale-up and process control of the preparation of nanocomposites, as has been demonstrated during the scale-up exercise of section 10.2. The newly developed EDI could be used to compare dispersion methods, processing conditions, resin systems and conductive fillers, offering direct and quantitative evaluation of dispersion.

Impedance spectroscopy of the neat unsaturated polyester resin during cure is in line with other thermosetting resins, but the behaviour of the nanocomposite is radically different. Its impedance spectrum is governed by two components: the re-aggregated carbon nanotubes and the interphase between aggregates. Using equivalent circuit modelling the evolution of the two components during cure is observed separately, giving the ability to monitor, control and optimise re-aggregation (see figures 8.6 and 8.7). The presence of aggregates and interphase has been reported in literature, e.g. [29, 31], but the contribution of the interphase to the electrical properties of the composite had been ignored so far.

The electric performance of cured nanocomposites for filler loadings between 0.05 and 0.30 wt% has been measured, giving a percolation threshold of 0.026 wt% and a maximum conductivity of $1.3 \cdot 10^{-1}\ S/m$ at the loading of 0.30 wt %. Figure 11.1 compares the re-

sults of this study with other thermosetting CNT nanocomposites reported in literature. The

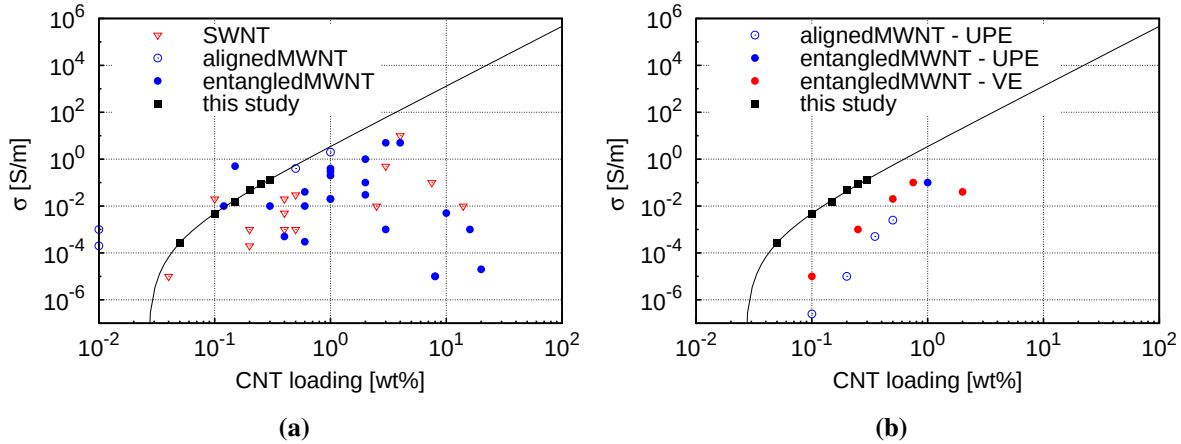

Figure 11.1: Comparison of the conductivity of the nanocomposites prepared in this study with (a) CNT-epoxy nanocomposites and (b) other thermosetting nanocomposites. Solid lines denote extrapolation of experimental data by equation 2.2. Data as reviewed in 2007 by [1] and reported in later works [39, 42].

conductivity of the nanocomposites prepared in this study is comparable with the best results obtained using entangled MWNT in epoxy resins and considerably higher than the best results obtained with unsaturated polyesters and vinyl esters. Figure 11.1 suggests that further improvement may be sought by using aligned multiwalled nanotubes or single walled nanotubes. However, the high cost of production of the filler should be taken into account.

The electrical properties of the nanocomposites prepared are adequate for using the nanocomposite for a conductivity-demanding application such as electrodeposition and resistance heating, as shown in figures 10.8 and 10.10.

The process of dispersion has been scaled up to the 20 kg scale. Scale-up is not completed at this stage. However, the points that need to be addressed to develop the industrial processing and application of the nanomaterials have been identified. In addition, reccomandations on how to progress further the scale up have been outlined.

11.2 Suggestions for further investigations

Carbon nanotube damage by processing

Irregular carbon nanotube structures have been observed by TEM, as shown in figure 5.6. The presence of defects has been observed for horn ultrasonication processing, but cannot be excluded for high shear mixing as well. The Philips CM20 scanning TEM lacks of the resolution needed to understand how and why the nanotubes are damaged, as can be seen in figure 11.2. A study of the irregularities introduced by processing, carried out using high-

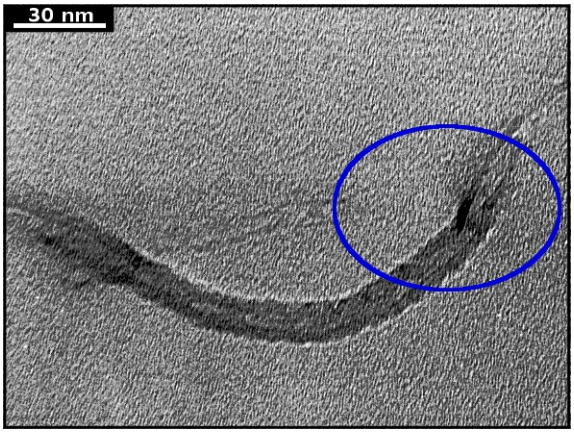

(a)

Figure 11.2: Buckling of carbon nanotubes in nanocomposites prepared by horn sonication

resolution TEM, could provide useful insights on the nature of the damage, its effects on nanocomposite properties and how damage can be avoided.

Thermosetting versus thermoplastic CNT composites

There is a marked difference of the levels of conductivity reported for thermosetting and thermoplastic nanocomposites [1]. The high conductivity of thermosetting has been related to re-aggregation during cure in several studied [30, 31, 41], and other works investigating how CNTs re-aggregates in thermoplastics, using impedance spectroscopy [49, 106, 125–128]. These results, as the example shown in figure 11.3, bear interesting similarities with

the re-aggregation during cure observed in this study. The causes of the difference between

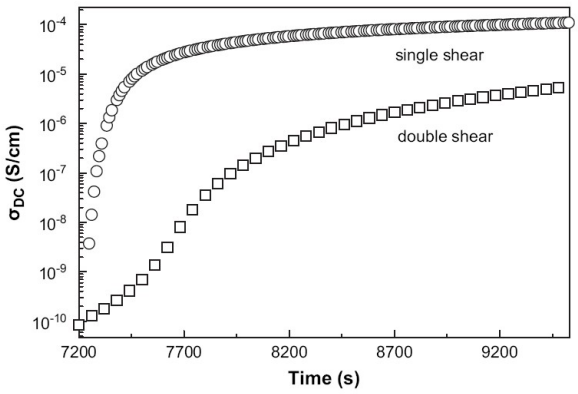

Figure 11.3: Conductivity recovery after shear application of a polycarbonate-MWNT composite [106]

thermosetting and thermoplastic nanocomposites have not been ascertained yet. Equivalent circuit modelling and the corresponding monitoring of the components contributing to the conductive network could be used effectively for addressing open questions in this area.

Direct evaluation of dispersion by image analysis

Rheology and liquid conductivity measurements are valuable tools to derive the level of dispersion of a mixture in real-time and on-line, respectively. A direct, quantitative assessment of dispersion would still be useful to characterise the dispersion of a preparation, a process or a nanocomposite, as has been attempted in [39] using TEM micrographs. Figure 11.4 is an example of the results of image analysis carried out on the optical micrographs obtained in this study[1]. Some of the original micrographs are shown in figure 5.3 on page 70 and an example of the image processing is illustrated in figure 11.5. Shear mixing causes a decrease of aggregate dimension and area covered. The technique needs to be developed further to be used for characterisation, but the example shown here exemplify the potential of using optical micrographs and image analysis for the direct assessment of nanotube dispersion.

[1]Ten micrographs analysed per sample

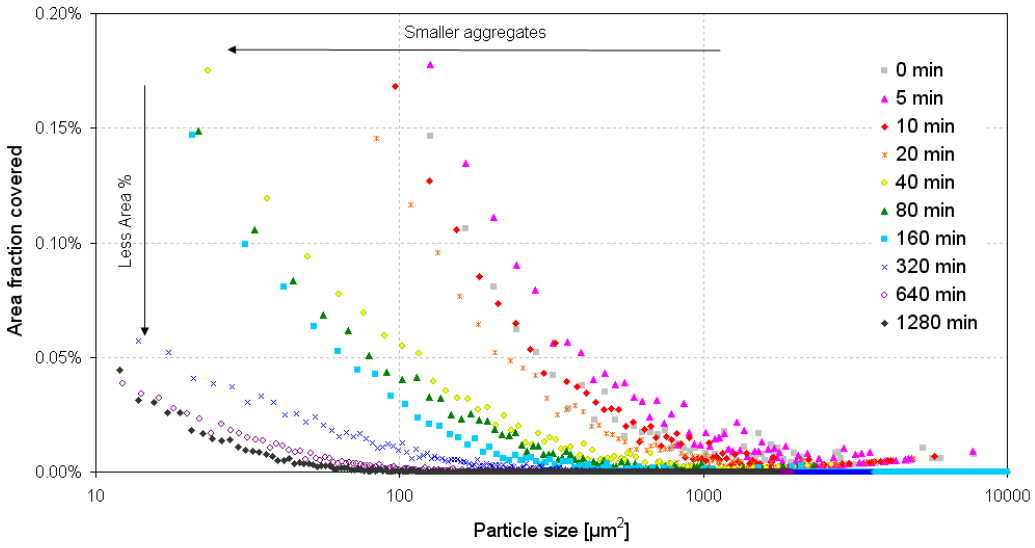

Figure 11.4: Image analysis of CNT aggregates of a CNT/UPE mixture during high shear mixing

Theoretical treatment of the excluded volume of re-aggregated filler structures

The theoretical treatment of conductive composites is not able to predict the electrical properties of a CNT nanocomposite. This shortcoming may be due to the two limit cases (see section 2.2), which do not consider partially re-aggregated structures of particles. A theoretical investigation of such structures could help to quantify the physical reasons of the conductivity enhancement by re-aggregation.

Optimisation of liquid conductivity sensor for process control purposes

The sensor described in chapter 7 has been shown to monitor effectively the evolution of dispersion during processing. Issues such as the need of temperature correction and the signal-to-noise ratio should be addressed to augment its applicability to industrial preparation of carbon nanotube composites.

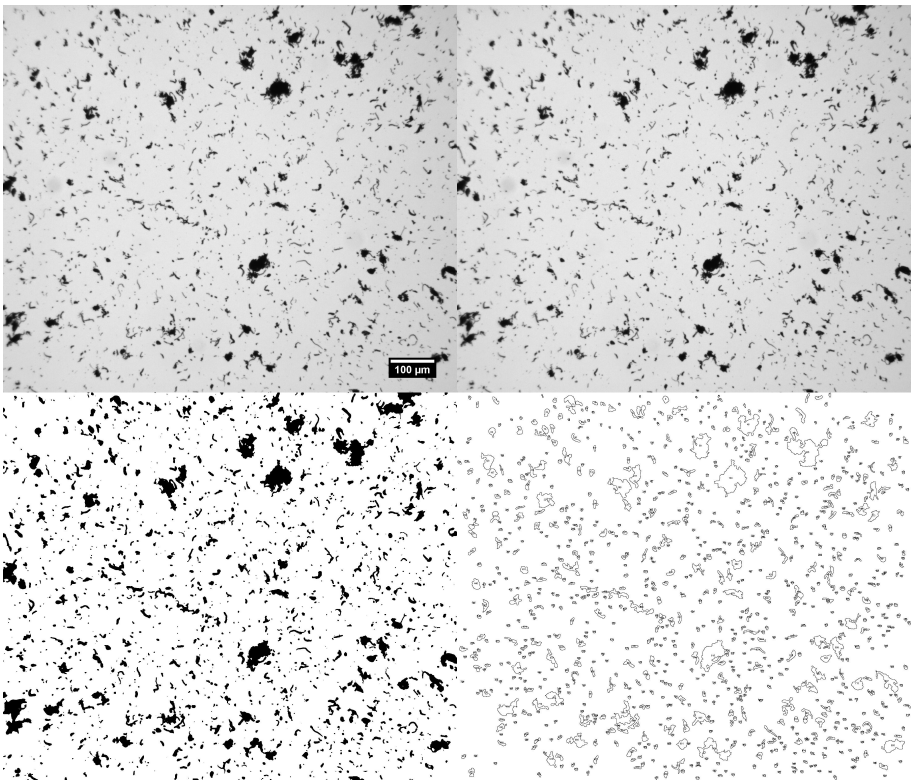

Figure 11.5: Example of image processing. Top row: 8.3 mm^2 section of the optical micrograph and scale bar; illumination-adjusted image. Bottom row: threshold image; outlines of the aggregates. 0.10 wt% CNTs in UPE, shear mixed for 5 minutes.

Investigation of the factors affecting dispersion

The electric dispersion index (EDI) developed here could be used to investigate which factors affect dispersion and how, e.g. resin chemistry and viscosity, type of filler, dispersion method and processing conditions. This may help to optimise the preparation of nanocomposites on lab and industrial scale. The scope of the EDI application could be extended to thermoplastic carbon nanotube composites.

Correlation between EDI and solid conductivity

During the scale up excercise, an interesting agreement between the EDI of the liquid mixture and the efficiency of the solid composite after cure has been found (see section 10.3). If EDI predicts the electrical conductivity of the final material, its use increases the control

over the performance of the final product. This would also be of major importance for cost optimisation of the nanocomposites processing.

Cure monitoring for the optimisation of electrical properties

This study showed how to monitor the development of a conductive network of nanotubes during thermosets cure. This could be exploited to further adjust the cure parameters, e.g. initiator, catalyst (for UPE), hardener-to-epoxy ratio (for epoxy), initial temperature and cure program, and to determine conditions optimal for the production of nanocomposites with the desired electrical properties.

Chapter 12

Conclusions

The main conclusions from this study are:

Dispersion of carbon nanotubes in unsaturated polyester resins

- combination of triple roll milling and horn sonication results in good dispersion
- combination of triple roll milling and high shear mixing gives equally good dispersion and is more industrially scalable
- as-produced nanotubes morphology influences the mechanism of dispersion
- rheology measurements offer a simple and quantitative assessment of dispersion
- on-line conductivity measurement offers the advantage of on-line monitoring
- the 'electrical dispersion index' quantifies dispersion on a 0 to 1 scale, allowing easy comparison of different preparations

Cure monitoring

- impedance spectroscopy analyses the conductive network morphology during cure
- equivalent circuit modelling data analysis separates the contributions to the signal
- electrical conductivity improves during cure due to carbon nanotube re-aggregation
- the resin-rich interphase between aggregates contributes to the overall conductivity
- cross-linking reaction affects the nanocomposite electrical properties

Electrical properties of nanocomposites prepared

- percolation threshold is 0.026 wt% filler loading
- conductivity is $1.3 \cdot 10^{-1}$ S/m at 0.30 wt% filler loading
- results are comparable to state-of-the-art nanocomposite
- materials prepared are usable for medium/high demanding commercial applications

Appendix A

Experimental details

A.1 Liquid electrical conductivity sensor

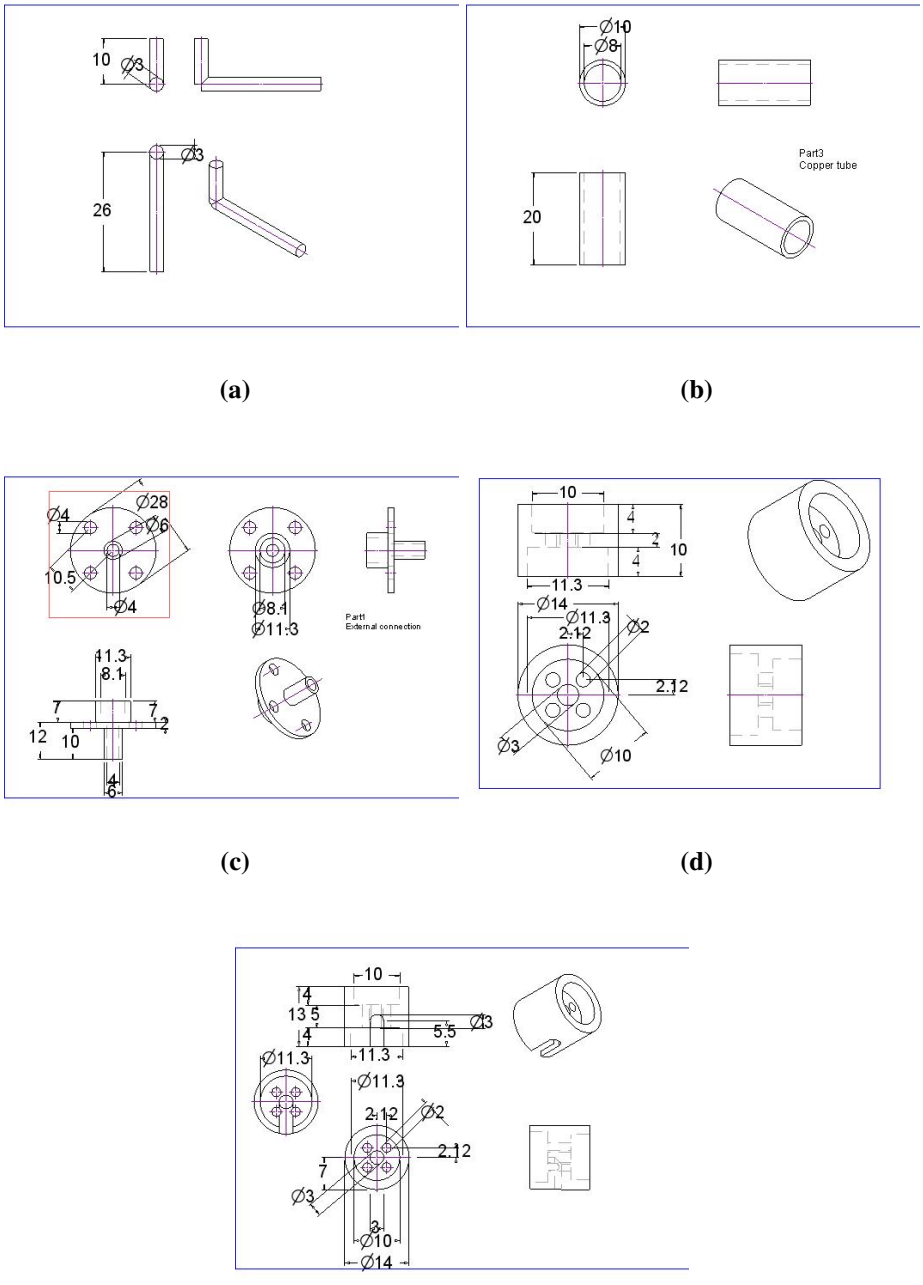

(a) **(b)**

(c) **(d)**

(e)

Figure A.1: Drawings of the components of the online resistivity cell; the material is copper for parts (a) and (b), polyoxymethylene for parts (c), (d) and (e).

A.2 Temperature correction

```
Option Explicit
Option Base 1
Sub Run()
Dim infinite As Double
Dim SegmentCount As Integer
Dim t As Integer
Dim InvTemp() As Double
Dim logResist() As Double
Dim Resist() As Double
Dim AveResist As Double
Dim AveTime As Double
Dim Time() As Double
Dim logRo As Double
Dim B As Double
Dim rsq As Double
Dim i As Integer, iStart As Integer, iStop As Integer, iStep
   As Integer
Dim arrsize As Integer
Dim j As Integer
Dim Tnot As Double
i = Cells(4, 8) 'first data point for RvsT fitting
iStep = Cells(2, 8)
Tnot = Cells(3, 8)
infinite = 0.0000001
SegmentCount = 0
Do While (Cells(i + 1, 1) <> "")
    iStart = i
searchnext:
    i = i + iStep
    If Cells(i, 4) < Cells(i + iStep, 4) Then
        t = 1
        ElseIf Cells(i, 4) > Cells(i + iStep, 4) Then
        t = -1
        Else
        t = 0
    End If

    If Cells(i, 4) > Cells(i - iStep, 4) Then
        t = t
        ElseIf Cells(i, 4) < Cells(i - iStep, 4) Then
```

```
        t = -t
        Else
        t = 0
    End If

    If t = 1 Then GoTo searchnext
    If t = -1 Then
        iStop = i
        SegmentCount = SegmentCount + 1
    End If
    arrsize = (iStop - iStart)
    ReDim InvTemp(arrsize)
    ReDim logResist(arrsize)
    ReDim Resist(arrsize)
    ReDim Time(arrsize)
    For j = 0 To arrsize - 1
        Time(j + 1) = Cells(iStart + j, 1)
        InvTemp(j + 1) = 1 / (273.15 + Cells(iStart + j, 4))-
            1 / (27.15 + Tnot)
        logResist(j + 1) = Log(Cells(iStart + j, 3))
        Resist(j + 1) = Cells(iStart + j, 3)
    Next j
    AveTime = Application.Average(Time)
    AveResist = Application.Average(Resist)
    B = Application.Slope(logResist, InvTemp)
    logRo = Application.Intercept(logResist, InvTemp)
    rsq = Application.rsq(logResist, InvTemp)
    Cells(SegmentCount, 10) = AveTime
    Cells(SegmentCount, 11) = AveResist
    Cells(SegmentCount, 12) = B
    Cells(SegmentCount, 13) = logRo
    Cells(SegmentCount, 14) = Exp(logRo)
    Cells(SegmentCount, 15) = rsq
    i = iStop
Loop
End Sub
```

A.3 Dielectric data interpolation

```
Sub RCinterpol()
Dim I As Integer, II As Integer
```

```
Dim time(1 To 3) As Double
Dim f(1 To 3) As Double
Dim C(1 To 3) As Double
Dim R(1 To 3) As Double
Dim Temp(1 To 3) As Double
I = 1
Sheets(2).Name = "RCinterpolated"
Sheets(2).Cells(1, 1) = "time"
Sheets(2).Cells(1, 2) = "freq"
Sheets(2).Cells(1, 3) = "C"
Sheets(2).Cells(1, 4) = "R"
Sheets(2).Cells(1, 5) = "Temp"
Sheets(2).Cells(1, 6) = ""

    While Sheets(1).Cells(I, 1) <> ""

    'get intial values
    time(1) = Sheets(1).Cells(I, 1)
    f(1) = Sheets(1).Cells(I, 2)
    C(1) = Sheets(1).Cells(I, 3)
    R(1) = Sheets(1).Cells(I, 4)
    Temp(1) = Sheets(1).Cells(I, 7)

        'get next value with same freq
        II = I + 1
        While Sheets(1).Cells(II, 2) <> f(1)
        II = II + 1
        Wend
    time(2) = Sheets(1).Cells(II, 1)
    f(2) = Sheets(1).Cells(II, 2)
    C(2) = Sheets(1).Cells(II, 3)
    R(2) = Sheets(1).Cells(II, 4)
    Temp(2) = Sheets(1).Cells(II, 7)

        'calculate average time for the series
        If f(1) = 10000000# Then
        time(3) = (time(1) + time(2)) / 2
        Temp(3) = (Temp(1) + Temp(2)) / 2
        End If

    'calculate interpolated value
    f(3) = f(1)
```

```
    R(3) = (R(2) * (time(3) - time(1)) + R(1) * (time(2) -
       time(3))) / (time(2) - time(1))
    C(3) = (C(2) * (time(3) - time(1)) + C(1) * (time(2) -
       time(3))) / (time(2) - time(1))

    'print results
    Sheets(2).Cells(I + 1, 1) = time(3)
    Sheets(2).Cells(I + 1, 2) = f(3)
    Sheets(2).Cells(I + 1, 3) = C(3)
    Sheets(2).Cells(I + 1, 4) = R(3)
    Sheets(2).Cells(I + 1, 5) = Temp(3)

    I = I + 1
    Wend
End SubOption Explicit
Sub RCinterpol()
Dim I As Integer, II As Integer
Dim time(1 To 3) As Double
Dim f(1 To 3) As Double
Dim C(1 To 3) As Double
Dim R(1 To 3) As Double
Dim Temp(1 To 3) As Double
I = 1
Sheets(2).Name = "RCinterpolated"
Sheets(2).Cells(1, 1) = "time"
Sheets(2).Cells(1, 2) = "freq"
Sheets(2).Cells(1, 3) = "C"
Sheets(2).Cells(1, 4) = "R"
Sheets(2).Cells(1, 5) = "Temp"
Sheets(2).Cells(1, 6) = ""

    While Sheets(1).Cells(I, 1) <> ""

    'get intial values
    time(1) = Sheets(1).Cells(I, 1)
    f(1) = Sheets(1).Cells(I, 2)
    C(1) = Sheets(1).Cells(I, 3)
    R(1) = Sheets(1).Cells(I, 4)
    Temp(1) = Sheets(1).Cells(I, 7)

        'get next value with same freq
        II = I + 1
        While Sheets(1).Cells(II, 2) <> f(1)
```

```
        II = II + 1
        Wend
    time(2) = Sheets(1).Cells(II, 1)
    f(2) = Sheets(1).Cells(II, 2)
    C(2) = Sheets(1).Cells(II, 3)
    R(2) = Sheets(1).Cells(II, 4)
    Temp(2) = Sheets(1).Cells(II, 7)

        'calculate average time for the series
        If f(1) = 10000000# Then
        time(3) = (time(1) + time(2)) / 2
        Temp(3) = (Temp(1) + Temp(2)) / 2
        End If

    'calculate interpolated value
    f(3) = f(1)
    R(3) = (R(2) * (time(3) - time(1)) + R(1) * _
    (time(2) - time(3))) / (time(2) - time(1))
    C(3) = (C(2) * (time(3) - time(1)) + C(1) * _
    (time(2) - time(3))) / (time(2) - time(1))

    'print results
    Sheets(2).Cells(I + 1, 1) = time(3)
    Sheets(2).Cells(I + 1, 2) = f(3)
    Sheets(2).Cells(I + 1, 3) = C(3)
    Sheets(2).Cells(I + 1, 4) = R(3)
    Sheets(2).Cells(I + 1, 5) = Temp(3)

    I = I + 1
    Wend
End Sub
```

A.4 Genetic algorithm fitting of impedance spectra

Subroutine *RunGAscan* loads the impedance data, calls the subroutine *GA*, compares the results with the criterion of acceptance, decides whether to repeat the fit and manages the consecutive spectra. Subroutine *GA* performs the core operations of the genetic algorithm search. Subroutine *Zfunction* defines the mathematical model of the equivalent circuit (see figure 4.11 and equation 4.12).

RunGAscan

```
Option Explicit
Public ExpLogW() As Double, ExpLogReZ() As Double, ExpLogImZ
   () As Double
Public Noexppoint As Integer, paramnumber As Integer, SS As
   Integer, trimHigh As Integer
Public S As Integer
Public R1exp As Double, R2exp As Double, lambda As Double '
   regularisation parameters
 _
Public fitresult() As Double, reg() As Double
Public Sub rungaScan()
Dim ScanN As Integer, startS As Integer
Dim I As Integer
Dim vData As Integer, trimLow As Integer, attempts As Integer
   , stepS As Integer
Dim NoexppointOrig As Integer
Dim fitnesslimit As Double
Dim PrintRes As Boolean, attemptsMAX As Integer
'input the number of parameters
paramnumber = 5
ReDim fitresult(paramnumber + 1) As Double, reg(1 To
   paramnumber) As Double
'input the initial scan
startS = 20
'input the number of scans to fit
ScanN = 205
'input the maximum number of iterations
attemptsMAX = 49
'input the nuber of points in a sweep
NoexppointOrig = 29
'trimming. Specify high freq trim and low freq trim
trimHigh = 0
trimLow = 0
'Prepare the first row of sheet2 for results
Worksheets("Sheet1").Cells(1, 1) = "ScanNumber"
Worksheets("Sheet1").Cells(1, 2) = "R1"
Worksheets("Sheet1").Cells(1, 3) = "R2"
Worksheets("Sheet1").Cells(1, 4) = "C1"
Worksheets("Sheet1").Cells(1, 5) = "C2"
Worksheets("Sheet1").Cells(1, 6) = "R0"
```

```
Worksheets("Sheet1").Cells(1, 7) = "fitness"
Worksheets("Sheet1").Cells(1, 8) = "attempts"
Worksheets("Sheet1").Cells(1, 9) = "trimlow"
returnpoint:
attempts = 1
stepS = 1
If ScanN = 0 Then stepS = -1 'for the scans S<startS

For S = startS To ScanN Step stepS
    'input
    Noexppoint = NoexppointOrig - trimHigh - trimLow
    ReDim ExpLogW(1 To Noexppoint)
    ReDim ExpLogReZ(1 To Noexppoint)
    ReDim ExpLogImZ(1 To Noexppoint)
    SS = S * NoexppointOrig + 1 'set the position of the
       first cell in a scan
    'populate the input arrays
    vData = 0
        For I = 1 To Noexppoint
            If Worksheets("data").Cells(SS + I + trimHigh, 5)
                > 0 Then
                vData = vData + 1
                ExpLogW(vData) = Worksheets("data").Cells(SS
                   + I + trimHigh, 1)
                ExpLogReZ(vData) = Worksheets("data").Cells(
                   SS + I + trimHigh, 2)
                ExpLogImZ(vData) = Worksheets("data").Cells(
                   SS + I + trimHigh, 3)
            End If
        Next I
    Noexppoint = vData
    ReDim Preserve ExpLogW(1 To Noexppoint)
    ReDim Preserve ExpLogReZ(1 To Noexppoint)
    ReDim Preserve ExpLogImZ(1 To Noexppoint)
    I = I
    'call the runga sub
    runga
    'check the quality of the result and decide if to repeat
       the fit
    PrintRes = False
    SS = S + 2
    fitnesslimit = 1.2 * Worksheets("Sheet1").Cells(SS -
       stepS, paramnumber + 2)
```

```
    Worksheets("Sheet1").Cells(SS, paramnumber + 3) =
       attempts
    If fitresult(0) < fitnesslimit Then
        PrintRes = True
        attempts = 1
    ElseIf attempts > attemptsMAX Then
        attempts = 1
    Else
        S = S - stepS
        attempts = attempts + 1
    End If
    'print the best result of repeated fittings
    If attempts = 2 Or fitresult(0) < Worksheets("Sheet1").
       Cells(SS, paramnumber + 2) Then PrintRes = True
    'swap R1C1<->R2C2 if necessary
    If PrintRes = True Then
        If (fitresult(1) + fitresult(3)) > (fitresult(2) +
           fitresult(4)) Then
            fitresult(6) = fitresult(1)
            fitresult(1) = fitresult(2)
            fitresult(2) = fitresult(6)
            fitresult(6) = fitresult(3)
            fitresult(3) = fitresult(4)
            fitresult(4) = fitresult(6)
        End If
        For I = 1 To paramnumber
            Worksheets("Sheet1").Cells(SS, I + 1) = 10 ^
               fitresult(I)
        Next I
        Worksheets("Sheet1").Cells(SS, 1) = SS - 2
        Worksheets("Sheet1").Cells(SS, paramnumber + 2) =
           fitresult(0)
        Worksheets("Sheet1").Cells(SS, paramnumber + 4) =
           trimLow
    End If
Next S
'continue for S<startS
If ScanN <> 0 Then
    ScanN = 0
    trimLow = 5
    GoTo returnpoint
End If
End Sub
```

GA

```
Option Explicit
Public apppath As String
Dim GenIndividual As Integer, generation As Integer
Dim OpenF1 As String, OpenF2 As String, OpenF3 As String
Dim GenStep As Integer, SolvedFlag As Integer
Dim StepofGen As Integer
Public Sub runga()
Dim measurement As Double, rndfactor As Double, Averagesigma
    As Double, invfitness1 As Double, ball As Double,
    totalfitness As Double, roulette As Double, deviationsigma
     As Double, totalsigma As Double, exchange As Double, norm
     As Double, rest As Double, mutation As Double, modelvalue
     As Double, invfitness As Double, Averagefitness As Double
    , Deviationfitness As Double
Dim ReproduceNumber As Integer, crossover As Integer,
    gennumber As Integer, crossoverdigit As Integer,
    crossoverdigit1 As Integer, crossoverPRM As Integer,
    crossoverdigit2 As Integer, DigitNumber As Integer, k As
    Integer, PRM As Integer, n As Integer, m As Integer,
    SurviveNumber As Integer, SampleNumber As Integer,
    NumberofGenerations As Integer, StackPosition As Integer,
    TopIndividual As Integer, I As Integer, J As Integer,
    parent1 As Integer, parent2 As Integer, individual As
    Integer, NotAlreadyinStack As Integer, Flag As Integer
Dim OpenFLO1 As String, OpenFLO2 As String, OpenFL61 As
    String, Sensor As Integer
Dim Arr() As Variant
'required input
     'paramnumber as integer
     'Noexppoint
     'ExpLogW(Noexppoint)
     'ExpLogReZ(Noexppoint)
     'ExpLogImZ (Noexppoint)
ReDim Range(1 To paramnumber) As Double, mean(1 To
    paramnumber) As Double
'Dim Noexppoint As Integer 'alraedy declared in rungascan
Dim exppoint As Integer, counter As Integer
'Define initial value of the parameters
'set the initial parameters mean
mean(1) = ExpLogReZ(Noexppoint)
```

```
mean(2) = mean(1)
mean(3) = -10
mean(4) = -10
mean(5) = 2
'Define initial range of the parameters
Range(1) = 0.5 * mean(1)
Range(2) = 0.5 * mean(2)
Range(3) = 0.3 * mean(3)
Range(4) = 0.3 * mean(4)
Range(5) = 0.5 * mean(5)
'get real random numbers, using "time" as seed value
Randomize
'input
'-----------------------------------------------------------
SolvedFlag = 0
'Accuracy of the solution. Resolution 2^digitnumber-1
DigitNumber = 41
'input
SampleNumber = 199
'input
ReproduceNumber = 199
'input
SurviveNumber = 3
'input
NumberofGenerations = 100
'input
mutation = 0.05
'input
exchange = 0.5
'input
'crossover = 0.6
ReDim sigma(SampleNumber) As Double, param(0 To 1,
   SampleNumber, paramnumber) As Double, Fitness(0 To
   SampleNumber) As Double
ReDim best(1 To SampleNumber) As Integer
ReDim digit(DigitNumber, SampleNumber, 0 To 1, paramnumber)
   As Integer
ReDim regfactor(0 To SampleNumber) As Double 'regularisation
'First Generation
    For PRM = 1 To paramnumber
        For individual = 1 To SampleNumber
            param(0, individual, PRM) = mean(PRM) + ((Rnd(Rnd
               ) - 0.5) * Range(PRM))
```

```
        Next individual
    Next PRM
'Digitise first generation
For PRM = 1 To paramnumber
    For individual = 1 To SampleNumber
        norm = Int((param(0, individual, PRM) - (mean(PRM) -
           Range(PRM))) / (2 * Range(PRM)) * (2 ^ (
           DigitNumber) - 1))
        For m = DigitNumber To 1 Step -1
            rest = 0
            For n = DigitNumber To m + 1 Step -1
                rest = digit(n, individual, 0, PRM) * 2 ^ (n
                   - 1) + rest
            Next n
            digit(m, individual, 0, PRM) = Int((norm - rest)
               / 2 ^ (m - 1))
            Next m
    Next individual
Next PRM
'.....................................................
For generation = 2 To NumberofGenerations
    rndfactor = Rnd(Rnd)
'Dedigitalasation of the previous generation
    For PRM = 1 To paramnumber
        For individual = 1 To SampleNumber
            norm = 0
            For n = 1 To DigitNumber
                norm = digit(n, individual, 0, PRM) * 2 ^ (n
                   - 1) + norm
            Next n
            param(0, individual, PRM) = (mean(PRM) - Range(
               PRM)) + (2 * Range(PRM)) * norm / (2 ^ (
               DigitNumber) - 1)
                ' print PRM(?) in sheet3
                'If PRM = 1 Then
                'Worksheets("sheet3").Cells(individual,
                   generation) = param(0, individual, PRM)
                'End If
        Next individual
    Next PRM
'Fitness measurement
    For individual = 1 To SampleNumber
       invfitness = 0
```

```
        GenIndividual = individual
        counter = 0
        For exppoint = 1 To Noexppoint
                counter = counter + 1
                'input
                'define arguments of the model
                Arr = Z(10 ^ ExpLogW(exppoint), 10 ^ param(0,
                    individual, 1), 10 ^ param(0, individual,
                    2), 10 ^ param(0, individual, 3), 10 ^
                   param(0, individual, 4), 10 ^ param(0,
                   individual, 5))  ', 10 ^ param(0,
                   individual, 6)) ', param(0, individual, 7)
                   )
                invfitness = (Abs((Arr(0) - (10 ^ ExpLogReZ(
                   exppoint)))) ^ 2 + Abs((Arr(1) - (10 ^
                   ExpLogImZ(exppoint)))) ^ 2) + invfitness
                   'ColeCole distance fit
        Next exppoint
        I = I
        invfitness = invfitness / counter
        Fitness(individual) = 1 / (invfitness)
    Next individual
     '.....................................................
    Fitness(0) = -8065014
'Sort  the sample
    For StackPosition = 1 To SampleNumber
            For individual = 1 To SampleNumber
            NotAlreadyinStack = 1
                For TopIndividual = 1 To StackPosition - 1
                    If best(TopIndividual) <> individual Then
                        Flag = 1
                    Else
                        Flag = 0
                    End If
                    NotAlreadyinStack = Flag *
                       NotAlreadyinStack
                Next TopIndividual
            If Fitness(individual) > Fitness(best(
               StackPosition)) And NotAlreadyinStack = 1 Then
                best(StackPosition) = individual
        Next individual
    Next StackPosition
```

```
    'fill generation number, fitness and parameter value in
       sheet2
    '         Worksheets("sheet2").Cells(S * 36 + 1,
       generation) = generation - 1
    '         Worksheets("sheet2").Cells(S * 36 + 8,
       generation) = 1 / Fitness(best(1))
    '         Worksheets("sheet2").Cells(S * 36 + 9,
       generation) = regfactor(best(1))
    '         For PRM = 1 To paramnumber
    '                 Worksheets("sheet2").Cells(S * 36 + PRM
       + 1, generation) = param(0, best(1), PRM)
    '         Next PRM
'.....................................................
'Best  in the next Generation
    For I = 1 To SurviveNumber
        For PRM = 1 To paramnumber
            For m = 1 To DigitNumber
                digit(m, I, 1, PRM) = digit(m, best(I), 0,
                   PRM)
            Next m
        Next PRM
    Next I
'Calculation of fitness average and deviation
    Averagefitness = 0
    For I = 1 To ReproduceNumber
        Averagefitness = Averagefitness + Fitness(best(I)) /
           ReproduceNumber
    Next I
    totalfitness = Averagefitness * ReproduceNumber
    Deviationfitness = 0
    For I = 1 To ReproduceNumber
        Deviationfitness = Deviationfitness + (Averagefitness
           - Fitness(best(I))) ^ 2 / ReproduceNumber
    Next I
    Deviationfitness = Deviationfitness ^ 0.5
    If Deviationfitness <> 0 Then
        For I = 1 To ReproduceNumber
            sigma(best(I)) = 1 + (Fitness(best(I)) -
               Averagefitness) / (2 * Deviationfitness)
            If sigma(best(I)) < 0 Then sigma(best(I)) = 0
        Next
    Else
       For I = 1 To ReproduceNumber
```

```
            sigma(best(I)) = 1 + (Fitness(best(I)) -
               Averagefitness) / (2 * 10 ^ -6)
            If sigma(best(I)) < 0 Then sigma(best(I)) = 0
        Next
    End If
    Averagesigma = 0
    totalsigma = 0
    For I = 1 To ReproduceNumber
        Averagesigma = Averagesigma + sigma(best(I)) /
           ReproduceNumber
        totalsigma = sigma(best(I)) + totalsigma
    Next I
    'Adaptive mutation
    mutation = 0.5 * Exp(-4 * (Abs(Deviationfitness /
       Averagefitness)) ^ 0.5)
'.....................................................
    For J = SurviveNumber + 1 To SampleNumber Step 2
'Parents Selection
       ball = Rnd(Rnd) * totalsigma
        roulette = 0
        For I = 1 To ReproduceNumber
            roulette = sigma(best(I)) + roulette
            If roulette > ball Then
                parent1 = best(I)
                I = ReproduceNumber
            End If
        Next I
        ball = Rnd(Rnd) * totalsigma
        roulette = 0
        For I = 1 To ReproduceNumber
            roulette = sigma(best(I)) + roulette
            If roulette > ball Then
                parent2 = best(I)
                I = ReproduceNumber
            End If
        Next I
'.....................................................
' reproduction
'uniform
        For PRM = 1 To paramnumber
            For m = 1 To DigitNumber
                If Rnd(Rnd) > exchange Then
```

```
                    digit(m, J, 1, PRM) = digit(m, parent1,
                       0, PRM)
                    digit(m, J + 1, 1, PRM) = digit(m,
                       parent2, 0, PRM)
                Else
                    digit(m, J, 1, PRM) = digit(m, parent2,
                       0, PRM)
                    digit(m, J + 1, 1, PRM) = digit(m,
                       parent1, 0, PRM)
                End If
                If Rnd(Rnd) < mutation Then
                    digit(m, J, 1, PRM) = Abs(digit(m, J, 1,
                       PRM) - 1)
                End If
                If Rnd(Rnd) < mutation Then
                    digit(m, J + 1, 1, PRM) = Abs(digit(m, J
                       + 1, 1, PRM) - 1)
                End If
            Next m
        Next PRM
            For PRM = 1 To paramnumber
                For m = 1 To DigitNumber
                    If Rnd(Rnd) < mutation Then
                        digit(m, J, 1, PRM) = Abs(digit(m, J,
                           1, PRM) - 1)
                    End If
                    If Rnd(Rnd) < mutation Then
                        digit(m, J + 1, 1, PRM) = Abs(digit(m
                           , J + 1, 1, PRM) - 1)
                    End If
                Next m
            Next PRM
    Next J
    For J = 1 To SampleNumber
        For PRM = 1 To paramnumber
            For m = 1 To DigitNumber
                digit(m, J, 0, PRM) = digit(m, J, 1, PRM)
            Next m
        Next PRM
    Next J
If SolvedFlag = 1 Then GoTo 110
Next generation
110
```

```
 'store the final of fit in fitresult() for runGAscan
    fitresult(0) = 1 / Fitness(best(1))
    For I = 1 To paramnumber
     fitresult(I) = param(0, best(1), I)
    Next I
End Sub
```

Zfunction

```
Function Z(w, R1, R2, C1, C2, R0)
k = k
Dim ReZ As Double
Dim ImZ As Double
Dim Arr() As Variant
ReDim Arr(1)
ReZ = R1 / (1 + (R1 * C1 * w) ^ 2) + R2 / (1 + (R2 * C2 * w)
   ^ 2) + R0
ImZ = R1 ^ 2 * C1 * w / (1 + (R1 * C1 * w) ^ 2) + R2 ^ 2 * C2
    * w / (1 + (R2 * C2 * w) ^ 2)
Arr(0) = ReZ
Arr(1) = ImZ
Z = Arr
End Function
```

Bibliography

[1] W. Bauhofer and J. Z. Kovacs. A review and analysis of electrical percolation in carbon nanotube polymer composites. *Composites Science and Technology*, 69(10): 1486–1498, 8 2009.

[2] M. Moniruzzaman and K. I. Winey. Polymer nanocomposites containing carbon nanotubes. *Macromolecules*, 39(16):5194–5205, 2006.

[3] J. N. Coleman, U. Khan, W. J. Blau, and Y. K. Gun'ko. Small but strong: A review of the mechanical properties of carbon nanotube-polymer composites. *Carbon*, 44(9): 1624–1652, 2006.

[4] M. Endo, M. S. Strano, and P. M. Ajayan. *Potential applications of carbon nanotubes*, volume 111. 2008.

[5] S. Iijima. Helical microtubules of graphitic carbon. *Nature*, 354(6348):56–58, 1991.

[6] M. Meyyappan. *Carbon nanotubes: science and applications*. Boca Raton, FL : CRC Press, 2005. ISBN 0849321115.

[7] Y. Gogotsi. *Nanotubes and Nanofibers (Advanced Materials)*. Boca Raton, FL : CRC Press, 2006. ISBN 0849393876.

[8] P. J. F. Harris. *Carbon Nanotubes and Related Structures*. Cambridge University Press, Cambridge, 2003. ISBN 0521005337.

[9] Wikimedia Foundation. Wikimedia commons. URL `commons.wikimedia.org`.

[10] B. O. Boskovic. Carbon nanotubes and nanofibres. *Nanotechnology Perceptions*, 3(3): 141–158, 2007.

[11] I. W. Chiang, B. E. Brinson, A. Y. Huang, P. A. Willis, M. J. Bronikowski, J. L. Margrave, R. E. Smalley, and R. H. Hauge. Purification and characterization of single-wall carbon nanotubes (SWNTs) obtained from the gas-phase decomposition of CO (HiPco process). *Journal of Physical Chemistry B*, 105(35):8297–8301, 2001.

[12] J. Sumfleth, K. Prehn, M. H. G. Wichmann, S. Wedekind, and K. Schulte. A comparative study of the electrical and mechanical properties of epoxy nanocomposites reinforced by cvd- and arc-grown multi-wall carbon nanotubes. *Composites Science and Technology*, 70(1):173–180, 2010.

[13] X. L Xie, Y. W Mai, and X. P Zhou. Dispersion and alignment of carbon nanotubes in polymer matrix: A review. *Materials Science and Engineering R: Reports*, 49(4): 89–112, 2005.

[14] V. Krstic, S. Roth, and M. Burghard. Phase breaking in three-terminal contacted single-walled carbon nanotube bundles. *Physical Review B - Condensed Matter and Materials Physics*, 62(24):R16353–R16355, 2000.

[15] S. Datta. Electrical resistance: An atomistic view. *Nanotechnology*, 15(7):S433–S451, 2004.

[16] P. Poncharal, C. Berger, Y. Yi, Z. L. Wang, and W. A. De Heer. Room temperature ballistic conduction in carbon nanotubes. *Journal of Physical Chemistry B*, 106(47): 12104–12118, 2002.

[17] R. Schueler, J. Petermann, K. Schulte, and H. P Wentzel. Agglomeration and electrical percolation behavior of carbon black dispersed in epoxy resin. *Journal of Applied Polymer Science*, 63(13):1741–1746, 1997.

[18] M. L. Clingerman, J. A. King, K. H. Schulz, and J. D. Meyers. Evaluation of electrical

conductivity models for conductive polymer composites. *Journal of Applied Polymer Science*, 83(6):1341–1356, 2002.

[19] M. L. Clingerman, E. H. Weber, J. A. King, and K. H. Schulz. Development of an additive equation for predicting the electrical conductivity of carbon-filled composites. *Journal of Applied Polymer Science*, 88(9):2280–2299, 2003.

[20] S. Kirkpatrick. Percolation and conduction. *Reviews of Modern Physics*, 45(4):574–588, 1973.

[21] D. S. McLachlan, C. Chiteme, C. Park, K. E. Wise, S. E. Lowther, P. T. Lillehei, E. J. Siochi, and J. S. Harrison. AC and DC percolative conductivity of single wall carbon nanotube polymer composites. *Journal of Polymer Science, Part B: Polymer Physics*, 43(22):3273–3287, 2005.

[22] A. Celzard, E. McRae, C. Deleuze, M. Dufort, G. Furdin, and J. F. Mareche. Critical concentration in percolating systems containing a high-aspect-ratio filler. *Physical Review B - Condensed Matter and Materials Physics*, 53(10):6209–6214, 1996.

[23] I. Balberg, C. H. Anderson, S. Alexander, and N. Wagner. Excluded volume and its relation to the onset of percolation. *Physical Review B*, 30(7):3933–3943, 1984.

[24] F. Dalmas, R. Dendievel, L. Chazeau, J. Y Cavaille, and C. Gauthier. Carbon nanotube-filled polymer composites. numerical simulation of electrical conductivity in three-dimensional entangled fibrous networks. *Acta Materialia*, 54(11):2923–2931, 2006.

[25] F. Hussain, M. Hojjati, M. Okamoto, and R. E. Gorga. Review article: Polymer-matrix nanocomposites, processing, manufacturing, and application: An overview. *Journal of Composite Materials*, 40(17):1511–1575, 2006.

[26] E. T. Thostenson, C. Li, and T. W Chou. Nanocomposites in context. *Composites Science and Technology*, 65(3-4):491–516, 2005.

[27] E. T. Thostenson, Z. Ren, and T. W Chou. Advances in the science and technology of carbon nanotubes and their composites: A review. *Composites Science and Technology*, 61(13):1899–1912, 2001.

[28] P. J. F. Harris. Carbon nanotube composites. *International Materials Reviews*, 49(1): 31–43, 2004.

[29] C. A. Martin, J. K. W. Sandler, M. S. P. Shaffer, M. K Schwarz, W. Bauhofer, K. Schulte, and A. H. Windle. Formation of percolating networks in multi-wall carbon-nanotube-epoxy composites. *Composites Science and Technology*, 64(15):2309–2316, 2004.

[30] J. K. W. Sandler, J. E. Kirk, I. A. Kinloch, M. S. P. Shaffer, and A. H. Windle. Ultra-low electrical percolation threshold in carbon-nanotube-epoxy composites. *Polymer*, 44(19):5893–5899, 2003.

[31] M. B. Bryning, M. F. Islam, J. M. Kikkawa, and A. G. Yodh. Very low conductivity threshold in bulk isotropic single-walled carbon nanotube-epoxy composites. *Advanced Materials*, 17(9):1186–1191, 2005.

[32] M. H. G. Wichmann, J. Sumfleth, B. Fiedler, F. H. Gojny, and K. Schulte. Multiwall carbon nanotube/epoxy composites produced by a masterbatch process. *Mechanics of Composite Materials*, 42(5):395–406, 2006.

[33] C. A. Martin, J. K. W. Sandler, A. H. Windle, M. K Schwarz, W. Bauhofer, K. Schulte, and M. S. P. Shaffer. Electric field-induced aligned multi-wall carbon nanotube networks in epoxy composites. *Polymer*, 46(3):877–886, 2005.

[34] A. Moisala, Q. Li, I. A. Kinloch, and A. H. Windle. Thermal and electrical conductivity of single- and multi-walled carbon nanotube-epoxy composites. *Composites Science and Technology*, 66(10):1285–1288, 2006.

[35] F. H. Gojny, M. H. G. Wichmann, B. Fiedler, I. A. Kinloch, W. Bauhofer, A. H. Windle,

and K. Schulte. Evaluation and identification of electrical and thermal conduction mechanisms in carbon nanotube/epoxy composites. *Polymer*, 47(6):2036–2045, 2006.

[36] A. Allaoui, S. Bai, H. M. Cheng, and J. B. Bai. Mechanical and electrical properties of a MWNT/epoxy composite. *Composites Science and Technology*, 62(15):1993–1998, 2002.

[37] J. A. Kim, D. G. Seong, T. J. Kang, and J. R. Youn. Effects of surface modification on rheological and mechanical properties of CNT/epoxy composites. *Carbon*, 44(10): 1898–1905, 2006.

[38] S. Arepalli, S. W. Freiman, S. A. Hooker, and K. D. Migler. Measurement issues in single-wall carbon nanotubes. Technical Report Special Publication (NIST SP) - 1071, NIST, 2008.

[39] J. Vera-Agullo, A. Gloria-Pereira, H. Varela-Rizo, J. L. Gonzalez, and I. Martin-Gullon. Comparative study of the dispersion and functional properties of multiwall carbon nanotubes and helical-ribbon carbon nanofibers in polyester nanocomposites. *Composites Science and Technology*, 69(10):1521–1532, 2009.

[40] P. Potschke, A. R. Bhattacharyya, A. Janke, S. Pegel, A. Leonhardt, C. Taschner, M. Ritschel, S. Roth, B. Hornbostel, and J. Cech. Melt mixing as method to disperse carbon nanotubes into thermoplastic polymers. *Fullerenes Nanotubes and Carbon Nanostructures*, 13(SUPPL. 1):211–224, 2005.

[41] J. Z. Kovacs, B. S. Velagala, K. Schulte, and W. Bauhofer. Two percolation thresholds in carbon nanotube epoxy composites. *Composites Science and Technology*, 67(5): 922–928, 2007.

[42] E. T. Thostenson, S. Ziaee, and T. W Chou. Processing and electrical properties of carbon nanotube/vinyl ester nanocomposites. *Composites Science and Technology*, 69 (6):801–804, 2009.

[43] J. Sandler, M. S. P. Shaffer, T. Prasse, W. Bauhofer, K. Schulte, and A. H. Windle. Development of a dispersion process for carbon nanotubes in an epoxy matrix and the resulting electrical properties. *Polymer*, 40(21):5967–5971, 1999.

[44] D. Qian, E. C. Dickey, R. Andrews, and T. Rantell. Load transfer and deformation mechanisms in carbon nanotube-polystyrene composites. *Applied Physics Letters*, 76 (20):2868–2870, 2000.

[45] N. Grossiord, J. Loos, O. Regev, and C. E. Koning. Toolbox for dispersing carbon nanotubes into polymers to get conductive nanocomposites. *Chemistry of Materials*, 18(5):1089–1099, 2006.

[46] EXAKT Vertriebs GmbH. Three roll mills - the main benefits. URL `www.exakt.de`.

[47] T. Hielscher. Ultrasonic production of nano-size dispersions and emulsions. In *European Nano Systems 2005*, Paris, France, 14-16 December 2005. TIMA Editions.

[48] K. L. Lu, R. M. Lago, Y. K. Chen, M. L. H. Green, P. J. F. Harris, and S. C. Tsang. Mechanical damage of carbon nanotubes by ultrasound. *Carbon*, 34(6):814–816, 1996.

[49] S. Pegel, P. Potschke, G. Petzold, I. Alig, S. M. Dudkin, and D. Lellinger. Dispersion, agglomeration, and network formation of multiwalled carbon nanotubes in polycarbonate melts. *Polymer*, 49(4):974–984, 2008.

[50] M. S. P. Shaffer, X. Fan, and A. H. Windle. Dispersion and packing of carbon nanotubes. *Carbon*, 36(11):1603–1612, 1998.

[51] Y. H Liao, O. Marietta-Tondin, Z. Liang, C. Zhang, and B. Wang. Investigation of the dispersion process of SWNTs/SC-15 epoxy resin nanocomposites. *Materials Science and Engineering A*, 385(1-2):175–181, 2004.

[52] J. N. Coleman, S. Curran, A. B. Dalton, A. P. Davey, B. McCarthy, W. Blau, and R. C. Barklie. Percolation-dominated conductivity in a conjugated-polymer-carbon-

nanotube composite. *Physical Review B - Condensed Matter and Materials Physics*, 58(12):R7492–R7495, 1998.

[53] T. Kimura, H. Ago, M. Tobita, S. Ohshima, M. Kyotani, and M. Yumura. Polymer composites of carbon nanotubes aligned by a magnetic field. *Advanced Materials*, 14 (19):1380–1383, 2002.

[54] A. T. Seyhan, F. H. Gojny, M. Tanoglu, and K. Schulte. Critical aspects related to processing of carbon nanotube/unsaturated thermoset polyester nanocomposites. *European Polymer Journal*, 43(2):374–379, 2007.

[55] R. Ramasubramaniam, J. Chen, and H. Liu. Homogeneous carbon nanotube/polymer composites for electrical applications. *Applied Physics Letters*, 83(14):2928–2930, 2003.

[56] D. D. L. Chung. Electrical applications of carbon materials. *Journal of Materials Science*, 39(8):2645–2661, 2004.

[57] Hyperion Catalysis. Automotive applications, 2007. URL `www.fibrils.com/automotive2.htm`.

[58] ASTM. D4935-99 standard test method for measuring the electromagnetic shielding effectiveness of planar materials.

[59] R. Schmitt. *EMC*. Electromagnetics Explained: A Handbook for Wireless/RF, EMC, and High-speed Electronics. Newnes, 2002.

[60] YSHIELD. EMR-protection. URL `www.yshield.com`.

[61] Energytechpro. Electrocoat system. URL `www.energytechpro.com`.

[62] K. I. Winey, T. Kashiwagi, and M. Mu. Improving electrical conductivity and thermal properties of polymers by the addition of carbon nanotubes as fillers. *MRS Bulletin*, 32(4):348–353, 2007.

[63] P. Phillips. Analyzing the future of e-coat growth, April 2006 . URL www.coatingsworld.com.

[64] G. Gardiner. Lightning strike protection for composite structures. *Compositesworld*, 07/2006 . URL www.compositesworld.com/articles/lightning-strike-protection-for-composite-structures.aspx.

[65] LM Glasfiber. Effective lightning protection. URL www.lmglasfiber.com/Products/Lightning.aspx.

[66] Boyce components introduces electrically conductive resin. *NetComposites*, 14/08/2006. URL www.netcomposites.co.uk/news.asp?3904.

[67] Z. Wu, Z. Chen, X. Du, J. M. Logan, J. Sippel, M. Nikolou, K. Kamaras, J. R. Reynolds, D. B. Tanner, A. F. Hebard, and A. G. Rinzler. Transparent, conductive carbon nanotube films. *Science*, 305(5688):1273–1276, 2004.

[68] F. Kremer and A. Schonhals. *Theory of Dielectric Relaxation*, chapter 1. Broadband Dielectric Spectroscopy. Springer, 1 edition, 2002-12-16 2002. ISBN 3540434070.

[69] J. Mijovic. *Dielectric spectroscopy of reactive network-forming polymers*, chapter 9. Broadband Dielectric Spectroscopy. Springer, 1 edition, 2002. ISBN 3540434070.

[70] J. R. Macdonald. *Impedance Spectroscopy. Emphasizing Solid Material and Systems*. John Wiley and Sons, New York, 1987.

[71] J. W. Schultz. Dielectric spectroscopy in analysis of polymers. *Encyclopedia of Analytical Chemistry*, 2006.

[72] S. D. Senturia and N. F. Sheppard. Dielectric analysis of thermoset cure. *Advances in Polymer Science*, 80:1–47, 1986.

[73] A. Schonhals and F. Kremer. *Analysis of dielectric spectra*, chapter 3. Broadband

Dielectric Spectroscopy. Springer, 1 edition, 2002-12-16 2002. ISBN 3540434070.

[74] A. A. Skordos. PhD thesis: Modelling and monitoring of resin transfer moulding, September 2000. Cranfield University, United Kingdom.

[75] M. Mitchell. *An introduction to genetic algorithms*. MIT Press, Cambridge, Mass., 1996. ISBN 0262631857.

[76] M. C. Kazilas, A. A. Skordos, and I. K. Partridge. Parameter estimation in equivalent circuit analysis of dielectric cure monitoring signals using genetic algorithms. *Inverse Problems in Science and Engineering*, 13(2):157–176, 2005.

[77] A. A. Skordos and I. K. Partridge. Determination of the degree of cure under dynamic and isothermal curing conditions with electrical impedance spectroscopy. *Journal of Polymer Science, Part B: Polymer Physics*, 42(1):146–154, 2004.

[78] L. Valentini, D. Puglia, E. Frulloni, I. Armentano, J. M. Kenny, and S. Santucci. Dielectric behavior of epoxy matrix/single-walled carbon nanotube composites. *Composites Science and Technology*, 64(1):23–33, 2004.

[79] Nanocyl. Nc7000 material safety data sheet.

[80] Nanocyl s.a. Nc7000 data sheet. URL `www.nanocyl.com/products/industrial/7000.php`.

[81] A. Maynard. Safenano community. URL `community.safenano.org/blogs/andrew_maynard/default.aspx`.

[82] Royal Commission on Environmental Pollution. Novel materials and applications. URL `www.rcep.org.uk/novelmaterials.htm`.

[83] ETC Group. Nanotechnology. URL `www.etcgroup.org/en/issues/nanotechnology.html`.

[84] BSI. PD 6699-2:2007 guide to safe handling and disposal of manufactured nano-

materials. URL www.worldwidestandards.com/shop/products_view.php?prod=43579.

[85] C. A. Poland, R. Duffin, I. Kinloch, A. Maynard, W. A. H. Wallace, A. Seaton, V. Stone, S. Brown, W. MacNee, and K. Donaldson. Carbon nanotubes introduced into the abdominal cavity of mice show asbestos-like pathogenicity in a pilot study. *Nature Nanotechnology*, 3(7):423–428, 2008.

[86] K. Donaldson, L. Tran, L. A. Jimenez, R. Duffin, D. E. Newby, N. Mills, W. MacNee, and V. Stone. Combustion-derived nanoparticles: A review of their toxicology following inhalation exposure. *Particle and Fibre Toxicology*, 2, 2005.

[87] Health and Safety Executive. Novel material in the environment: the case of nanotechnology, 03/09 2009. URL www.hse.gov.uk/PUBNS/web38.pdf.

[88] Scott Bader Company. *Crystic Composites Handbook*. 2003.

[89] R. A. Panther. *Unsaturated polyester resins*. Handbook of polymer-fibre composites. Longman Group, UK, 1994.

[90] NIST database. Styrene. URL webbook.nist.gov/cgi/cbook.cgi?ID=C100425&Units=SI&Mask=4#Thermo-Phase.

[91] A. Daire. Low-voltage measurement techniques. *Evaluation Engineering*, 44(6):40–46, 2005.

[92] J. Fraden. *Chapter 16. Temperature Sensors*. Handbook of Modern Sensors - Physics, Designs and Applications. Springer - Verlag, 3rd edition, 2003. ISBN 0387007504.

[93] J. Z. Kovacs, K. Andresen, J. R. Pauls, C. P. Garcia, M. Schossig, K. Schulte, and W. Bauhofer. Analyzing the quality of carbon nanotube dispersions in polymers using scanning electron microscopy. *Carbon*, 45(6):1279–1288, 2007.

[94] A. Battisti, A. A. Skordos, and I. K. Partridge. Monitoring dispersion of carbon nano-

tubes in a thermosetting polyester resin. *Composites Science and Technology*, 69(10): 1516–1520, 2009.

[95] P. J. Carreau. Rheological equations from molecular network theories. *Trans Soc Rheol*, 16(1):99–127, 1972.

[96] K. Yasuda, R. C. Armstrong, and R. E. Cohen. Shear flow properties of concentrated solutions of linear and star branched polystyrenes. *Rheologica Acta*, 20(2):163–178, 1981.

[97] A. V. Shenoy. *Rheology of Filled Polymer Systems*. Springler-Verlag, 1999. ISBN 0412831007.

[98] D. Fylstra, L. Lasdon, J. Watson, and A. Waren. Design and use of the microsoft excel solver. *Interfaces*, 28(5):29–55, 1998.

[99] A. T. Seyhan, F. H. Gojny, M. Tanoglu, and K. Schulte. Rheological and dynamic-mechanical behavior of carbon nanotube/vinyl ester-polyester suspensions and their nanocomposites. *European Polymer Journal*, 43(7):2836–2847, 2007.

[100] A. W. K. Ma, M. R. Mackley, and S. S. Rahatekar. Experimental observation on the flow-induced assembly of carbon nanotube suspensions to form helical bands. *Rheologica Acta*, 46(7):979–987, 2007.

[101] S. S. Rahatekar, K. K. K. Koziol, S. A. Butler, J. A. Elliott, M. S. P. Shaffer, M. R. Mackley, and A. H. Windle. Optical microstructure and viscosity enhancement for an epoxy resin matrix containing multiwall carbon nanotubes. *Journal of Rheology*, 50 (5):599–610, 2006.

[102] J. Loos, A. Alexeev, N. Grossiord, C. E. Koning, and O. Regev. Visualization of single-wall carbon nanotube (SWNT) networks in conductive polystyrene nanocomposites by charge contrast imaging. *Ultramicroscopy*, 104(2):160–167, 2005.

[103] A. Battisti, A. A. Skordos, and I. K. Partridge. Dielectric monitoring of carbon nanotube network formation in curing thermosetting nanocomposites. *Journal of Physics D: Applied Physics*, 42(15), 2009.

[104] A. Dimopoulos, A. A. Skordos, and I. K. Partridge. Cure of a carbon nanotube modified multiphase epoxy- thermoplastic resin system. In *Proceedings of the 49th AIAA/ASME/ASCE/AHS/ASC Structures, Structural Dynamics, and Materials Conference*. Published by AIAA, Digital, 7 - 10 April 2008 2008.

[105] J. Mijovic and C. F. W. Yee. Use of complex impedance to monitor the progress of reactions in epoxy/amine model systems. *Macromolecules*, 27(25):7287–7293, 1994.

[106] I. Alig, T. Skipa, D. Lellinger, and P. Potschke. Destruction and formation of a carbon nanotube network in polymer melts: Rheology and conductivity spectroscopy. *Polymer*, 49(16):3524–3532, 2008.

[107] S. Andjelic, J. Mijovic, and F. Bellucci. Impedance spectroscopy of reactive polymers. 5. impedance as a measure of chemical and physical changes in glass formers. *Journal of Polymer Science, Part B: Polymer Physics*, 36(4):641–653, 1998.

[108] P. Heitjans and S. Indris. Diffusion and ionic conduction in nanocrystalline ceramics. *Journal of Physics Condensed Matter*, 15(30):R1257–R1289, 2003.

[109] J. T. S. Irvine, D. C. Sinclair, and A. R. West. Electroceramics : Characterization by impedance spectroscopy. *Advanced Materials*, 2(3):132–138, 1990.

[110] D. S. McLachlan, J. H Hwang, and T. O. Mason. Evaluating dielectric impedance spectra using effective media theories. *Journal of Electroceramics*, 5(1):37–51, 2000.

[111] G. Sauti and D. S. McLachlan. Impedance and modulus spectra of the percolation system silicon-polyester resin and their analysis using the two exponent phenomenological percolation equation. *Journal of Materials Science*, 42(16):6477–6488, 2007.

[112] D. S. Mclachlan. Analytical functions for the DC and AC conductivity of conductor-insulator composites. *Journal of Electroceramics*, 5(2):93–110, 2000.

[113] S. K. Kim, M. Miyayama, and H. Yanagida. Electrical anisotropy and a plausible explanation for dielectric anomaly of Bi4Ti3O12 single crystal. *Materials Research Bulletin*, 31(1):121–131, 1996.

[114] E. T. Thostenson and T. W Chou. On the elastic properties of carbon nanotube-based composites: Modelling and characterization. *Journal of Physics D: Applied Physics*, 36(5):573–582, 2003.

[115] P. I. Karkanas. PhD thesis: Cure modelling and monitoring of epoxy/amine resin systems, 1998. School of Industrial and Manufacturing Science. Cranfield University.

[116] J. Baur and E. Silverman. Challenges and opportunities in multifunctional nanocomposite structures for aerospace applications. *MRS Bulletin*, 32(4):328–334, 2007.

[117] R. H. Baughman, A. A. Zakhidov, and W. A. De Heer. Carbon nanotubes - the route toward applications. *Science*, 297(5582):787–792, 2002.

[118] J. Robertson. Realistic application of CNTs. *Materials Today*, 7(9):46–52, 2004.

[119] N. Pottish. Nanoparticles, nanotubes and nanocomposites. *Composites technology*, 2005. URL `www.compositesworld.com/articles/nanoparticles-nanotubes-and-nanocomposites.aspx`.

[120] A. Beigbeder, P. Degee, S. L. Conlan, R. J. Mutton, A. S. Clare, M. E. Pettitt, M. E. Callow, J. A. Callow, and P. Dubois. Preparation and characterisation of silicone-based coatings filled with carbon nanotubes and natural sepiolite and their application as marine fouling-release coatings. *Biofouling*, 24(4):291–302, 2008.

[121] L. Boger, M. H. G. Wichmann, L. O. Meyer, and K. Schulte. Load and health monitoring in glass fibre reinforced composites with an electrically conductive nanocomposite

epoxy matrix. *Composites Science and Technology*, 68(7-8):1886–1894, 2008.

[122] M. Schlesinger and M. Paunovic. *Modern electroplating*. John Wiley and Sons, 2000. ISBN 0471168246.

[123] MDC Max Daetwyler AG. Starbase light weight cylinder system. URL `www.daetwyler.com/user_content/editor/files/Fact_sheet_starbase_en/fs_stbas_eng_eu.pdf`.

[124] L. Lin. Mechanisms of pigment dispersion. *Pigment and Resin Technology*, 32(2):78, 2003.

[125] I. Alig, D. Lellinger, M. Engel, T. Skipa, and P. Potschke. Destruction and formation of a conductive carbon nanotube network in polymer melts: In-line experiments. *Polymer*, 49(7):1902–1909, 2008.

[126] I. Alig, T. Skipa, M. Engel, D. Lellinger, S. Pegel, and P. Potschke. Electrical conductivity recovery in carbon nanotube-polymer composites after transient shear. *Physica Status Solidi (B) Basic Research*, 244(11):4223–4226, 2007.

[127] P. Potschke, M. Abdel-Goad, I. Alig, S. Dudkin, and D. Lellinger. Rheological and dielectrical characterization of melt mixed polycarbonate-multiwalled carbon nanotube composites. *Polymer*, 45(26):8863–8870, 2004.

[128] P. Potschke, S. M. Dudkin, and I. Alig. Dielectric spectroscopy on melt processed polycarbonate - multiwalled carbon nanotube composites. *Polymer*, 44(17):5023–5030, 2003.